Aus dem Institut für Insektenbiotechnologie
Professur für Naturstoffforschung mit Schwerpunkt
Insektenbiotechnologie der

In vitro and *in vivo* characterization of darobactin derivatives

Kumulative - Dissertation

zur Erlangung des Doktorgrades (Dr. rer. nat.)
im Fachbereich Agrarwissenschaften, Ökotrophologie und Umweltmanagement der Justus-Liebig-Universität Gießen

vorgelegt von

Jil-Christine Kramer
geboren in Fritzlar

Gießen, Mai 2025

Mit Genehmigung des Fachbereichs 09
Agrarwissenschaften, Ökotrophologie und Umweltmanagement
der Justus-Liebig-Universität Gießen

Prüfungskommission:

1. Gutachter:	**Prof. Dr. Till F. Schäberle**
2. Gutachter:	**Prof. Dr. Kai Thormann**
3. Prüfer:	Prof. Dr. Marc F. Schetelig
4. Prüferin:	Prof. Dr. Elena Evguenieva-Hackenberg
Vorsitzender:	Prof. Dr. Jan Siemens

Erklärung gemäß der Promotionsordnung des Fachbereichs 09 vom 07. Juli 2004 § 17 (2)

„Ich erkläre: Ich habe die vorgelegte Dissertation selbständig und ohne unerlaubte fremde Hilfe und nur mit den Hilfen angefertigt, die ich in der Dissertation angegeben habe.

Alle Textstellen, die wörtlich oder sinngemäß aus veröffentlichten Schriften entnommen sind, und alle Angaben, die auf mündlichen Auskünften beruhen, sind als solche kenntlich gemacht.

Bei den von mir durchgeführten und in der Dissertation erwähnten Untersuchungen habe ich die Grundsätze guter wissenschaftlicher Praxis, wie sie in der „Satzung der Justus-Liebig-Universität Gießen zur Sicherung guter wissenschaftlicher Praxis" niedergelegt sind, eingehalten."

Datum Unterschrift

Inhalt

Summary

Antibiotics are our major weapon to fight infectious diseases. Many of today's standard medical procedures, such as organ transplants or cancer treatments, are only possible through the use of antibiotics, and they have drastically increased the average human lifespan. But we are about to lose this huge advantage as we are facing an antimicrobial resistance crisis. Some microorganisms are no longer susceptible to antibiotics, making infectious diseases very difficult to treat. Alongside to tuberculosis, the most problematic pathogens are Gram-negative bacteria, like *Acinetobacter baumannii*, *Escherichia coli*, *Klebsiella pneumoniae* and *Pseudomonas aeruginosa*. Since not many novel antibiotics have been discovered since the so-called 'golden age' of antibiotic discovery, we are in urgent need of new treatment options. A lot of the antibiotics discovered during this period were natural products, which still represent a source of great potential for the discovery of new antibiotics.

The discovery of the natural product darobactin A (DAR A) is a good example, marking a major step forward in the fight against the looming antimicrobial resistance crisis. The compound shows activity against all the important Gram-negative pathogens and has a novel mode of action with no known cross-resistance to antibiotics available on the market. By targeting BamA, a part of a complex in the outer membrane of Gram-negative bacteria responsible for the folding and integrating of outer membrane proteins, DAR A acts on the outside of the bacterial cell wall. This avoids the major problem of antibiotics having to cross both the inner and outer cell membrane to reach a target inside of Gram-negative bacteria. With DAR A opening up a new class of BamA inhibitors, many derivatization studies were initiated to optimize the structure of this compound. In addition to exchanging amino acids in the sequence of the cyclic heptamer, genome mining approaches have been used to identify other DAR producers and find natural derivatives.

In the first project of this work, this approach led to the discovery of the DAR biosynthetic gene cluster in *P. luteoviolacea* H33, which was found to contain additional genes next to the ones encoding for DAR. This strain produces three new DAR variants: bromodarobactin, dehydrodarobactin and dehydrobromodarobactin. One of these genes revealed to be a flavin-dependent tryptophan halogenase with a novel fold. This halogenase, DarH, brominates the

N-terminal tryptophan of DAR A to form bromodarobactin. The enzyme was purified and further characterized. *In vitro* and heterologous expression studies *in vivo* showed that DarH can also brominate a DAR derivative and catalyze the iodination of tryptophan. Furthermore, activity assays with bromodarobactin revealed increased activity and plasma binding compared to DAR A.

To further increase the activity of DAR A or to optimize the pharmacokinetics of the compound, in the second project of this dissertation a technique was developed to replace the natural amino acids by non-canonical amino acids. This was achieved by adapting the amber stop codon suppression technique for the production of DAR A derivatives. An altered aminoacyl-tRNA synthase that accepts non-canonical amino acids is used in combination with a tRNA that recognizes a nonsense codon. This nonsense codon is integrated into the biosynthetic gene cluster at the desired position of exchange by mutation. In the case of DAR A, the codon at position seven of the heptapeptide has been changed, resulting in the production of darobactin A F7F with a 4-fluoro-L-phenylalanine, darobactin A F7I (4-iodo-L-phenylalanine), darobactin A F7F_5 (2,3,4,5,6-pentafluoro-L-phenylalanine) and darobactin A F7OMe (4-methoxy-L-phenylalanine). Darobactin A F7F could be purified in large scale, was characterized by NMR experiments and showed a similar activity compared to DAR A in activity assays.

Zusammenfassung

Antibiotika gehören zu den wichtigsten Werkzeugen der modernen Medizin. Nur dank ihnen können Infektionskrankheiten wirksam bekämpft werden, wodurch sich die Lebenserwartung der Menschen heutzutage deutlich erhöht hat. Auch medizinische Eingriffe wie Organtransplantationen oder Chemotherapien, die unseren medizinischen Fortschritt ausmachen, werden erst durch Antibiotika möglich. Leider sorgen resistente Erreger dafür, dass wir diesen Fortschritt immer mehr verlieren und uns eine antimikrobielle Resistenzen Kriese bevorsteht. Wenn Bakterien resistent werden, also Abwehrmechanismen gegen ein Antibiotikum entwickeln, sind die entsprechenden Infektionen nur noch sehr schwer zu behandeln. Neben resistenten Tuberkuloseerregern stellen vor allem Gram-negative Bakterien wie *Acinetobacter baumannii*, *Escherichia coli*, *Klebsiella pneumoniae* und *Pseudomonas aeruginosa* ein großes Problem dar. Leider wurden nach dem sogenannten Goldenen Zeitalter der Antibiotikaentdeckung nicht mehr viele neue antibiotisch wirksame Substanzen entdeckt, so dass wir dringend neue Behandlungsmöglichkeiten für diese Krankheitserreger benötigen. Viele der damals entdeckten Antibiotika sind Naturstoffe und diese Klasse birgt auch heute noch ein großes Potenzial für die Entdeckung neuer Antibiotika.
Ein gutes Beispiel dafür ist die Entdeckung des Naturstoffes Darobactin A (DAR A). Das Antibiotikum ist wirksam gegen alle wichtigen Gram-negativen Erreger und hat einen neuartigen Wirkmechanismus, so dass keine Kreuzresistenzen zu kommerziell erhältlichen Antibiotika zu erwarten sind. Das Antibiotikum bindet an BamA, einem Teil eines Komplexes in der äußeren Membran Gram-negativer Bakterien. Dieser faltet Proteine der äußeren Zellmembran und integriert sie anschließend. Durch diesen Wirkmechanismus wird das große Problem umgangen, welches bei der Behandlung von Infektionen mit Gram-negativen Bakterien besteht, nämlich dass der Wirkstoff zwei Zellmembranen überwinden muss, um sein Ziel im Inneren des Bakteriums zu erreichen. Damit begründet DAR A eine neue Klasse von BamA-Inhibitoren und inspirierte zahlreiche Derivatisierungsstudien. Einige dieser Studien beschäftigen sich mit dem Austausch einzelner Aminosäuren des Peptidgrundgerüsts von DAR A, andere nutzen Genomdatenbanken, um Bakterien zu identifizieren, die ebenfalls DAR produzieren.

Letzteres führte in der ersten Studie dieser Arbeit zur Entdeckung des DAR Biosyntheseclusters in *P. luteoviolacea* H33, welches neben den ursprünglichen Genen zur DAR Expression noch weitere unbekannte Gene enthält. Der Stamm selbst produziert drei neue DAR Derivate: Bromodarobactin, Dehydrodarobactin und Dehydrobromodarobactin. Eines der unbekannten Gene konnte als Flavin-abhängige Tryptophan-Halogenase identifiziert werden. Die Halogenase DarH zeichnet sich durch eine bisher unbekannte Teilstruktur aus und katalysiert die Bromierung des *N*-terminalen Tryptophans des DAR A Grundgerüsts, wodurch Bromodarobactin entsteht. Das Enzym wurde aufgereinigt und durch *in vitro* und heterologe *in vivo* Expressionsstudien charakterisiert. Dadurch konnte gezeigt werden, dass nicht nur DAR A, sondern auch ein anderes DAR Derivat bromiert werden kann und außerdem eine Iodierung des Tryptophans möglich ist. Bromodarobactin selbst zeigt während *in vitro* Studien eine höhere Aktivität und eine besser Plasmabindung im Vergleich zu DAR A.

Um eine verbesserte Aktivität von DAR A zu erreichen oder die pharmakokinetischen Eigenschaften des Antibiotikums zu verbessern, wird in der zweiten Studie dieser Arbeit die „amber stop codon suppression"-Technik dazu genutzt proteinogene Aminosäuren des DAR A Grundgerüsts gegen nicht-proteinogene Aminosäuren auszutauschen. Hierzu wird eine Aminoacyl-tRNA Synthase benötigt die so modifiziert ist, dass sie nicht-proteinogene Aminosäuren als Substrat nutzen kann. Diese wird in Verbindung mit einer tRNA verwendet, die das Anticodon eines Stopcodons trägt. Das Stopcodon wird mit molekularbiologischen Methoden an der gewünschten Stelle in das Gencluster von DAR A eingefügt. In diesem Fall wurde das Phenylalanin an Position sieben des DAR A Grundgerüsts ausgetauscht. Dies ermöglichte die heterologe Expression von vier neuen Derivaten: Darobactin A F7F durch die Integration von 4-Fluoro-L-Phenylalanin, sowie Darobactin A F7I (4-Iodo-L-Phenylalanin), Darobactin A $F7F_5$ (2,3,4,5,6-Pentafluoro-L-Phenylalanin) und Darobactin A F7OMe (4-Methoxy-L-phenylalanin). Darobactin A F7F wurde in größerem Maßstab aufgereinigt und seine Struktur durch NMR-Experimente bestätigt. In Aktivitätstests zeigte die Substanz eine ähnliche Aktivität wie DAR A.

1. Introduction

1.1 The antimicrobial resistance crisis

Antimicrobial drugs are used to treat a wide range of infectious diseases caused by bacteria (antibiotics), viruses (antivirals), fungi (antifungals) or other parasites. When these organisms are no longer affected by the drugs, antimicrobial resistance (AMR) occurs. AMR is a natural process and has been observed since the first antimicrobial drugs were discovered, but the process is heavily driven by the misuse and overuse of these drugs (O'Neill, 2016). Antibiotics are often used in livestock for the treatment of diseases as well as for control or prevention, resulting in the development of resistant microbes in animals (Figure 1A). If feces are used as fertilizers and the food crops are not properly cleaned or if animal meat is not properly handled or cooked, the resistant microbes can be transferred to humans. Another transmission route is directly from human to human, either in general public or during hospitalization (U. S. Centers for Disease Control and Prevention, 2024). Approximately 700,000 patients worldwide suffer from infections with resistant microbes each year, which is still less than the number of people who suffer from diabetes, cancer or road traffic accidents (Figure 1B). However, this number is estimated to increase to 10 million people per year, making AMR the leading cause of death by 2050 (O'Neill, 2016).

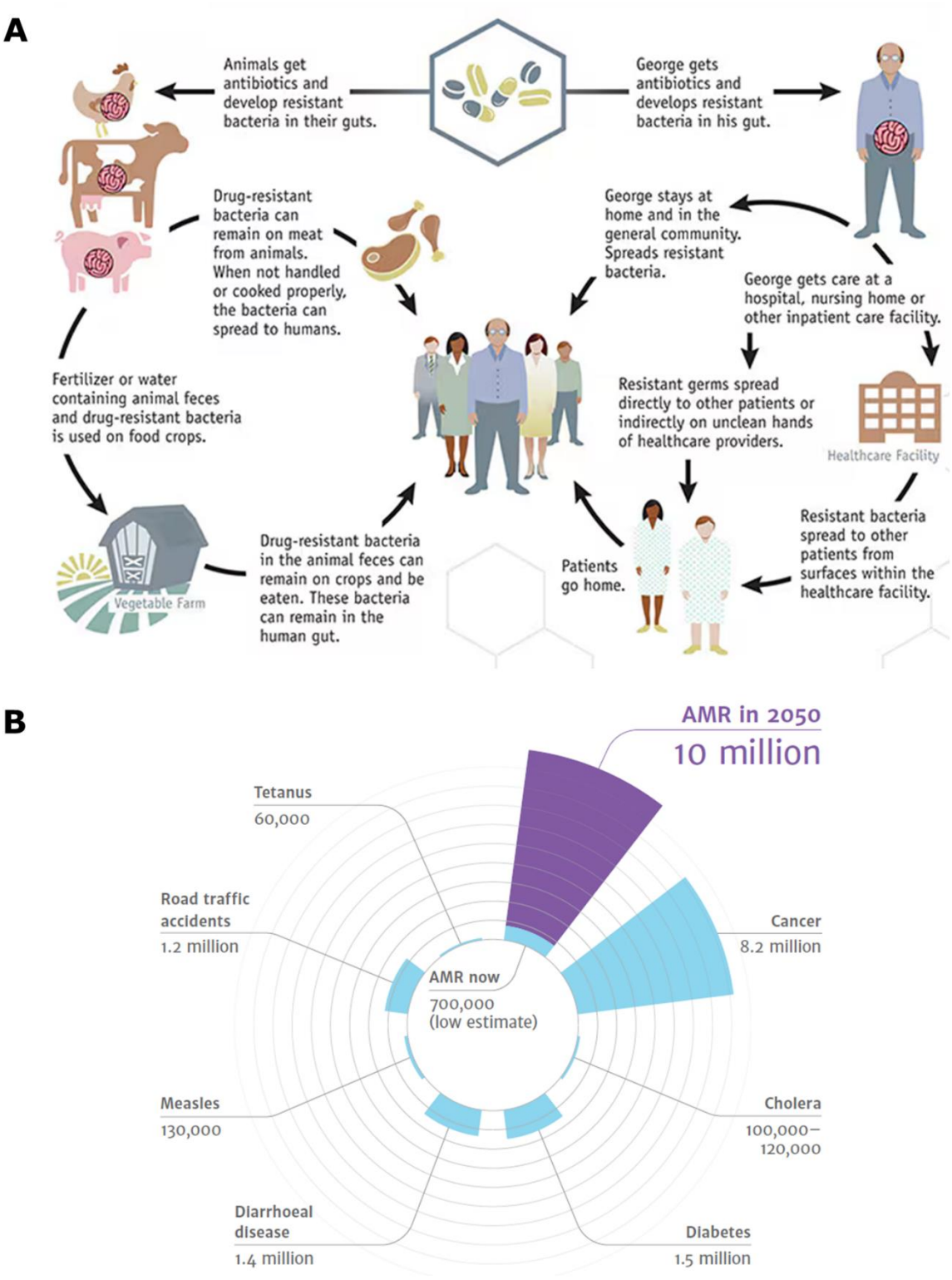

Figure 1: How antimicrobial resistance spreads and the consequences. A: Scheme showing examples of how antimicrobial resistance spreads (adapted from: U. S. Centers for Disease Control and Prevention, 2024). **B:** Estimated deaths attributed to different diseases and road traffic accidents per year (O'Neill, 2016).

The excess costs to the US health care system caused by infections with resistant microbes is approximately USD 20 billion per year (Smith and Coast, 2013). In particular, during the COVID-19 pandemic, which caused a major disruption to the healthcare system itself, the number of hospitalized COVID-19 patients with resistant microbial infections increased dramatically (Segala *et al.*, 2021; Yang *et al.*, 2024). According to the WHO (2024), apart from tuberculosis, the pathogens for which we most urgently need new antibiotics for are Gram-negative bacteria. The top three strains with "critical" status are carbapenem-resistant *Acinetobacter baumannii* and *Escherichia coli* as well as β-lactamase-producing *Klebsiella pneumoniae*. Carbapenem-resistant *Pseudomonas aeruginosa* has recently been reclassified from the "critical" to the "high" status (WHO, 2024). Infections with resistant microbes are on the rise, and the infections are no longer just associated with hospitals or care facilities, resulting in the fact that we are facing an AMR crisis. Due to our reliance on antimicrobial drugs to fight life-threatening diseases such as tuberculosis and malaria or to support patients with a weak immune systems during organ transplants or chemotherapy, new antibiotics are urgently needed to avoid losing ground in modern medicine (O'Neill, 2016).

1.2 Antibiotic discovery in the past, present and future

The antibiotic era began in 1910, when Paul Ehrlich invented Salvarsan for the treatment of syphilis (Figure 2) (Gelpi *et al.*, 2015). Inspired by his work, Gerhard Domagk developed sulfonamides 20 years later, which became the first broad-spectrum antimicrobials in clinical use, with resistance emerging just a few years later (Otten, 1986; Hutchings *et al.*, 2019). In 1928, Alexander Fleming (1929) discovered penicillin, and its structure was elucidated by Dorothy Hodgkin (1949) in 1945, paving the way for semi-synthetic derivatives of the compound to overcome the resistances already observed in 1940 (Hutchings *et al.*, 2019). Subsequently, the so-called 'golden age' of antibiotic discovery from 1940 to 1960 was initiated by Selman Waksman, who systematically studied microorganisms as producers of antibiotics (Katz and Baltz, 2016). He identified the class of actinomycetes as potent natural product (NP) producers and discovered the NP streptomycin as the first agent active against tuberculosis (Waksman *et al.*, 2010). NPs are secondary metabolites produced by an organism (mainly bacteria and fungi). These compounds are not required for the growth of the organism and

some of them show antibacterial, antiviral, antifungal or anticancer activity (Newman and Cragg, 2016). The last class of NP antibiotics was discovered in the 1980s, leading to the fact that most of the antibiotics in clinical trials today are derivatives of known NP classes or synthetic antibiotics (Katz and Baltz, 2016; Hutchings *et al.*, 2019).

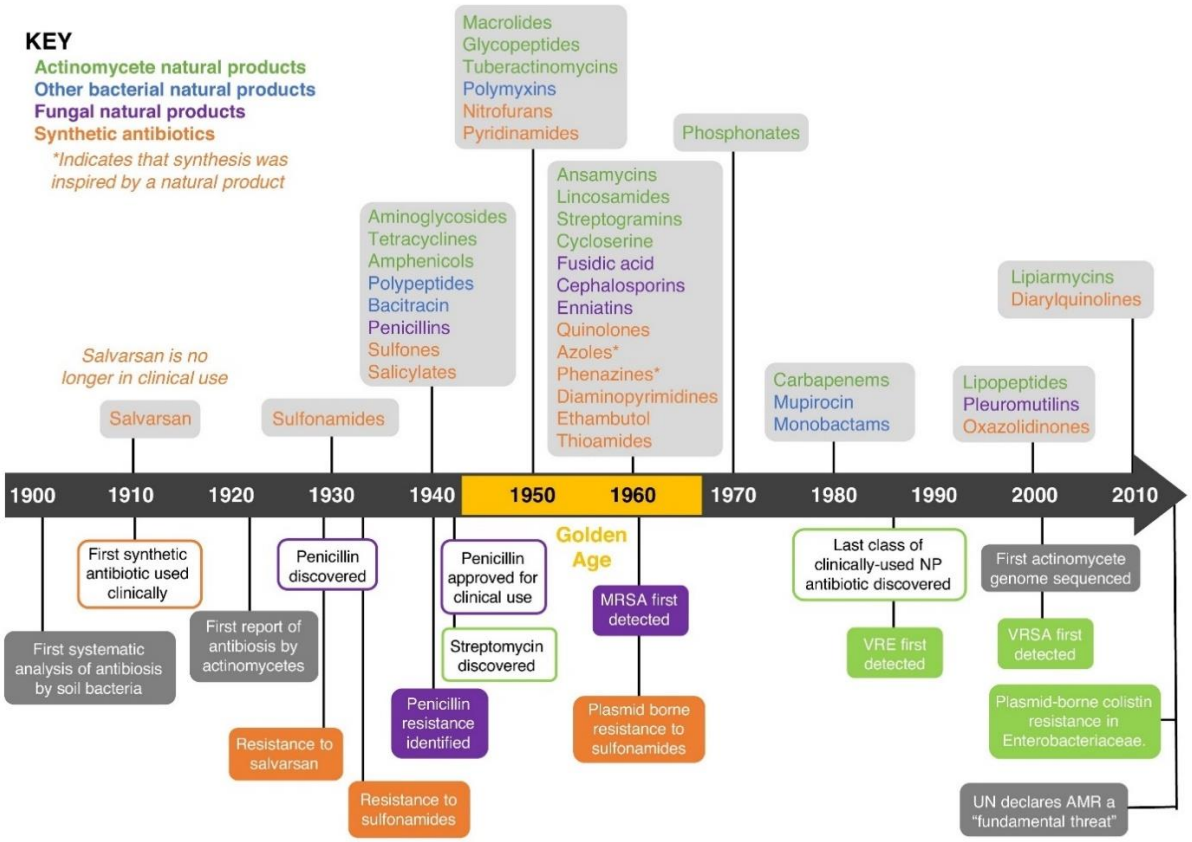

Figure 2: Timeline of antibiotics and antibiotic classes reaching the market. The top of the timeline shows the antibiotics colored according to their origin (green: actinomycetes, blue: other bacteria, purple: fungi, orange: synthetic). The bottom shows the first emergence of resistance and key events in antibiotic discovery (Hutchings *et al.*, 2019).

With the dawn of the genomic era, whole genome sequencing of pathogens revealed potential antibiotic targets which are essential for their survival. High-throughput screening was expected to enable to the discovery of a large number of compounds binding to these targets, leading to huge investments by pharmaceutical companies in these platforms. However, this strategy failed and the resulting financial losses have led companies to exit the antibiotic discovery business (Livermore, 2011; Da Ribeiro Cunha *et al.*, 2019). The median cost of bringing a new antibiotic to the market is USD 985 million, and antibiotics are usually only needed for a short period of time (Ventola, 2015; Hernandez *et al.*,

2020). Drugs for chronic diseases, which are typically administered throughout a patient's lifetime, are estimated to have a net present value three times higher than a new antibiotic (Power, 2006; Ventola, 2015). Therefore, antibiotic discovery and development seems to be a rather unattractive business for pharmaceutical industry and the development of new antibiotics is mainly handled by small or medium-sized companies, resulting in an insufficient clinical pipeline (WHO, 2021). From 2017 to 2023, there have been 97 antibiotics or combination therapies including an antibiotic in the clinical antibacterial pipeline. Of these, 57 are traditional antibiotics and 40 are non-traditional antibiotics. Most of the traditional antibiotics (32) are active against the WHO bacterial priority pathogens, 19 against *M. tuberculosis*, five against *C. difficile* and one against *H. pylori*. From these 32 antibacterial compounds, active against the WHO priority pathogens, only 12 fulfill at least one of the WHO innovation criteria (new chemical class, new target, new mode of action or the absence of cross-resistance). Only four of these new compounds are active against the multidrug-resistant Gram-negative bacteria in the WHO "critical" group. In addition, only 16 antibiotics have been approved for the market between July 2017 and December 2023 and most of them are classified as reserve antibiotics, which further supports the urgent need for new antibacterial compounds (WHO, 2023).

1.3 Natural products as antimicrobial agents

NPs have been and continue to be a promising compound class for the discovery of new antibiotics (Hutchings *et al.*, 2019; Newman and Cragg, 2020). Especially microorganisms are able to produce a variety of NPs to kill competitors, protect themselves, for predation purposes or as signaling molecules for interaction within their species or with their eukaryotic host (Seipke *et al.*, 2012; Klassen, 2014; Traxler and Kolter, 2015). These properties make NPs, especially those produced by microorganisms, a good source for antibiotic discovery (Katz and Baltz, 2016). Many of these compounds produced by bacteria, which are easy to cultivate, were discovered during the golden age of antibiotic discovery, and rediscovery of these compounds became a problem soon (Hutchings *et al.*, 2019). This can be circumvented by sampling in under-explored environments that were inaccessible or unknown during this period or taking a closer look at symbiotic bacteria, such as those living associated with sponges or insects (Kaltenpoth, 2009; Palaniyandi

et al., 2013; Wilson *et al.*, 2014; Payne *et al.*, 2015). Furthermore, advanced tools for genome mining have revealed that the majority of the potential NPs of a microorganism are not expressed under standard laboratory conditions, leading to a new field of NP discovery (Figure 3) the genomic-driven NP discovery (Rutledge and Challis, 2015; Blin *et al.*, 2019). Next generation sequencing is used to access the whole genome sequence of an organism of interest (Rutledge and Challis, 2015). Bioinformatic tools like antiSMASH (Medema *et al.*, 2011), SMURF (Khaldi *et al.*, 2010) or BAGEL3 (van Heel *et al.*, 2013) can be used to identify cryptic biosynthetic gene clusters (BGCs) within the genome (Rutledge and Challis, 2015).

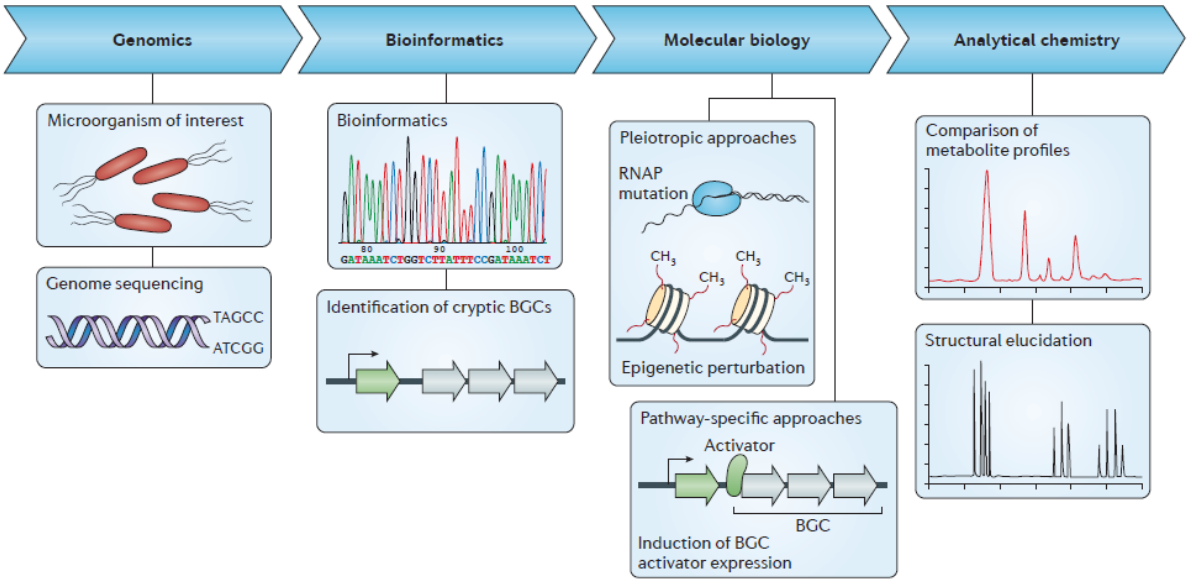

Figure 3: Overview of the process of genomic-driven NP discovery. The genome sequence of the microorganism of interest is obtained by whole genome sequencing and bioinformatical tools are used to predict biosynthetic gene clusters (BGCs). Afterwards cryptic gene clusters can be activated by different molecular biological approaches (e. g. pleiotropic approaches or pathway-specific approaches), the NP is identified in the culture broth and characterized by high-resolution mass spectrometry and NMR spectroscopy (Rutledge and Challis, 2015).

Afterwards, different molecular biologic approaches can be used to access a cryptic BGC. One option are pleiotropic approaches, which are more untargeted and therefore useful for high-throughput screenings. An example of this would be the variation of the growth conditions (Rutledge and Challis, 2015). This can be achieved by using different media and temperatures, co-cultivation, addition of unusual trace elements, addition of soil extracts or by triggering the organism with antibiotics to increase the selective pressure (Scherlach and Hertweck, 2006; Kawai *et al.*, 2007; Lincke *et al.*, 2010; Scherlach *et al.*, 2010; Tanaka *et al.*, 2010;

Seyedsayamdost, 2014; Rutledge and Challis, 2015). Furthermore, novel cultivation techniques such as the iChip allow the cultivation of previously under laboratory conditions 'unculturable microorganisms' directly in their natural environment (Nichols *et al.*, 2010; Gavrish *et al.*, 2014; Ling *et al.*, 2015). Other than triggering the microorganisms with external factors, intrinsic measures can be taken, such as modifying the RNA polymerase, ribosomal proteins, global regulators or histone modifying enzymes (Shima *et al.*, 1996; Rutledge and Challis, 2015).

In contrast to the pleiotropic approaches, pathway-specific approaches are more targeted and can be used when more knowledge is acquired about the BGC from bioinformatic analysis. Examples include, inducing the expression of BGC specific activator genes or deleting repressor genes. Another option could be refactoring combined with heterologous expression. Refactoring refers to replacing the natural promoter of the BGC with a constitutive promoter or one that can be stimulated by a known external stimulus. When there are no genetic tools for the natural producer available, or when the BGC contains only a few genes, the refactoring can be combined with the expression in a heterologous host. This technique is especially suitable for marine NPs, which are the most abundant biological NP resource, with more than 42,000 (https://marinlit.rsc.org/, 2024) compounds. On the one hand, their adaptation to high pressure, high salinity, low temperature and low light has driven the evolution of unique metabolic and biosynthetic pathways, but on the other hand, these adaptations make them difficult to cultivate in the laboratory (Zhao *et al.*, 2024).

Activation of the BGC by any of the above-mentioned techniques is followed by detecting changes in the metabolite profile of the NP producer or the heterologous host. High-performance liquid chromatography (HPLC) coupled with electrospray ionization mass spectrometry (ESI-MS) can be used to identify the masses of the metabolites, which vary between the extract with and without the activated BGC (Krug and Müller, 2014). When measured with high accuracy, the *m/z* ratio can be used to predict the molecular formula of the compound to assess the likelihood of discovering a novel compound, while the fragment ions produced in tandem mass spectrometry (MS/MS) can be used to get a first insight into the structure of the compound (Medema *et al.*, 2014; Mohimani *et al.*, 2014a; Mohimani *et al.*, 2014b). After purification of the target compound by various methods, nuclear magnetic

resonance (NMR) spectroscopy can be used for a final structural elucidation (Breton and Reynolds, 2013).

There are four main classes of NPs: non-ribosomal peptides (NRPs), polyketides, terpenes and, ribosomally synthesized and post-translationally modified peptides (RiPPs) (Rutledge and Challis, 2015). NRPs, polyketides and terpenes are classes of NPs that are biosynthesized in a modular fashion. There is always a starter unit, which is elongated and/or modified during the biosynthetic process by different enzymes in the assembly line. Since the function of the enzymes is known, structural predictions can sometimes be made prior to isolation (Hertweck, 2009; Oves-Costales *et al.*, 2009; Piel, 2010; Strieker *et al.*, 2010; Gao *et al.*, 2012). The BGC of RiPPs consists of a precursor peptide with possible regions of signaling function, leader peptides, recognition sites and the core peptide with the unmodified amino acid sequence of the RiPP. This precursor peptide is ribosomally produced, followed by different maturation steps involving the enzymes for the post-translational modifications and a subsequent proteolysis step to get the final RiPP (Arnison *et al.*, 2013).

1.4 Heterologous expression

As already mentioned above, microorganisms have a huge potential to express NPs, but many BGCs remain "silent" under laboratory conditions. Therefore, heterologous expression is a powerful tool for NP discovery (Rutledge and Challis, 2015; Katz and Baltz, 2016; Zhao *et al.*, 2024). From 2018 to 2023, at least 63 NP families were discovered in 50 studies by using heterologous expression. Once the BCG is identified, different cloning techniques can be used to integrate it into the heterologous expression host, which can be cultivated under laboratory conditions (Kadjo and Eustáquio, 2023).

Although this may sound like a straightforward workflow, heterologous expression provides its own challenges, starting with the selection of a suitable host organism (Watts *et al.*, 2021). For example, eukaryotic genes have introns and are GC-rich, whereas prokaryotic genes are mostly AT-rich without introns (Ullrich *et al.*, 2015; Parret *et al.*, 2016). Furthermore, genes within the prokaryotic phylum are not transcribed and translated with the same efficiency. In addition, the processing and the post-translational modification machinery may not function in the same manner and the messenger ribonucleic acid (mRNA) or the protein itself may be

degraded by the host cell machinery (Desai *et al.*, 2010; Genuth and Barna, 2018). In recent years some heterologous hosts such as *E. coli*, *Bacillus thuringiensis* and yeast have been established in different fields of heterologous expression (Celik and Calık, 2012; Rosano and Ceccarelli, 2014; Watts *et al.*, 2021). Especially for marine NPs, the heterologous hosts *S. coelicolor* or *S. lividans* are often chosen next to *E. coli* (Zhao *et al.*, 2024).

If a suitable heterologous host is not available, gene modifications can be made to match the characteristics of the host organism, a technique in which codon usage is an important factor (Welch *et al.*, 2009). There are 61 codons encoding for the twenty different canonical amino acids with additional three stop (nonsense) codons (Gustafsson *et al.*, 2004). Codons that encode for the same amino acid are called synonymous codons and their frequency of use varies from species to species (Sharp and Li, 1987; Hershberg and Petrov, 2008). Therefore, adapting the codon usage within the gene to the heterologous host can increase the expression rate or even allow the heterologous expression of a NP that would otherwise not be expressed (Watts *et al.*, 2021). In addition, using the correct Shine-Dalgarno sequence is important for an optimal expression, and the adaption the GC content of the gene can increase the mRNA stability, expression and export (Li *et al.*, 2012; Mordstein *et al.*, 2020). Heterologous expression requires knowledge of both the protein biosynthetic machinery of the original producer and the host organism. Therefore, increasing knowledge of the transcriptional and translational machinery will also increase the efficiency of heterologous expression as a tool in the future (Watts *et al.*, 2021).

1.5 Darobactin

A promising new antibiotic with huge potential to help us to tackle the coming AMR crisis is darobactin A (DAR A) (Imai *et al.*, 2019). DAR A is a RiPP with activity against the important drug-resistant pathogens *E. coli, P. aeruginosa*, *K. pneumoniae* and *A. baumannii*. It was discovered in 2019 by a classical bioactivity guided screening approach. A set of extracts from *Photorhabdus* and *Xenorhabdus* strains, living associated with the gut microbiome of nematode species, was screened against *E. coli* for inhibition zones in a nutrient agar diffusion test. The compound is produced by *Photorhabdus khanii* HGB1456 and possesses a novel mode of action (Imai *et al.*, 2019). It binds to BamA, a part of the β-barrel

assembly machinery (BAM), which is a complex that catalyzes the folding and integration of outer membrane proteins (OMPs) into the outer membrane (OM) of Gram-negative bacteria (Hagan *et al.*, 2010; Konovalova *et al.*, 2017; Imai *et al.*, 2019). BamA generally exists in two major conformations: the 'lateral open' and the 'lateral closed' state (Iadanza *et al.*, 2016). Studies with a DAR A derivative showed that the compound promotes the transition of BamA to the 'lateral closed' state, stabilizes this conformation and therefore prevents OMPs from entering the complex (Haysom *et al.*, 2023). Attempts to obtain resistant mutants at a concentration of four times the minimum inhibitory concentration (MIC), resulted in a resistance frequency of $8x10^{-9}$. This data suggests that a low resistance development against the novel antibiotic can be expected (Imai *et al.*, 2019). DAR A is a bicyclic heptapeptide with the amino acid sequence W^1-N^2-W^3-S^4-K^5-S^6-F^7, including an ether bond between W^1 and W^3 and a carbon-carbon bond between W^3 and K^5 (Figure 4A) (Imai *et al.*, 2019).

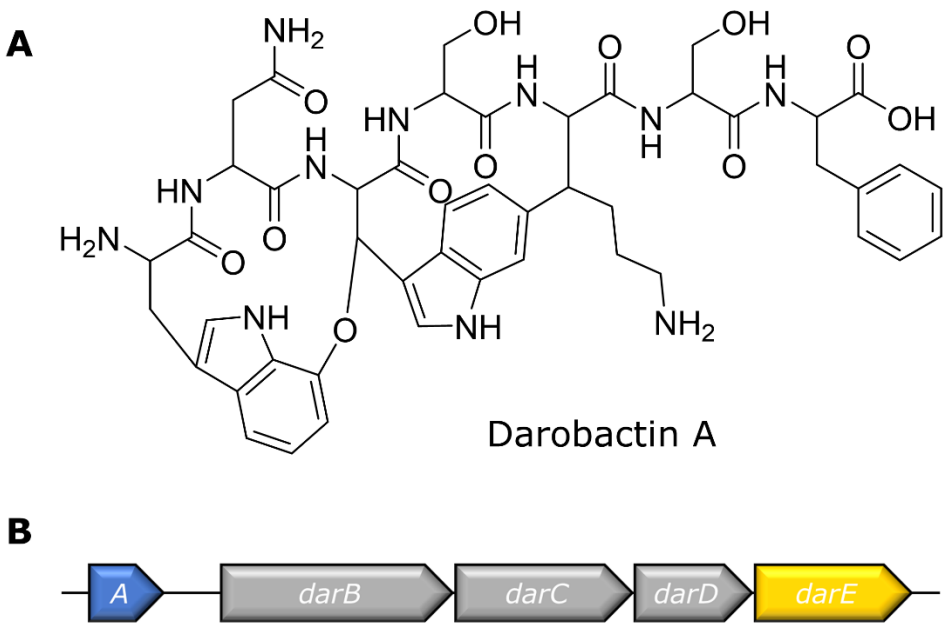

Figure 4: Darobactin A (DAR A) is a ribosomally synthesized and post-translationally modified heptapeptide. A: Structure of DAR A. **B:** BGC of DAR A.

The BGC consists of five genes: *darA*, *darB*, *darC*, *darD* and *darE* (Figure 4B). *DarA* encodes for the DAR A precursor peptide, *darBCD* encode for subunits of an ABC-transporter and *darE* for a radical S-adenosylmethionine (SAM) enzyme (Imai *et al.*, 2019). This radical SAM enzyme catalyzes the formation of the ether and

carbon-carbon crosslinks in the linear peptide (Imai *et al.*, 2019; Nguyen *et al.*, 2022). However, unlike other radical SAM enzymes, that only install crosslinks within already existing functional groups, DarE post-translationally integrates an oxygen atom (Nguyen *et al.*, 2022). Initially, this oxygen was assumed to be derived from water, as there have been no reports of radical SAM enzymes functioning under aerobic conditions due to the oxygen sensitivity of the [4Fe-4S] cluster (Gao *et al.*, 2012; Guo *et al.*, 2022; Nguyen *et al.*, 2022). However, later studies by Nguyen *et al.* (2022) showed that molecular oxygen is used, suggesting that DarE is the first reported radical SAM oxygenase. It remains unclear which of the crosslinks is installed first, but studies to clarify the exact mechanism of DarE are ongoing (Nguyen *et al.*, 2022; Nguyen *et al.*, 2024).

As DarE is the only post-translationally modifying enzyme in the DAR A BGC, a DAR minimal BGC was defined by Wuisan *et al.* (2021). In heterologous expression studies the authors showed that only *darA* and *darE* are required for a successful heterologous expression in *E. coli (Wuisan et al., 2021)*.

Since DAR A appears to be a promising new compound, its discovery inspired many studies to search for more active derivatives. This has been achieved either by biosynthetic engineering driven approaches, by exchanging amino acids at several positions of the heptapeptide or by random library generation with a subsequent activity based high throughput screening. Studies have focused on the replacement of amino acids at positions N^2, S^4, K^5, S^6 and F^7. For position seven, aromatic amino acids such as tryptophan or the naturally occurring phenylalanine revealed to be the most promising candidates. Positions W^1 and W^3 were conserved in all studies, as otherwise the ring closures are not possible. The most promising candidates discovered in these studies are DAR B and DAR B9 (DAR D22), with DAR B performing better during *in vivo* studies (Böhringer *et al.*, 2021; Groß *et al.*, 2021; Marner *et al.*, 2023; Seyfert *et al.*, 2023b; Seyfert *et al.*, 2023a; Böhringer *et al.*, 2024). Elongation or truncation of the DAR core peptide did not lead to a successful production of novel derivatives (Böhringer *et al.*, 2024). Other studies used databases to search for alternative DAR producers by blasting *darA* or *darE* (Böhringer *et al.*, 2021; Groß *et al.*, 2021). These genome-mining approaches also revealed DAR BGCs with additional enzymes for post-translational modification of the heptapeptide (Groß *et al.*, 2021; Böhringer *et al.*, 2023).

1.6 Dynobactin

Screening databases for the sequence of *darE* also revealed another class of antibiotics called dynobactins (DYN). Computational tools were used to analyze the genomic neighborhood of the genes and rank them according to their potential to be a RiPP. The most promising strains were fermented, the culture broth was concentrated and tested against a set of Gram-negative bacteria. An extract of *Photorhabdus australis* was found to be active. The bacterium possesses an operon encoding for a xenorceptide derivative, an operon encoding for a DAR derivative and the DYN A operon (Zhang *et al.*, 2021; Miller *et al.*, 2022). MS-based screening identified DYN A as the active compound, which is a decapeptide with the sequence: W^1-N^2-S^3-N^4-V^5-H^6-S^7-Y^8-R^9-F^{10}. Similar to DAR, the structure of DYN A includes two ring closures (Figure 5), a carbon-carbon bond between W^1 and N^4, and an unusual nitrogen-carbon bond between the imidazole of H^6 and Y^8 (Imai *et al.*, 2019; Miller *et al.*, 2022).

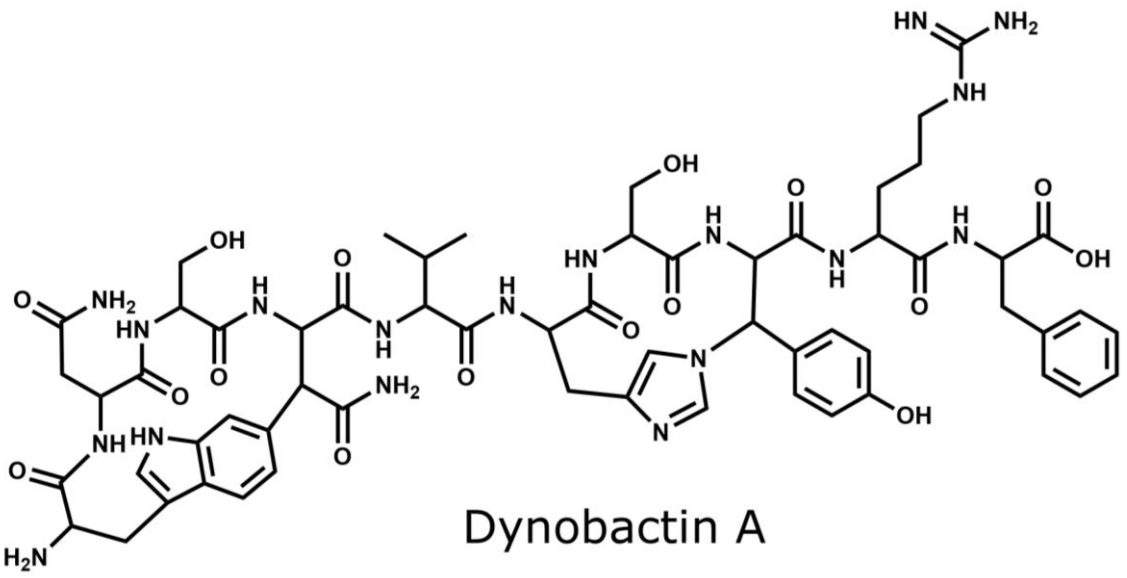

Figure 5: Structure of Dynobactin A.

The DYN A BGC consists of *dynA*, which encodes for the radical SAM, and *dynB*, which encodes for the precursor peptide (Miller *et al.*, 2022). Since there are only these two genes in the BGC, it was assumed that the two crosslinks are installed by *dynA*, which was later shown by Nguyen *et al.* (2024). Similar to DAR A, DYN A inhibits BamA, but the binding site is slightly different (Kaur *et al.*, 2021; Miller *et*

al., 2022). While the compound shows a higher activity during *in vitro* assays, DAR A is more potent in whole cell assays. These results suggest that the OM of the Gram-negative bacteria interferes more with DYN A than DAR A. This issue could be addressed in derivatization studies using DYN A as a lead structure for the optimization and discovery of novel BamA-targeting compounds (Miller *et al.*, 2022).

1.7 Other BamA inhibitors

DAR A was the first BamA inhibitor discovered, inducing and stabilizing the closed conformation of this OMP (Imai *et al.*, 2019; Haysom *et al.*, 2023). The later discovered DYN A has a similar BamA binding site and therefore shows an analogous mode of action (Miller *et al.*, 2022). BamA appears to be an interesting target, because it is located in the OM of Gram-negative bacteria (Tomasek and Kahne, 2021). Gram-negative bacteria possess this OM in addition to the inner membrane (Figure 6) (Silhavy *et al.*, 2010). The OM acts as an extra barrier for antibiotics that is not present in Gram-positive bacteria, making it more challenging to find Gram-negative active compounds (Nikaido, 2003; Storek *et al.*, 2024). This is mitigated by acting directly on targets located in the OM, as in the case of BamA. Furthermore, BamA is a conserved and essential target, which is involved in the folding and integration of OMPs. These OMPs have functions associated with cell division, nutrient transport, virulence, and cell wall synthesis or maintenance, and their disruption activates multiple stress response systems (Voulhoux *et al.*, 2003; Gerding *et al.*, 2007; Silhavy *et al.*, 2010; Typas *et al.*, 2010; Noinaj *et al.*, 2013; Qiao *et al.*, 2014; Okuda *et al.*, 2016; Tomasek and Kahne, 2021; Storek *et al.*, 2024).

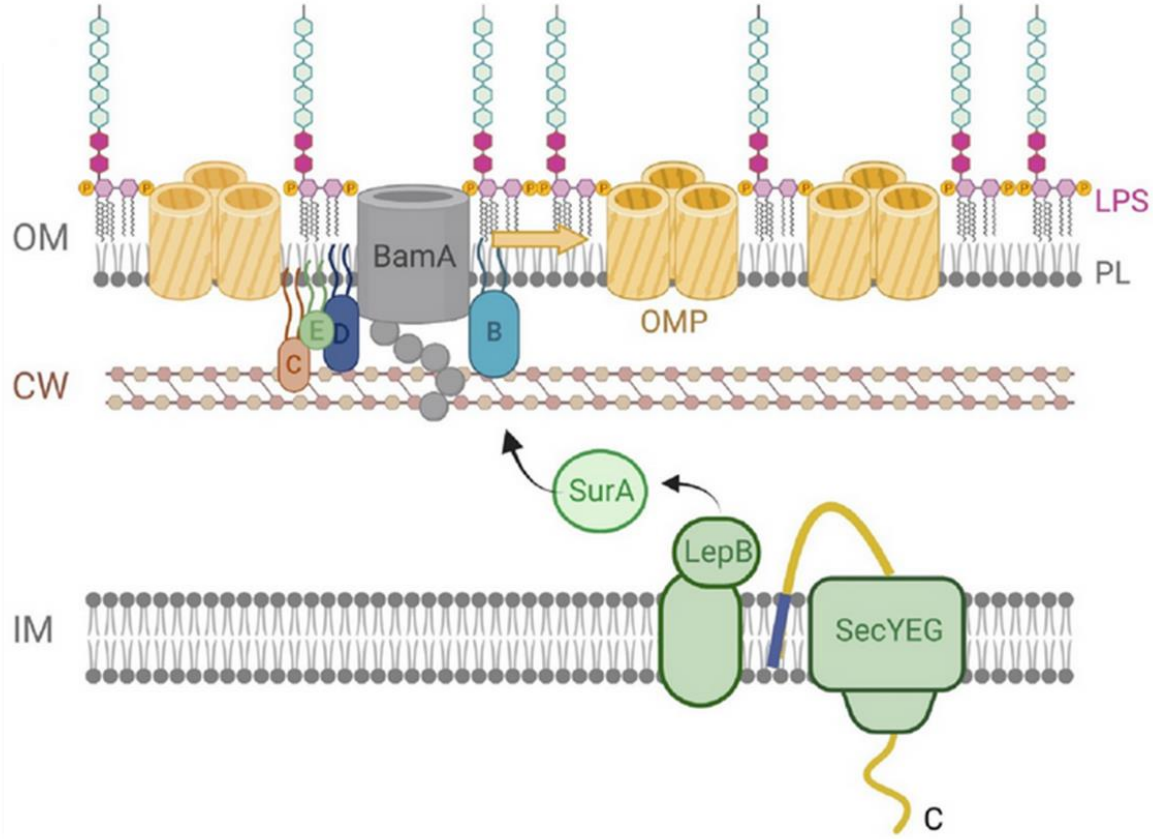

Figure 6: Illustration of the β-barrel assembly machinery (BAM) complex in Gram-negative bacteria. The graphic shows the inner membrane (IM) composed of phospholipids (PL, grey) and the outer membrane (OM) with PL and lipopolysaccharides (LPS, purple) on the outside. The periplasmatic space is located in between the IM and the OM, with a peptidoglycan cell wall (CW). The IM shows in green the processing enzymes for the transport of OM proteins into the periplasmatic space (Date and Wickner, 1981; Driessen *et al.*, 2001). SurA (light green), located in the periplasmatic space, delivers the OMPs to the BAM complex (Sklar *et al.*, 2007). BAM is located in the OM showing the different subunits: BamA (grey), BamB (cyan), BamC (orange), BamD (blue), BamE (green). Yellow barrels indicate β-barrel outer membrane proteins (OMP) (adapted from: Storek *et al.*, 2024).

As these properties make BamA such an interesting target, apart from DARs and DYN A, other substances with antibiotic activity that target BamA have been discovered. One class are BamA targeting antibodies (Storek *et al.*, 2018; Vij *et al.*, 2018). In a screening campaign, 3,000 antibodies were tested for their ability to bind to BamA, but only MAB1 showed antibiotic activity. The antibody is only active against *E. coli* as the binding region is not conserved. In studies with this antibody, decreased OMP biogenesis and OM permeabilization were observed, ultimately leading to cell death (Storek *et al.*, 2018). Another study observed the activation of a periplasmatic stress response, leading to the accumulation of unfolded OMPs, which can be toxic to Gram-negative bacteria (Mitchell and Silhavy, 2019).

Another class of compounds targeting BamA with a narrow species range are bacteriocins, which even inhibit the growth of species closely related to the producer (Riley and Wertz, 2002; Ghequire *et al.*, 2018; Matano *et al.*, 2021). Bacteriocins are peptides produced by bacteria with different modes of action, such as interfering with DNA, RNA or protein biosynthesis (Riley and Wertz, 2002). Examples of bacteriocins are the lectin-like bacteriocins produced by *Pseudomonas* or the bacteroidetocins produced by Bacteroidetes. The lectin-like bacteriocins inhibit BamA of other *Pseudomonas* species, while bacteroidetocins are active against various Bacteroidales species (Ghequire *et al.*, 2018; Matano *et al.*, 2021). The mode of action is still unknown, but during *in vitro* experiments the compounds induced cell envelope stress and morphological changes by BamA inhibition (Matano *et al.*, 2021).

More potent drug candidates that overcome the access issues associated with the antibodies and the narrow species spectrum ranges of the bacteriocins, are small molecule inhibitors, such as MRL-494 (Hart *et al.*, 2019; Storek *et al.*, 2024). The exact binding mechanism of MRL-494 is not fully understood, but it is known that the compound reduces OMP levels, thereby activating a periplasmatic stress response, leading to cell death by the accumulation of unfolded OMPs (Mitchell and Silhavy, 2019). Interestingly, the compound also kills the Gram-positive bacterium *Bacillus subtilis*. As an amphiphilic cationic peptide, it is proposed that MRL-494 acts similarly to antimicrobial peptides that non-specifically permeabilize membranes (Kundu, 2020). This would imply that the compound has two modes of action: the membrane-lytic mechanism observed in *B. subtilis* and the BamA targeting for Gram-negative bacteria (Wade *et al.*, 2022). The compound serves as a useful lead structure, but further optimization for Gram-positive/Gram-negative selectivity and potency is required (Storek *et al.*, 2024).

With the macrocyclic peptide PTB1-1, Sun *et al.* (2024) discovered a BamA inhibitor with a broader activity spectrum. In addition to *E. coli*, this compound is also active against *K. pneumoniae* and *A. baumannii.* No activity against non-fermenting Gram-negative bacteria was observed in their study. PTB1-1 appears to lock the lateral gate, preventing BamA from entering the lateral open state, resulting in reduced levels of OMPs. To discover the compound, a library of macrocyclic peptides consisting of both, canonical and non-canonical amino acids was screened against purified BamA and BAM complexes in a membrane-mimetic formulation. This initially led to the discovery of PTB1, which was then optimized

in a second screening approach to PTB1-1, this time against purified BamA only. The same study also led to the discovery of a second inhibitor, PTB2-1, which is only active against *E. coli*. PTB2-1 has a unique binding site, by binding deep into in the β-barrel lumen of BamA, it stabilizes the lateral open state. These two compounds are good examples of drug discovery by screening a library specifically against a target and show the potential of BamA inhibitors (Sun *et al.*, 2024).

However, not only can BamA be targeted directly, also the inhibition of the interaction between BamA and BamD, another part of the BAM complex, showed effects (Mori *et al.*, 2012; Hagan *et al.*, 2015). BamA and BamD interact directly in the cytoplasm and this interaction has been shown to be critical for the OMP folding (Ricci *et al.*, 2012; Sinnige *et al.*, 2015). In studies, short conserved regions of either BamD or BamA were expressed and resulted in increased permeability of the OM of the expression strain, leading to increased antibiotic unptake (Mori *et al.*, 2012; Hagan *et al.*, 2015). Although these small peptides lack drug-like properties and do not show antibiotic activity, this example demonstrates the suitability of the BamA-BamD protein-protein interaction as a drug target (Storek *et al.*, 2024).

A compound that inhibits the BamA-BamD interaction and has antibiotic activity by itself is IMB-H4. This compound was discovered by screening molecules using a BamA-BamD yeast two-hybrid system (Li *et al.*, 2020). By reducing the cytotoxicity and improving the potency of the compound, derivatives could become potent antibiotics (Storek *et al.*, 2024). However, they still have the major disadvantage of having to pass the OM, which is not the case for molecules that directly target BamA (Nikaido, 2003; Silhavy *et al.*, 2010; Storek *et al.*, 2024).

All of the compounds mentioned above have in common that they have a single target and therefore carry the risk that a single mutation is sufficient for the bacteria to develop resistance against these compounds (Storek *et al.*, 2024). For this reason, compound 8 was developed as a chimeric BamA inhibitor (Luther *et al.*, 2019). The compound consists of a peptidomimetic macrocycle that inhibits BamA and a polymyxin variant that targets lipid A of lipopolysaccharides (LPS). Both targets are located in the OM of Gram-negative bacteria and are essential (Trimble *et al.*, 2016; Tomasek and Kahne, 2021). Compound 8 appears to be active against difficult to treat bacteria such as *P. aeruginosa* and *A. Baumannii*, and was even active against strains that had already developed resistance against polymyxin (Luther *et al.*, 2019). Resistance development was also observed

against this chimeric compound, but it provides a good starting point for evaluating the potential of such compounds (Luther *et al.*, 2019; Storek *et al.*, 2024).
Overall, BamA is a promising new drug target with the potential to find more Gram-negative active compounds than the those already discovered, given the growing field of biotechnology (Storek *et al.*, 2024). Although BamA is conserved in all Gram-negative bacteria, the sequence is not highly conserved, making it difficult to find a BamA inhibitor with a broad spectrum of activity. The only highly conserved region is the lateral gate, which is targeted by DARs and DYN A (Imai *et al.*, 2019; Miller *et al.*, 2022; Storek *et al.*, 2024). Some promising drug candidates have already been discovered, but still need to be optimized for potency and specificity (Storek *et al.*, 2024).

1.8 Halogenases

One option for optimizing NPs is halogenation. Halogenation of a compound can have a significant effect on its activity and bioavailability (Neumann *et al.*, 2008). Examples are vancomycin or salinosporamide A, which are not active without their respective chlorine substituents (Harris *et al.*, 1985; Groll *et al.*, 2006). Also for DAR A a halogenated derivative was discovered. This halogenation is incorporated by DarH, which is a tryptophan halogenase (Böhringer *et al.*, 2023). In general, halogenases incorporate halogen atoms into NPs. By 2023, approximately 8,400 halogenated NPs had been reported (Gribble, 2024). The most prevalent halogenation in nature is chlorination, followed by bromination (Neumann *et al.*, 2008). The majority of marine organisms produce brominated compounds, whereas chlorination is preferred by terrestrial organisms (van Pée, 1996). Iodination and fluorination are rare in nature, and fluorination in particular is used in semi-synthetic derivatizations of NPs (Neumann *et al.*, 2008; Piccionello *et al.*, 2019). Since halogenated NPs can be very complex in their structures, the halogenases can use diverse substrates, but they can be classified according to their mechanism (van Pée, 1996; Ludewig *et al.*, 2020).
There are nucleophilic halogenases such as the 5’-fluoro-5’-deoxyadenosine synthase, which catalyzes the first step of fluoroacetate and 4-fluoro-L-threonine biosynthesis by mediating the nucleophilic attack of fluoride on S-adenosyl-L-methionine (Sanada *et al.*, 1986; Dong *et al.*, 2004). A very similar mechanism is

used by the halogenase that catalyzes the chlorination of salinosporamide A (Eustáquio *et al.*, 2008).

Radical halogenases are non-haem-iron α-ketoglutarate-dependent enzymes which halogenate unactivated aliphatic carbon centers (Ludewig *et al.*, 2020). An alkyl radical reacts with a halide to form an alkyl halide. In the case of syringomycin E, the methyl group of the L-threonine is chlorinated (Vaillancourt *et al.*, 2005).

Electrophilic halogenases in general halogenate electron-rich carbon centers (Neumann *et al.*, 2008). They are divided into two major groups, the haloperoxidases (HPOs) and the flavin-dependent halogenases (FDHs). The HPOs can be further subdivided into the haem-iron haloperoxidases and the vanadium-dependent haloperoxidases (V-HPOs). The reaction mechanism of both enzyme types is very similar, producing free hypohalous acid, which reacts with the substrate. In the case of the haem-iron haloperoxidases, the resting state haem reacts with H_2O_2, to form an intermediate capable of oxidizing the halide, whereas in V-HPOs a peroxovanadate intermediate catalyzes the oxidation (Ludewig *et al.*, 2020). The first characterized haem-iron haloperoxidase is called chloroperoxidase, which dichlorinates an activated carbon in caldariomycin (Hager *et al.*, 1966). V-HPOs are believed to catalyze, as vanadium-dependent bromoperoxidases, the majority of halogenations in marine organisms and they are abundant in marine seaweeds (Butler and Carter-Franklin, 2004). In contrast, vanadium-dependent chloroperoxidases are rare, occurring only in terrestrial fungi and two bacterial species involved in the biosynthesis of napyradiomycin (Winter *et al.*, 2007).

FDHs can act on free or carrier-bound substrates, for example catalyzing the chlorination of the precursor of the enediyne antibiotic C-1027 while bound to a peptidyl carrier protein during biosynthesis (Lin *et al.*, 2007; Ludewig *et al.*, 2020). The first described FDH acting on a free substrate was described in 2000 by Keller *et al.* (2000). PrnA catalyzes the chlorination of tryptophan during the biosynthesis of pyrrolnitrin (Keller *et al.*, 2000). Since then, many other members of the halogenase family have been discovered, such as RebH (Figure 7), which is involved in the biosynthesis of rebeccamycin (Yeh *et al.*, 2005; Neumann *et al.*, 2008). Both PrnA and RebH halogenate tryptophan at the C-7 position (Keller *et al.*, 2000; Yeh *et al.*, 2005). In contrast, FDHs involved in the biosynthesis of pyrroindomycin and thienodolin halogenate at position 5 and 6, demonstrating the

regioselectivity of these enzymes (van Pée and Zehner, 2003; Zehner *et al.*, 2005; Neumann *et al.*, 2008).

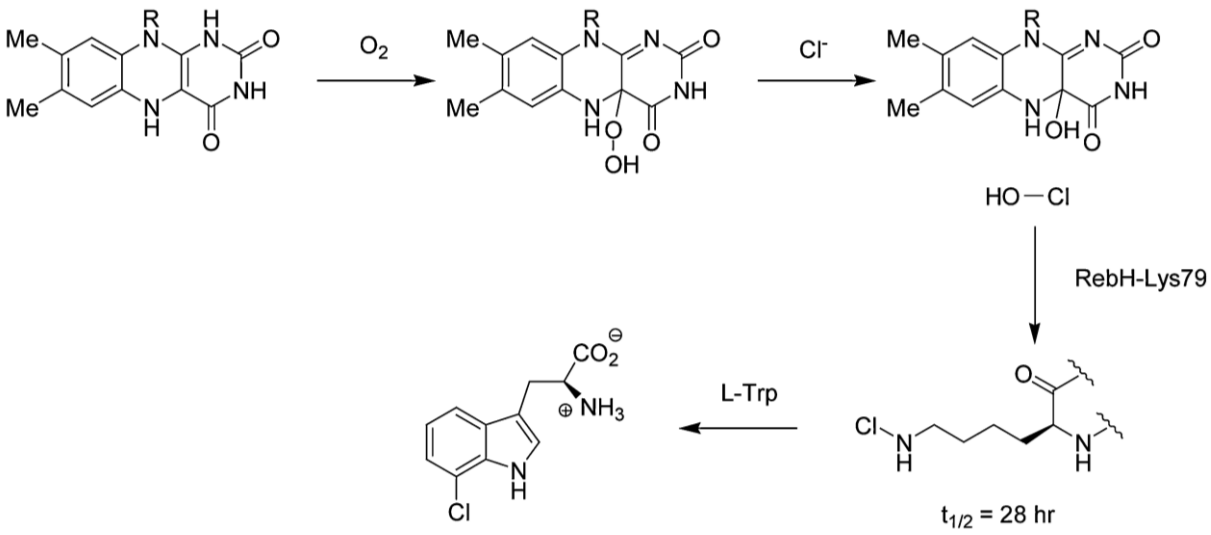

Figure 7: Reaction mechanism of the halogenation of tryptophan by RebH during rebeccamycin biosynthesis. Hypochlorous acid is formed by flavin and a lysine chloramine intermediate is formed by the enzyme, before the halogen is transferred to tryptophan (adapted from: Neumann *et al.*, 2008).

The reaction mechanism of FDHs (Figure 7) involves a hypohalite, similar to the other groups of the electrophilic halogenases, but molecular oxygen is used as the oxidant (Keller *et al.*, 2000; Neumann *et al.*, 2008). The reaction depends on the reduced flavin cofactor, oxygen, the halogenide (e.g. chloride) and a NAD(P)H-dependent flavin reductase, which subsequently reduces the oxidized cofactor (Zehner *et al.*, 2005; Neumann *et al.*, 2008). In the first step, the reduced flavin cofactor is oxidized by molecular oxygen to the corresponding hydroperoxide product (Neumann *et al.*, 2008). The distal oxygen of this hydroperoxide group is attacked by chloride to form hypochlorous acid, while the flavin cofactor is converted to the corresponding hydroxy derivative and subsequently regenerated by the NAD(P)H-dependent flavin reductase (Yeh *et al.*, 2006; Neumann *et al.*, 2008). A lysine, which is located in a conserved region of the FDHs, reacts with the hypochlorous acid to form a lysine chloramine species with a half-life of approximately 28 hours (Nightingale *et al.*, 2000; Yeh *et al.*, 2007). This species is less reactive than hypochlorous acid and therefore more selective for the final halogen transfer to tryptophan (Nightingale *et al.*, 2000). Conserved sequence motifs of FDHs and non-haem-iron halogenases have been used in large screenings for new NPs (Hornung *et al.*, 2007). For example, the antibiotic class of kutznerides

from the actinomycete *Kutzneria* sp. 744 was discovered using degenerated PCR probes (Broberg *et al.*, 2006; Pohanka *et al.*, 2006).

Although the mechanism of a relatively large number of halogenases has been elucidated, there are still some enzymes for which it remains unknown (Neumann *et al.*, 2008). For example, the halogenases in the NP family of the jamaicamide catalyze unusual alkenyl and alkynyl halogenations (Edwards *et al.*, 2004). Others use novel substrates, as in hectochlorin, which contains a dichlorinated methylene moiety (Ramaswamy *et al.*, 2007). As halogenations can have significant effects on the properties of a compound, the use of halogenases from other biosynthetic pathways to engineer NPs could improve their efficacy or optimize their pharmacokinetics. Therefore, it is important to understand the halogenation mechanism of these enzymes in more detail and to gain knowledge of the substrate specificity of the different halogenases (Neumann *et al.*, 2008).

2. Chapter 1: Discovery of new darobactin A derivatives by genome mining

DARs have great potential as antibiotics due to their activity against several Gram-negative pathogens (Imai *et al.*, 2019; Groß *et al.*, 2021; Marner *et al.*, 2023; Seyfert *et al.*, 2023b; Seyfert *et al.*, 2023a; Böhringer *et al.*, 2024). Therefore, the aim of this study was to identify more potent DAR derivatives by screening the amino acid sequence of DarE in databases. This revealed the DAR BGC in *P. luteoviolacea* H33 with two additional genes of unknown function, *darG* and *darH*. Fermentation of the original producer strain led to the discovery of three new DAR derivatives: bromodarobactin A (Br-DAR A), dehydrodarobactin A (DH-DAR A) and dehydrobromodarobactin A (DH-Br-DAR A). While the mechanism of the double bond formation and the function of DarG remain unknown, DarH was identified as a novel halogenase. This halogenase is responsible for the halogenation of the C-8 position of W^1 in DAR A. To fully elucidate the mechanism of this post-translational modification, *darH* was heterologously expressed in *E. coli* together with the DAR minimal BGC and the culture supernatant was analyzed by HRMS/MS based methods. Furthermore, *darH* attached to a His-tag was heterologously expressed to purify the enzyme for *in vitro* studies. Substrate specificity was tested by conducting *in vitro* studies with DAR B and the linear DAR heptapeptide, of which only the former could be halogenated. It was concluded that the halogenation is the last step in the maturation of Br-DAR A and takes place after the formation of the two rings. Furthermore, when testing different halogens in these *in vitro* studies, tryptophan could only be brominated or iodinated, but not fluorinated or chlorinated. Computational analysis of DarH revealed that the enzyme has a FAD- and NAD(P)-binding site as well as a unique C-terminal region. This C-terminal region is proposed to be involved in the binding and correct positioning of DARs in the active site of the enzyme. This novel C-terminal fold suggests that DarH belongs to a new class of flavin-dependent halogenases (Böhringer *et al.*, 2023; Kramer *et al.*, 2023).

Manuscript 1: Genome- and metabolome-guided discovery of marine BamA inhibitors revealed a dedicated darobactin halogenase

Status: published on 09/21/2023

Author's contributions: study design, heterologous expression experiments, protein purification, *in vitro* assay development, data analysis, manuscript writing, graphical abstract design, figure design SI.

Cell Chemical Biology

Genome- and metabolome-guided discovery of marine BamA inhibitors revealed a dedicated darobactin halogenase

Graphical abstract

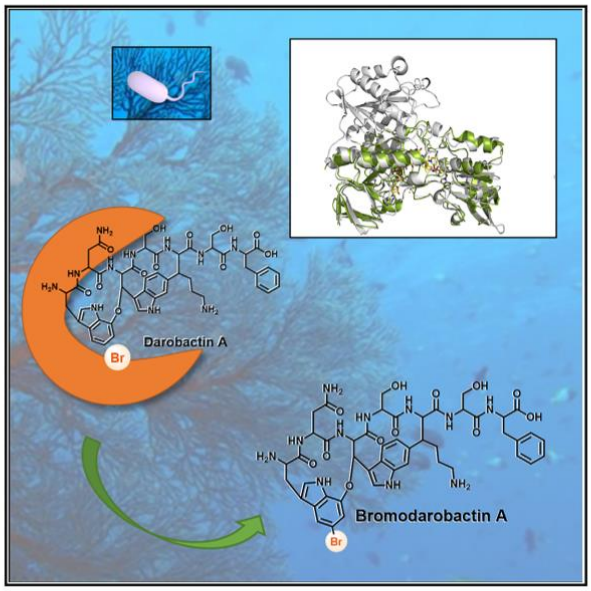

Authors

Nils Böhringer, Jil-Christine Kramer, Eugenio de la Mora, ..., Yvain Nicolet, Ute Mettal, Till F. Schäberle

Correspondence

Ute.Mettal@chemie.uni-giessen.de (U.M.), Till.F.Schaeberle@agrar.uni-giessen.de (T.F.S.)

In brief

Böhringer et al. identified brominated darobactin derivatives from *Pseudoalteromonas luteoviolacea* strains. The halogenase involved in the process was of a new type. The bromine substituent leads to higher activity against Gram-negative bacteria and altered physico-chemical properties. It paves the way for further modification.

Highlights

- Brominated and dehydrated darobactin derivates from *P. luteoviolacea* are identified
- Derivatives are active against multidrug-resistant Gram-negative bacteria
- They show altered physico-chemical properties (compared to source molecules)
- A new class of FAD-dependent halogenases harbors a novel fold and catalyzes bromination

Böhringer et al., 2023, Cell Chemical Biology *30*, 1–10
September 21, 2023
https://doi.org/10.1016/j.chembiol.2023.06.011

CellPress

Please cite this article in press as: Böhringer et al., Genome- and metabolome-guided discovery of marine BamA inhibitors revealed a dedicated darobactin halogenase, Cell Chemical Biology (2023), https://doi.org/10.1016/j.chembiol.2023.06.011

Cell Chemical Biology

CellPress

Article

Genome- and metabolome-guided discovery of marine BamA inhibitors revealed a dedicated darobactin halogenase

Nils Böhringer,[1,6,7] Jil-Christine Kramer,[1,7] Eugenio de la Mora,[2] Leo Padva,[1,3,8] Zerlina G. Wuisan,[1] Yang Liu,[1] Michael Kurz,[4] Michael Marner,[3] Hai Nguyen,[5] Patricia Amara,[2] Kenichi Yokoyama,[5] Yvain Nicolet,[2] Ute Mettal,[1,*] and Till F. Schäberle[1,3,6,9,*]

[1]Institute for Insect Biotechnology, Division for Natural Product Research, Justus-Liebig-University Giessen, Ohlebergsweg 12, 35392 Giessen, Germany
[2]University Grenoble Alpes, CEA, CNRS, IBS, Metalloproteins Unit, 38000 Grenoble, France
[3]Natural Product Department, Fraunhofer-Institute for Molecular Biology and Applied Ecology (IME), Ohlebergsweg 12, 35392 Giessen, Germany
[4]Research & Development, Integrated Drug Discovery, Sanofi-Aventis Deutschland GmbH, Industriepark Höchst, Bldg. G 849, 65926 Frankfurt am Main, Germany
[5]Duke University Medical Center, Department of Biochemistry, Duke University, 307 Research Drive, Rm 233 Nanaline H. Duke Building, Durham, NC 27710, USA
[6]German Center for Infection Research (DZIF), Partner Site Giessen-Marburg-Langen, Ohlebergsweg 12, 35392 Giessen, Germany
[7]These authors contributed equally
[8]Present address: Institute of Pharmaceutical Biology, University of Bonn, 53115 Bonn, Germany
[9]Lead contact
*Correspondence: Ute.Mettal@chemie.uni-giessen.de (U.M.), Till.F.Schaeberle@agrar.uni-giessen.de (T.F.S.)
https://doi.org/10.1016/j.chembiol.2023.06.011

SUMMARY

Darobactins represent a class of ribosomally synthesized and post-translationally modified peptide (RiPP) antibiotics featuring a rare bicyclic structure. They target the Bam-complex of Gram-negative bacteria and exhibit *in vivo* activity against drug-resistant pathogens. First isolated from *Photorhabdus* species, the corresponding biosynthetic gene clusters (BGCs) are widespread among γ-proteobacteria, including the genera *Vibrio*, *Yersinia*, and *Pseudoalteromonas* (*P.*). While the organization of the BGC core is highly conserved, a small subset of *Pseudoalteromonas* carries an extended BGC with additional genes. Here, we report the identification of brominated and dehydrated darobactin derivatives from *P. luteoviolacea* strains. The marine derivatives are active against multidrug-resistant (MDR) Gram-negative bacteria and showed solubility and plasma protein binding ability different from darobactin A, rendering it more active than darobactin A. The halogenation reaction is catalyzed by DarH, a new class of flavin-dependent halogenases with a novel fold.

INTRODUCTION

Darobactin A (**1**) was the first member from a class of novel ribosomally synthesized and post-translationally modified peptides (RiPPs), specifically bicyclic heptapeptides produced by various members of the *Photorhabdus* bacterial genus with prominent anti-Gram-negative activity.[1] Clinically relevant ESKAPE strains were inhibited in their growth (e.g., *Escherichia coli* AR350 (*mcr-1*) and *Klebsiella pneumoniae* ATCC BAA-1705 (KPC) with MICs of 2 and 4 μg/mL, respectively) *in vitro* by inhibition of the outer membrane chaperone BamA. In contrast, Gram-positive bacteria and the main group of Gram-negative gut symbionts (e.g., *Bacteroides fragilis* ATCC 25285) were not affected due to the absence or evolutionary high divergence of the target BamA architecture. In addition, *in vivo* activity was proven against *E. coli*, *K. pneumoniae*, and *Pseudomonas aeruginosa* in mouse infection models. The corresponding biosynthesis was linked to the five genes *darA-darE*. These translate into a precursor peptide, an ABC transporter system, and a radical SAM (rSAM) enzyme, whereby the latter is modifying the precursor peptide by catalyzing the intramolecular ring closure, resulting in two fused macrocycles and hence leading to a rigid heptapeptide structure. By heterologous expression, we could show that only the precursor peptide- and rSAM-encoding genes are essential for darobactin production.[2]

In silico analysis of available genome data revealed orthologs of the darobactin biosynthetic gene cluster (BGC) in further γ-proteobacteria lineages. While a majority of clusters were identified in species of the genera *Yersinia* and *Photorhabdus*, BGCs encoding for precursor peptides carrying a core amino acid composition identical to the darobactin A heptapeptide were also detected in genera that are predominantly found in

Please cite this article in press as: Böhringer et al., Genome- and metabolome-guided discovery of marine BamA inhibitors revealed a dedicated darobactin halogenase, Cell Chemical Biology (2023), https://doi.org/10.1016/j.chembiol.2023.06.011

Figure 1. Conserved organization of the darobactin BGC in genomes deposited in NCBI

Blue: *darA* encoding the precursor peptide, yellow: radical SAM enzyme, green: halogenase *darH*, and gray: others (e.g., transport-related and peptidase). The BGCs found in *Vibrio* and *Pseudoalteromonas* strains harbor additional open reading frames. *darH* is present in the strains *P. luteoviolaceae* H33, H33S, JG1, and sp. NC201.

marine habitats, i.e., several *Vibrio* and few *Pseudoalteromonas* strains. Bacteria of all these genera have in common that they are mostly associated with higher organisms. Furthermore, they represent talented natural product producers, biosynthesizing a plethora of (especially brominated) natural products, among others, the first antibiotic identified from the marine environment pentabromopseudilin,[3] and the bromoalterochromides.[4–6]

In this study, we investigated the closely related strains *Pseudoalteromonas luteoviolacea* H33 and H33S in which further genes are co-localized adjacent to the reported *darA-E* darobactin BGC core. These additional genes expand the chemical realm of darobactins beyond the alteration of amino acids. Three new analogs of **1** were identified, initially characterized, and the biosynthesis of the halogenated variants (**2** and **4**) was elucidated by *in vitro* and *in vivo* experiments. AlphaFold[7] modeling predicted the halogenating enzyme as a new class of flavin-dependent halogenases harboring a novel fold.

RESULTS AND DISCUSSION

Identification of putative darobactin producers and corresponding biosynthetic gene clusters

Screening public sequence databases with the DarE amino acid sequence as query revealed several BGCs consisting of the *darA-E* core, which we described earlier,[1,2] in several γ-proteobacteria (Figure 1).

However, the BGCs of the marine bacteria differ slightly: In *Vibrio* strains, the same organization as in the *Enterobacteriaceae* was observed, yet, an additional gene (*darG*, annotated as transporter encoding) is located downstream of the *darE* ortholog (Figure 1). A few *Pseudoalteromonas* strains harbor *darF* situated between *darA* and *darB* and the two genes *darG* and *darH* downstream of *darE*. The *darH* gene is specific for four strains (i.e., *P. luteoviolacea* H33, H33S, JG1, and *Pseudoalteromonas* sp. NC201, Table S1). It encodes for a putative protein annotated as putative FAD-dependent oxidoreductase. To avoid confusion, we adapt and expand the nomenclature introduced by Groβ and co-workers, who heterologously expressed *darF* and identified it as a darobactin protease that might contribute to self-resistance.[8] However, the halogenase *darH* was not described yet and no corresponding compounds have been identified so far.

Identification of darobactin derivatives from *Pseudoalteromonas luteoviolacea*

To test whether *P. luteoviolacea* H33 and H33S are naturally producing darobactin A and/or derivatives thereof, these strains were fermented in ten different media and after removal of the cells, a concentrate of the culture broth was prepared. Measurement of these aqueous extracts by UPLC-HRMS/MS and subsequent GNPS molecular networking[9] initially allowed the identification of a single node with an *m/z* consistent with the double-charged darobactin A ion in all extracts of both strains. Based on this observation, we further investigated the extracts using GNPS molecular networking by relaxing the settings to identify putative analogs. Thereby, an ion was identified (523.663 *m/z*) that showed structural similarity to darobactin A and did match the third isotope peak of an ion with an *m/z* of 522.6647 (Data S1). The mass difference to darobactin A (Δ 79.91 Da) supported a brominated derivative. Comparison of the measured and simulated isotopic ion patterns matched with the formula $C_{47}H_{54}N_{11}O_{12}Br$ $[M+2H]^{2+}$ (Figure S1). Furthermore, analysis of the UPLC-HRMS data revealed two peaks in the extracted ion chromatogram (EIC), with one of them corresponding to darobactin A ($C_{47}H_{55}N_{11}O_{12}$ $[M+2H]^{2+}$). The second peak, eluting after darobactin A on a reversed-phase column, derived from a double-charged ion with 482.7014 *m/z*. Being 2 Da lighter than darobactin A, it precisely fits the sum formula $C_{47}H_{53}N_{11}O_{12}$ (Δ 0.6 ppm). Analogously, the EIC of 523.663 *m/z* showed two peaks (Figures 2 and S6).

Both peaks in the EIC of $C_{47}H_{54}N_{11}O_{12}Br$ $[M+2H]^{2+}$ displayed the characteristic bromine isotope pattern. Again, the 2 Da mass difference and retention time shift indicated the presence of a double bond resulting from the formal loss of H_2. Comparison of the fragmentation patterns of the ions with 482.7014 *m/z*, 522.6647 *m/z*, and 521.6565 *m/z* corroborated their structural relation to darobactin A (for details see supplemental information and Figures S2–S5). Derivatives containing either halogens other than Br, or multiple halogenations of the darobactin backbone, were not detected. We propose to name the here-identified derivatives bromodarobactin A (**2**, $C_{47}H_{54}N_{11}O_{12}Br$), dehydrobromodarobactin A (**4**, $C_{47}H_{52}N_{11}O_{12}Br$), and dehydrodarobactin A (**3**, $C_{47}H_{53}N_{11}O_{12}$), respectively.

Structure elucidation

HRMS/MS fragmentation of both, **1** and **3** (Figures S2 and S4), yielded the same signature ions: N-terminal b_1^* (186.0550 *m/z*), a_1 (175.0866 *m/z*), and hydroxyindolylethanylium ions (160.0757 *m/z*) from W^1 as well as C-terminal y_1 (F^7) with 166.0863 *m/z* and y_2 (S^6-F^7) 253.1183 *m/z*. Furthermore, fragmentation of **1** showed y_5 (650.2933 *m/z*) and the internal cleavage ion N^2-W^3-S^4-K^5-S^6 (538.2045 *m/z*), which were shifted to 648.2776 *m/z* and 536.1888 *m/z*, respectively for the dehydro variant **3**. However, neither the characteristic 398.1823 *m/z* nor a dehydrogenated fragment could be detected. This indicated the double bond to be located on the W^3-S^4-K^5 segment. Fragmentation of **2** (Figure S3) yielded the C-terminal y_1, y_2, y_5, and the characteristic internal cleavage ions (e.g., N^2-W^3-S^4-K^5) of **1**. In contrast, the characteristic fragments corresponding to the N-terminus were shifted, revealing the presence of fragments congruent with b_1^* + ^{79}Br (263.9655 *m/z*), a ^{79}Br-bromohydroxyindolylethanylium ion (237.9862 *m/z*), and a corresponding b_5^* + ^{79}Br ion with 775.1834 *m/z*, all showing the Br-specific isotopic pattern. This indicated the bromination to be located at W^1, likely at the aromatic part of the indole moiety. Fragmentation of **4** (Figure S5) consequently showed a combination of the

Please cite this article in press as: Böhringer et al., Genome- and metabolome-guided discovery of marine BamA inhibitors revealed a dedicated darobactin halogenase, Cell Chemical Biology (2023), https://doi.org/10.1016/j.chembiol.2023.06.011

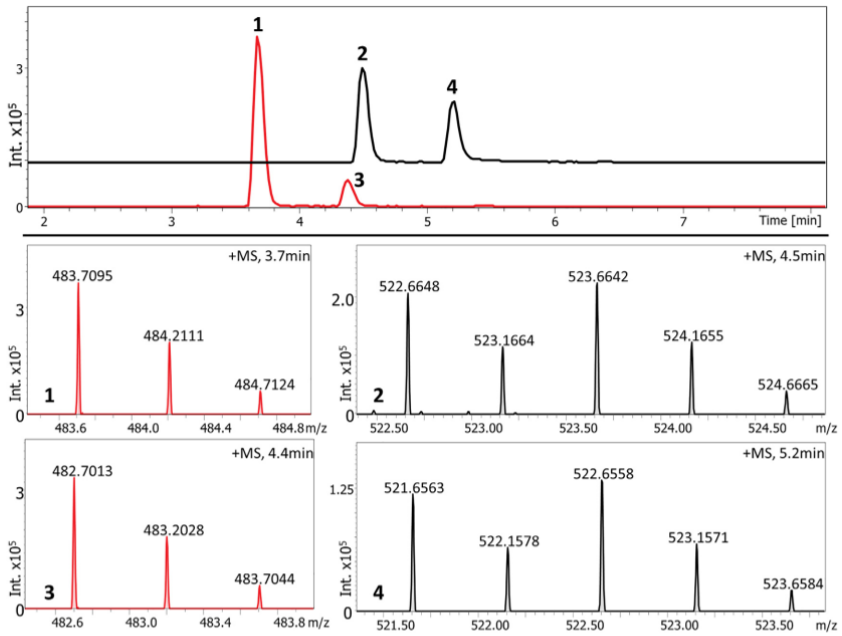

Figure 2. UPLC-HRMS analysis of a *P. luteoviolaceae* extract

Extracted ion chromatograms of **1** ($C_{47}H_{55}N_{11}O_{12}$ $[M+2H]^{2+}$ ±0.05, red) and **2** ($C_{47}H_{54}N_{11}O_{12}Br$ $[M+2H]^{2+}$ ±0.05, black) as well as the respective mass spectra of **1** (red peak 1), **3** (red peak 2), **2** (black peak 1), and **4** (black peak 2). All Δ m/z ≤ 1.15 ppm.

brominated *N*-terminal section of **2** and the −2 Da shifted core fragments.

To determine the position of the bromine and the double bond, NMR experiments were performed. However, only low sample amounts were obtained from all fermentation approaches and proved structure elucidation of the derivatives challenging. Especially compound supply of the dehydro variants **3** (^{1}H spectrum provided in Figures S81 and S82) and **4** was limited, which might be related to their presumed inherent instability. The position of the double bond was determined based on the obtained COSY (Figure S83), HSQC (Figure S84), and ROESY (Figure S85) data (outlined in the supplemental information), which identified the structural fragment *trans*-4,5-dehydrolysine (Figure 3, top).

In contrast to **1**, measurement in D_2O did not result in well-resolved spectra for bromodarobactin A (**2**) and dehydrobromodarobactin A (**4**). Hence, DMSO-d_6 was used as an alternative solvent for the presumably more hydrophobic brominated derivatives. Yet, **4** displayed only limited solubility in DMSO-d_6, thus further complicating NMR measurement. Consequently, while for **2** ^{1}H (Figures S37–S45), COSY (Figures S46–S56), TOCSY (Figures S57–S64), NOESY (Figures S65–S67), ROESY (Figures S68–S71), and HSQC (Figures S72–S80) spectra could be obtained, **4** only yielded ^{1}H (Figures S86–S89) and COSY (Figures S90 and S91) spectra. Due to the lack of HMBC data, comparison with darobactin A (**1**) was an important cornerstone for the structural assignment of the marine darobactin derivatives. So far, spectral data for **1** had only been reported in water/D_2O-based solvent systems,[1] so that spectra (^{1}H (Figures S16–S19), COSY (Figures S20–S23), TOCSY (Figures S24–S27), NOESY (Figures S28–S30), HSQC (Figures S31–S33), and HMBC (Figures S34–S36)) of **1** had to be re-measured in DMSO-d_6 to enable such comparison. In contrast to compounds **2** and **4**, NMR data of derivative **3** were obtained by measurement in a D_2O/MeCN-d_3 (2:1) solvent mixture.

The structural assignment of bromodarobactin A (**2**), given in Table S3 as well as Figures S14 and S15, is a result of the obtained homonuclear correlations (COSY, TOCSY, NOESY, and ROESY) in combination with a comparison of the obtained ^{1}H and HSQC spectra to the corresponding spectra of **1**.

The most significant difference between the ^{1}H-NMR spectra of bromodarobactin A (**2**) and darobactin A (**1**) is the observed downfield shift for the indole NH signal of the N-terminal tryptophan residue for the brominated derivative. The COSY correlation between the shifted NH proton (NH-4, δ_H = 11.32 ppm; (Figures S47, S53, S54, and S56) and the multiplet at δ_H = 7.27 ppm corresponding to H-4 (as determined by comparison of the HSQC spectra) allowed us to infer that indeed the indole NH of the N-terminal tryptophan is influenced by the bromine atom. In addition, the second indole NH signal (NH-19, δ_H = 11.08 ppm), which was almost identical to the corresponding

Please cite this article in press as: Böhringer et al., Genome- and metabolome-guided discovery of marine BamA inhibitors revealed a dedicated darobactin halogenase, Cell Chemical Biology (2023), https://doi.org/10.1016/j.chembiol.2023.06.011

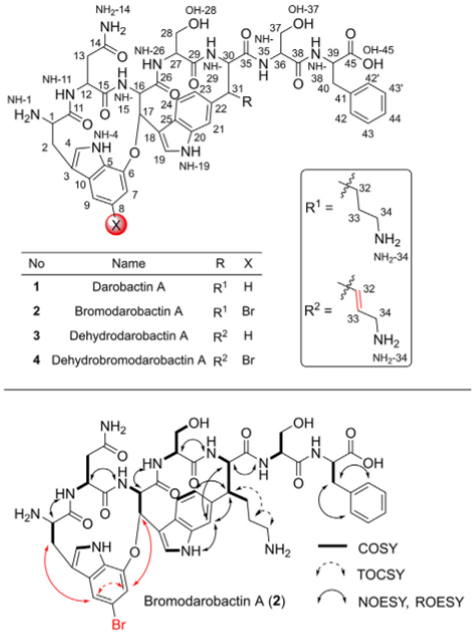

Figure 3. Chemical structures and NMR correlations of darobactin derivatives

Top: Molecular structure of naturally occurring darobactin derivatives. Darobactin A as well as halogenated and dehydrogenated variants are displayed. Bottom: Key correlations for the structure elucidation of bromodarobactin A. The most important correlations with respect to the position of the bromine atom are highlighted in red.

signal of **1**, showed a COSY correlation to a CH signal (δ_H = 7.86 ppm) which was unambiguously identified as H-19. Hence, bromination took place on W[1].

Even though the indole NH NMR signal exhibits a significant shift upon bromination, the observed COSY coupling of H-4 to NH-4 precludes bromine attachment to C-4, leaving C-7 to C-9 as the only possible sites. Inspection of the aromatic region of the HSQC spectrum showed two distinct peaks at δ_C = 109.2 and 114.1 ppm, which were assigned to C-7 and C-9, respectively. Based upon the HSQC correlation of C-9 (δ_C = 114.1 ppm) to the corresponding proton signal at δ_H = 7.04 ppm, it is apparent that H-9 exhibits a singlet structure. Such a singlet for H-9 should only be observed, if the bromine atom occupies the meta-position relative to the oxygen atom of the ether bridge. Likewise, the signal for H-7 is expected to be a singlet in case the bromine atom resides on C-8. The singlet structure of H-7 can still be recognized among the aromatic proton signals and the TOCSY spectrum displays a correlation between the singlet signals of H-9 and H-7 (Figure S63). The meta-substitution pattern is corroborated by the observed NOESY correlations between H-2 and H-9 as well as between H-7 and H-17.

Biosynthesis of bromodarobactin A

To verify that the *in silico* predicted BGC corresponds to the biosynthesis of darobactin A (**1**) and marine derivatives thereof, it was aimed to heterologously express the compounds in a genetically accessible strain. This would also allow an in-depth investigation of the BGC. Hence, codon-optimized $darA_{Pse}$ and $darE_{Pse}$ (the subscript $_{Pse}$ indicates the origin of the genes from *P. luteoviolacea* H33) were heterologously expressed in *E. coli*. However, applying the same setup as was used before for *Photorhabdus*-derived genes,[2] no production of any analog was observed. Therefore, in addition to pLP02 (harboring $darA_{Pse}$ and $darE_{Pse}$), the co-expression of different chaperones was tested. Indeed, a condition using pLP02 in combination with the GroEL chaperones[10] resulted in low, but detectable darobactin A (**1**) expression. This verified, as shown before with *Photorhabdus*-derived genes, that solely $darA_{Pse}$ and $darE_{Pse}$ are sufficient to produce **1**.

Since attempts to genetically modify the *P. luteoviolacea* H33(S) wild-type strains failed, in the next step, we attempted heterologous production of bromodarobactin A (**2**) in *E. coli*. Therefore, $darH_{Pse}$ (annotated as FAD-dependent oxidoreductase) was added to constructs carrying either *Photorhabdus* or *Pseudoalteromonas darA* + *darE*. Production was only observed using suitable conditions, e.g., lowered incubation temperature and co-expression of the GroEL chaperone, thus enabling detection of **1** and **2**. By replacing KBr in the medium with KI, KF, and KCl, we were also able to detect iodinated darobactin A in similar amounts as bromodarobactin A (**2**), while fluorinated and chlorinated derivatives were absent (Data S2–S7). These results demonstrated that $DarH_{Pse}$ is responsible for halogenation of **1**.

To further characterize $DarH_{Pse}$ *in vitro*, it was heterologously expressed in *E. coli* and purified by affinity chromatography using an N-terminal His-tag (Data S8). $DarH_{Pse}$ was co-purified with FAD (Data S15). Upon incubation of the purified $DarH_{Pse}$ with darobactin A (**1**) and NADH, the production of bromodarobactin A (**2**) was observed by HPLC and LCMS (Figure 4, Data S9 and S10). This activity required NAD(P)H but no flavin reductase is needed, suggesting either an inherent flavin reductase function of $DarH_{Pse}$ or co-purification of an *E. coli* FAD reductase (Figures 4, S8, S9, and Data S15). $DarH_{Pse}$ catalyzed a single turnover after ~60 min (Data S13). While this rate was unexpectedly slow, it was comparable to the rate of DarE catalysis[11] (60–120 min per turnover) and may represent the overall flux of this biosynthetic pathway. We also tested the activity of $DarH_{Pse}$ using full-length DarA with both ether and C-C crosslinking and did not detect the formation of brominated products (Data S14). These observations support that $DarH_{Pse}$ catalyzes the bromination after proteolytic cleavage of the leader and the follower peptides (Figure 5).

To test whether the absence of fluorinated darobactin A in the *in vivo* assays was caused by the negative effect of KF on bacterial growth, KF was also tested in the *in vitro* assay. However, fluorinated darobactin was not detected (Data S11). To analyze if $DarH_{Pse}$ also catalyzes bromination of other darobactins, the assay was repeated with darobactin B[12] and indeed the brominated variant was observed (Data S12 and Figure S8). To gain further insights into the substrate promiscuity, we synthesized the linear heptapeptide W-N-W-S-K-S-F by solid-phase peptide

Please cite this article in press as: Böhringer et al., Genome- and metabolome-guided discovery of marine BamA inhibitors revealed a dedicated darobactin halogenase, Cell Chemical Biology (2023), https://doi.org/10.1016/j.chembiol.2023.06.011

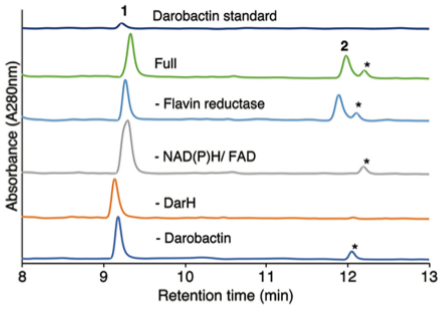

Figure 4. HPLC chromatograms of the DarH assays
$DarH_{Pse}$ (100 μM) was incubated with darobactin A (100 μM) sodium bromide (25 mM), NAD(P)H (1.0 mM), FAD (10 μM), and flavin reductase (10 μM). Shown are HPLC UV chromatograms of the darobactin A standard, the complete condition (Full) and controls without flavin reductase, NAD(P)H/FAD, DarH, or darobactin A. * marks an unrelated peak from assay components.

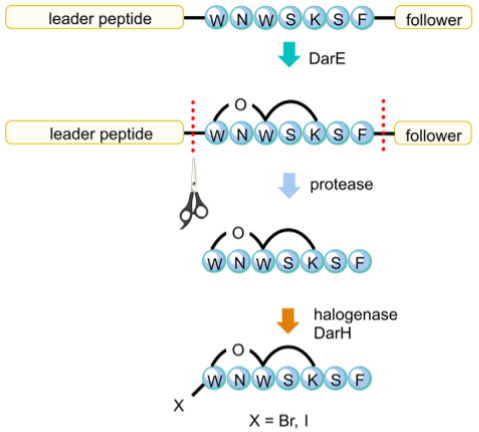

Figure 5. Schematic biosynthetic hypothesis for the formation of halogenated darobactin A
The linear precursor peptide DarA is modified by DarE, thereby installing the two intramolecular rings. Subsequently, the heptapeptide is cleaved off the leader and follower peptide by a not yet identified protease(s), yielding darobactin A (**1**). The latter is halogenated by DarH. The timing of the formal dehydrogenation remains elusive until now.

synthesis, but no halogenation was observed for this compound in the *in vitro* assay (Figure S7).

In contrast to the clear biosynthetic origin of **2**, the enzymes catalyzing the formal dehydrogenation of darobactins could not be identified until now. Heterologous expression experiments, using *darF* and *darH*, did not result in detectable formation of dehydrodarobactins under the tested conditions.

$DarH_{Pse}$ belongs to a new class of FAD-dependent oxidoreductases

To get further insights into this newly identified halogenase, homologous sequences were searched and identified with identity percentages >36% in UniProtKB and SwissProt databases, most of them annotated as FAD-dependent oxidoreductases but also as pyridine nucleotide-disulfide oxidoreductases, thioredoxin reductases, ferredoxin-NADP reductases, or even as a cation diffusion facilitator. None of the top 250 hits is annotated as flavin-dependent halogenase. Interestingly, homologs are widely distributed in nature, with sequences from bacteria, plants, and metazoan being found among the first 250 hits.

We searched for homologous sequences in the PDB to obtain more information about the structure-function relationship. As a result, we obtained homologs with sequence identity lower than 27%. All homologs are part of the family of FAD/NAD(P) binding proteins. The low sequence identity is common among the members of this family, but structural conservation is high even for proteins with identity percentages lower than 15%.[13] Phylogenetic analysis showed that $DarH_{Pse}$ is grouped with the flavin-containing putative monooxygenase from *S. aureus* (pdb id 3d1c) and with the disulfide reductase YpdA, also from *S. aureus* (pdb id 7a7b), while tryptophan halogenases are clustered as an independent group (Figure 6A). This result was confirmed by a further search in the Pfam database, in which both, DarH homologs and YpdA-like proteins, are classified in family PF13738, annotated as Pyr_redox_3, while known Trp halogenases, like MibH, belong to family PF04820, annotated as Trp halogenases. Other flavin-dependent halogenases like CmsL[14] or CndH[15] were not found among the top hits.

To confirm the structural homology with FAD/NAD(P) binding proteins, we calculated an AlphaFold (AF) model[7] that was superimposed with representative members from the three clusters derived from the phylogenetic analysis. Superimposition of the $DarH_{Pse}$ AF model with the selected homologs showed that the only significant structural conservation between $DarH_{Pse}$ and the tryptophan halogenase MibH from *Microbiospora* sp. is the FAD binding domain that comprises 160 amino acid residues from the N-terminus (RMSD = 3.4 Å for 157 residues, Figure 6B), while both, the FAD and NAD(P) binding sites, comprising up to 323 amino acid residues, are structurally conserved in the closest structural homolog YpdA (RMSD = 2.1 Å for 288 residues, Figure 6C). While the structures of both FAD and NAD(P) binding domains superimpose with low RMSD (2.1–2.4 Å) with structures from members of cluster I, the C-terminus (residues 369–505) has no counterpart in any experimentally determined structure available in databases, including the FAD/NAD(P)-dependent oxidoreductases deposited. Using the DALI server,[17] structural homologs were only found when the search included AF-predicted models. For example, DALI found 22% sequence identity in 128 residues (RMSD = 2.5 Å, after superimposition with $DarH_{Pse}$ AF model), with a human FAD-dependent oxidoreductase (AF-Q8IWF2-F1), whose exact function is unknown, yet supporting the universal spreading of the folding in nature. We thus hypothesized that the C-terminal domain is a novel fold that has evolved to fulfill different biological functions, and possibly, in the case of DarH, the recognition of its substrate.

Please cite this article in press as: Böhringer et al., Genome- and metabolome-guided discovery of marine BamA inhibitors revealed a dedicated darobactin halogenase, Cell Chemical Biology (2023), https://doi.org/10.1016/j.chembiol.2023.06.011

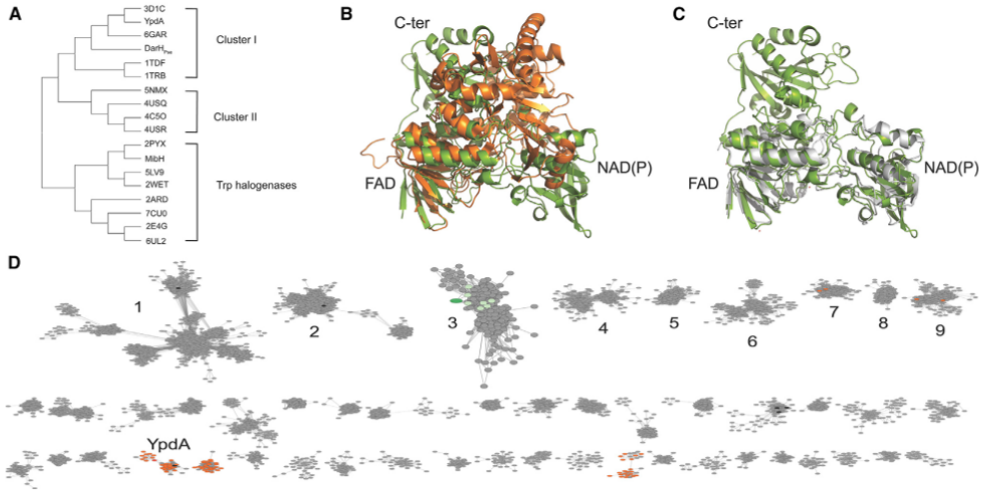

Figure 6. Phylogenetic and in silico structural analysis of DarH. Sequence-based maximum likelihood (ML) phylogenetic tree
(A) showing the three clusters formed by representative homolog sequences deposited in the PDB.
The pdb codes of each model are shown on the right. The central panel (B) shows the structural alignment of the DarH$_{Pse}$ AlphaFold model (green) with the Trp halogenase MibH from *Microbiospora sp.* (pdb code 5uao, orange) and the right panel (C) the superimposition with the disulfide reductase YpdA from *S. aureus* (pdb code 7a7b, gray). DarH$_{Pse}$ contains both an FAD and NAD(P) binding domains and a C-terminal domain without structural homologs in the PDB. (D) SSN analysis of PF13738 shows DarH$_{Pse}$ (green) and direct neighbor nodes (pale green) placed in Cluster 3 (green). Nodes represented in orange correspond to YpdA homologs. A zoom in of Cluster 3 is shown to highlight the position of DarH.

We performed a sequence similarity network (SSN) analysis[18] to get more information about the relations of DarH with other members of the PF13738 family. SSN revealed that the members of the family are distributed in multiple clusters that can be divided into two groups according to the length of their sequence: proteins smaller and larger than 400 amino acid residues (Figure S10, yellow nodes). We selected this threshold value because it corresponds to the maximum sequence length observed in the simplest YpdA-like protein containing only FAD and NAD(P) binding domains. Proteins larger than 400 residues are mainly located in the upper part of the SSN, in the most populated clusters, including DarH and homolog sequences, which are located in a well-defined cluster (Figure 6D, Cluster 3). As described previously, none of the proteins belonging to this cluster are annotated as halogenases, most of them are simply annotated either as FAD-dependent oxidoreductase domain-containing proteins or as uncharacterized proteins. Because of the lack of consistent functional annotation in this group of proteins, it is not possible to determine if the observed clusters belong to functional groups. Thus, we selected structural similarity, based on AF models deposited in Uniprot, as a criterion to evaluate the correct selection of clusters. AF models from all members of Cluster 3, larger than 400 amino acid residues, are characterized by the presence of the novel C-terminal domain of DarH$_{Pse}$. In contrast, members of Clusters 1 and 2, contain insertion domains in the N-terminus. An example of it is the cold-active flavin-dependent monooxygenase from *Janthinobacterium svalbardensis* (pdb id 8acs).[19] Cluster 4 is mainly composed of YpdA-like proteins without N-terminal, C-terminal, or other kinds of domain extensions, while members of Cluster 5 contain a C-terminal extension α-helical domain. Based on these results we conclude that the clusters obtained by SSN represent true structural groups.

Detailed analysis of multiple sequence alignments (MSAs) and structural comparison of homologs revealed that conserved motifs and residues involved in FAD and NAD(P) binding are present in DarH$_{Pse}$ (Figure S11). To obtain further insight into the function-structure relationship of DarH$_{Pse}$ we then investigated whether FAD could fit into the DarH$_{Pse}$ AF model and how it could be orientated with respect to the C-terminal domain. We calculated the putative binding sites in the protein using the SiteMap program (see supplemental information for details).[20–22] When the halogenase is superimposed to YpdA (chain C pdb id 7a7b), the FAD bound to YpdA fits in the first-ranked binding site of DarH$_{Pse}$ while the NADP bound to YpdA fits partially (Figures 7A and S12). Thus, the top-ranked binding site (binding site 1) is common to both proteins and to other FAD/NAD(P) binding proteins. Docking of FAD in DarH$_{Pse}$ (Figure S13) suggested the residues that are important for binding. Comparison of sequences and structural features of the FAD binding sites in DarH$_{Pse}$ and YpdA confirms the crucial interactions and points out that AF most probably failed to correctly model Y46 rotamer that interacts with FAD in YpdA. We cannot exclude that other sidechains may be misplaced by AF. Part of binding site 1 is delineated by residues identified by sequence comparison such as the NAD(P) binding motif (Figure S13A).

Please cite this article in press as: Böhringer et al., Genome- and metabolome-guided discovery of marine BamA inhibitors revealed a dedicated darobactin halogenase, Cell Chemical Biology (2023), https://doi.org/10.1016/j.chembiol.2023.06.011

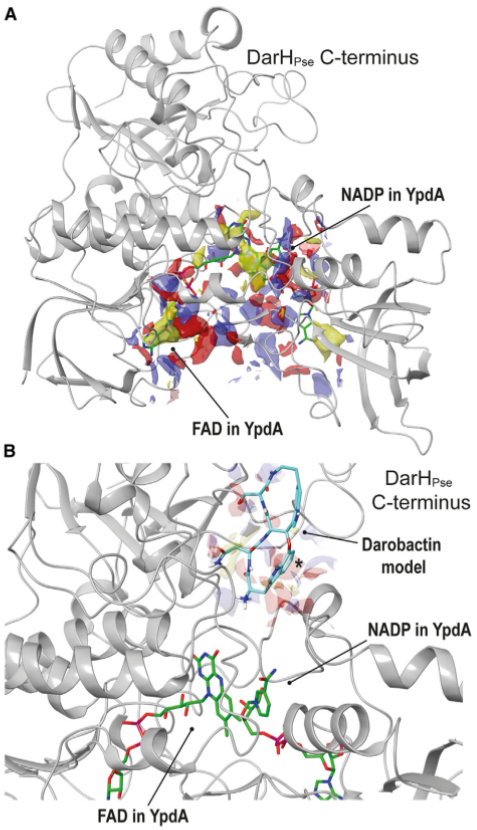

Figure 7. Identification of putative binding sites in DarH *in silico* model

(A) The YpdA structural model (C chain, pdb id 7a7b) was superimposed to the DarH$_{Pse}$ AF one. Only the FAD and NAD of YpdA are shown as sticks with C, N, O, and P atoms colored in green, blue, red, and purple, respectively. The whole DarH$_{Pse}$ AF structure is displayed as gray ribbons. The first putative binding site we identified (see supplemental information), binding site 1, where the red, blue, and yellow surfaces correspond to hydrogen-bond donors, hydrogen-bond acceptors, and hydrophobic regions, respectively, is displayed. A zoom of binding site 1 is shown in Figure S12.

(B) Binding site 3 (Data S16, color code as in A) is displayed in the DarH$_{Pse}$ AF model, (gray ribbons). Part of this cavity lies about 14 Å (shortest distance) from FAD.

Interestingly, the remaining four putative binding sites identified by the SiteMap program, are specific to DarH$_{Pse}$ since they are all located in the unique C-terminal domain (Data S16). Out of the four sites, binding site 3 is the only one that sits in a region close enough to the FAD riboflavin and the NAD(P) nicotinamide moieties; this suggests that it could be a good candidate to host the substrate (Data S16). Yet, the approximate distance of 14 Å suggests the hypobromous acid intermediate should migrate from the FAD site to reach the darobactin binding site, as has been shown in other halogenases.[23,24] Overall, our results support the hypothetical role of the C-terminal domain of darobactin halogenase in binding and correct positioning of its substrate and demonstrate that DarH$_{Pse}$ is a new class of flavin-dependent halogenases characterized by a novel fold.

Biological activity of marine darobactin analogs

Compounds **2** and **4** were purified from natural producer strains after optimizing fermentation conditions. The respective MIC values were determined against a panel of clinically relevant Gram-negative pathogens; among them MDR isolates like the *mcr-1* positive strain *E. coli* NRZ14408. Darobactin A (**1**) showed MIC values of 4–8 μg/mL against the tested strains (*E. coli* ATCC 35218 and clinical isolates, *K. pneumoniae* DSM30104, *P. aeruginosa* [PAO 1 and 750], and *S. enterica* ATCC13076) but >64 μg/mL against *A. baumannii* ATCC19606. Bromodarobactin A (**2**) performed better, showing MICs of 1–2 μg/mL against all strains, except *A. baumannii* (32 μg/mL) (Data S17). Binding to human serum albumin (HSA) and α_1-acid glycoprotein (AGP) (in physiological ratio, 24:1) increased with the modifications in comparison to **1** (e.g., **1**: 36.4%, **2**: 45.2%, **4**: 74.4%, and warfarin: 98.9%).

BamA inhibitors like darobactin A (**1**) have been overlooked in many bioactivity-screening campaigns. However, the encoding BGC is widespread in multiple genera of the γ-proteobacteria family. These genera are all associated with eukaryotic organisms, which pose the question if these bicyclic heptapeptides are of importance in a holobiontic system. Here, we described darobactin analogs of marine origin from closely related *P. luteoviolacea* strains, whose biosynthesis is encoded by a BGC that carries more genes than the previously investigated BGC from nematophilic *Photorhabdus* strains. The dedicated halogenase DarH expands the darobactin class by site-specific bromination of the bicyclic scaffold. It specifically catalyzes modification at the C-5 position (indole numbering; corresponds to C-8 in bromodarobactin A) of the N-terminal tryptophan moiety. DarH specifically acts on the mature natural product and unlike other RiPP modification enzymes, interaction with a leader of the precursor is not required. To the best of our knowledge, up to now only two more RiPP halogenases were described. One of them, the FAD-dependent chlorinase MibH, catalyzes tryptophan-5-chlorination during NAI-107 biosynthesis.[25] This chlorinase specifically recognizes the post-translationally modified precursor carrying a macrocyclic scaffold without the leader peptide as substrate. Recently, the FAD-dependent brominase SrpI was identified by mining for halogenating enzymes in sponge metagenomes. SrpI and the corresponding precursor peptide were heterogously expressed and Agarwal and co-workers observed a broad-spectrum region-specific peptidyl tryptophan-6-brominase activity, since also partially cyclodehydrated peptide variants and even linear precursors were brominated.[26] Hence, in contrast to MibH and DarH, SrpI can brominate an unmodified linear peptide. Both brominases of marine origin (i.e., SrpI and DarH) lack any promiscuity toward chlorination. This specificity should be of importance to avoid contamination with the much higher abundant chloride in the

Please cite this article in press as: Böhringer et al., Genome- and metabolome-guided discovery of marine BamA inhibitors revealed a dedicated darobactin halogenase, Cell Chemical Biology (2023), https://doi.org/10.1016/j.chembiol.2023.06.011

marine habitat. The bromination opens a way for further structural modification of the bicyclic heptapeptides, e.g., by Pd-catalyzed Suzuki-Miyaura cross-coupling with boronic acids that was applied for the derivatization of indole alkaloids.[27,28] The genus *Pseudoalteromonas* is well known for brominated natural products and several enzymes are well-understood, e.g., Bmp2 catalyzes the bromination of its carrier protein-tethered substrate proline toward pentabromopseudilin biosynthesis.[29] It is reasonable to assume that DarH would follow the same chemistry as other reported FAD-dependent halogenases. Reduced flavin FADH would react with molecular oxygen to produce a peroxyflavin intermediate, which would convert the Br^- ion to hypobromous acid. This Br-OH species is then positioned by a lysine side chain for the subsequent attack by the electron-rich indole moiety.[23,30,31] Further studies will determine the exact darobactin halogenation mechanism by DarH. In contrast to bromination, the biosynthetic origin of darobactin desaturation remains elusive. For the clustered gene *darF,* a protease activity was described and adding it to our heterologous system did not result in detectable formation of **3**. Until now, it is not clear if any of the transport-related proteins are involved in this reaction, and even in *trans* modification by dehydrogenases or desaturases from the producer genetic background cannot be ruled out.

Peculiarly, the BGC encoding the new darobactin analogs was only detected in a few closely related *Pseudoalteromonas* strains, which all were isolated from the same geographic region in the Pacific Ocean. Halogenation and desaturation are both modifications resulting in higher hydrophobicity of the compounds. Hence, the more "sticky" molecules likely represent an adaption toward the lifestyle of *Pseudoalteromonas*, which are sessile and associated with higher organisms. The higher hydrophobicity limits the diffusion of the molecules into the free water column and therewith the dilution and loss of inhibitory activities. This is well in tune with our observation that biosynthesis of darobactins is associated with biofilm formation of *P. luteoviolacea* H33 and H33S.

In an antimicrobial activity screening against a panel of clinically relevant Gram-negative pathogens, the MIC of **2** was improved compared to **1**. Based on the crystal structure of **1** bound to its target BamA, **1** interacts with the lateral gate through the peptidic backbone and the W^1 indole ring is not involved in the interaction.[30] Thus, even though it cannot be excluded, bromination of the W^1 indole should not affect the binding of the molecule to its target. Therefore, we propose that bromination improves membrane permeability and results in the increased activity. Conversely, the desaturation of K^5 resulted in slightly higher MICs against the panel tested. The increase in rigidity of the molecule may affect BamA binding. This effect toward activity was observed against the strains tested and it cannot be excluded that this might be a specific adaption to yet unidentified competitors of *P. luteoviolacea* in its habitat.

The change in solubility of the marine darobactins might be beneficial for further development of this compound class into a marketable drug. Even though the chemical total synthesis of darobactin derivatives comes within reach with the previously published total synthesis of darobactin A,[32,33] the halogenation performed by nature still provides a promising starting point for targeted derivatization as it might be a more "step economic" approach, providing satisfying overall yields. Furthermore, the molecules showed stronger plasma protein binding than **1**. Hence, the equilibrium to free compound in plasma will be altered and suggests a longer elimination half-life. This might be advantageous if longer exposure times to the compound are desired and could reduce dosing intervals. The effects of the modifications on tissue penetration and further pharmacokinetics and pharmacodynamics (PK/PD) of the bicyclic heptapeptides will be investigated in future studies. In combination with mutasynthetic derivatization of the darobactin core structure, this will yield optimized molecules for further development of BamA inhibitors.

Limitations of the study

This study is a proof of concept to identify new derivatives of a bioactive compound and to clarify the function of an unknown gene by heterologous expression. This enabled the discovery of a more active derivative of darobactin A. However, for the time being, the new derivative is only accessible in low amounts, which limits the analysis to *in vitro* MIC data. Further *in vivo* studies are not yet possible.

SIGNIFICANCE

There is an unmet medical need to develop new antibiotics especially against Gram-negative bacteria, since even recently licensed drugs are often not efficient to treat infections caused by antimicrobial-resistant (AMR) pathogens. The bicyclic heptapeptides presented here attack a new target, i.e., BamA, and do not show cross-resistance or toxicity. The naturally occurring derivatives of the recently discovered molecule class possess altered properties, which will impact pharmacokinetics and pharmacodynamics. The characterization of the enzymes involved in the biosynthesis and the application of them for heterologous expression approaches will enable further targeted modification of the promising natural product in the future. Thereby, the repertoire of molecules can be enlarged to foster lead nomination for future development. Such a multi-omics approach as applied in this study to discover new natural products could serve as a blueprint for future studies.

STAR★METHODS

Detailed methods are provided in the online version of this paper and include the following:

- KEY RESOURCES TABLE
- RESOURCE AVAILABILITY
  - Lead contact
  - Materials availability
  - Data and code availability
- METHOD DETAILS
  - Detection of bromodarobactin A, dehydrobromodarobactin A and dehydrodarobactin A by UPLC-HRMS
  - Isolation of darobactin derivatives
  - Determination of MIC values of darobactin A and darobactin analogs
  - Plasma protein binding assay
  - HRMS/MS analysis

SUPPLEMENTAL INFORMATION

Supplemental information can be found online at https://doi.org/10.1016/j.chembiol.2023.06.011.

ACKNOWLEDGMENTS

We would like to thank Tillman Harder and Lone Gram for keeping the strains *P. luteoviolacea* H33 and H33S strains alive and for the provision of them. Linda Falgenhauer is thanked for providing the clinical *E. coli* isolates, Mona Abdullahi for technical assistance, and Jean-Marie Pohl for helpful discussion. In addition, we would like to acknowledge the support of Brigitte Weinl-Boulakhrouf for IR spectra, and of Heike Hausmann and the JLU NMR facility for measurements. P.A. appreciates the help from the staff of the computing facility provided by the Commissariat à l'Energie Atomique et aux Energies Alternatives (CEA/DRF/GIPSI), Saclay and CCRT, Bruyères-le-Châtel. This work was supported by the French National Research Agency (ANR-20-CE44-0005). This work used the platforms of the Grenoble Instruct-ERIC center (ISBG; UMS 3518 CNRS-CEA-UGA-EMBL) within the Grenoble Partnership for Structural Biology (PSB), which is supported by FRISBI (ANR-10-INBS-05-02) and GRAL, and financed within the Université Grenoble Alpes graduate school (Ecoles Universitaires de Recherche) CBH-EUR-GS (ANR-17-EURE-0003). The work in the Schäberle lab was supported by the State Ministry of Higher Education, Research and Arts of the state Hessen through the LOEWE program for the Center for Insect Biotechnology and Bioresources and the German Federal Ministry of Education and Research (BMBF, via grant GBi2S and DZIF TTU 09.918).

AUTHOR CONTRIBUTIONS

Conceptualization: T.F.S.; Methodology: N.B. and J-C.K.; Investigation: N.B., J-C.K., E.d.l.M., L.P., Z.G.W., Y.L., M.K., M.M., H.N., P.A., and U.M.; Data Analysis: N.B., J-C.K., E.d.l.M., L.P., Z.G.W., Y.L., M.K., M.M., H.N., P.A., and U.M.; Writing – Original Draft: N.B., J-C.K., E.d.l.M., M.M., H.N., U.M., and T.F.S.; Visualization: N.B., J-C.K., E.d.l.M., M.M., H.N., P.A., and U.M.; Supervision: K.Y., Y.N., and T.F.S. Project Administration: T.F.S.; Funding Acquisition: K.Y., Y.N., and T.F.S.

Lead contact: Prof. Dr. Till F. Schäberle (Till.F.Schaeberle@agrar.uni-giessen.de).

DECLARATION OF INTERESTS

The authors declare no competing interest.

Received: January 24, 2023
Revised: May 5, 2023
Accepted: June 13, 2023
Published: July 13, 2023

REFERENCES

1. Imai, Y., Meyer, K.J., Iinishi, A., Favre-Godal, Q., Green, R., Manuse, S., Caboni, M., Mori, M., Niles, S., Ghiglieri, M., et al. (2019). A new antibiotic selectively kills Gram-negative pathogens. Nature *576*, 459–464. https://doi.org/10.1038/s41586-019-1791-1.
2. Wuisan, Z.G., Kresna, I.D.M., Böhringer, N., Lewis, K., and Schäberle, T.F. (2021). Optimization of heterologous Darobactin A expression and identification of the minimal biosynthetic gene cluster. Metab. Eng. *66*, 123–136. https://doi.org/10.1016/j.ymben.2021.04.007.
3. Burkholder, P.R., Pfister, R.M., and Leitz, F.H. (1966). Production of a pyrrole antibiotic by a marine bacterium. Appl. Microbiol. *14*, 649–653. https://doi.org/10.1128/am.14.4.649-653.1966.
4. Sobolevskaya, M.P., Smetanina, O.F., Speitling, M., Shevchenko, L.S., Dmitrenok, P.S., Laatsch, H., Kuznetsova, T.A., Ivanova, E.P., and Elyakov, G.B. (2005). Controlling production of brominated cyclic depsipeptides by Pseudoalteromonas maricaloris KMM 636T. Lett. Appl. Microbiol. *40*, 243–248. https://doi.org/10.1111/j.1472-765X.2005.01635.x.
5. Speitling, M., Smetanina, O.F., Kuznetsova, T.A., and Laatsch, H. (2007). Bromoalterochromides A and A', unprecedented chromopeptides from a marine Pseudoalteromonas maricaloris strain KMM 636T. J. Antibiot. *60*, 36–42. https://doi.org/10.1038/ja.2007.5.
6. Suria, A.M., Tan, K.C., Kerwin, A.H., Gitzel, L., Abini-Agbomson, L., Bertenshaw, J.M., Sewell, J., Nyholm, S.V., and Balunas, M.J. (2020). Hawaiian Bobtail Squid Symbionts Inhibit Marine Bacteria via Production of Specialized Metabolites, Including New Bromoalterochromides BAC-D/D'. mSphere *4*. https://doi.org/10.1128/mSphere.00166-20.
7. Jumper, J., Evans, R., Pritzel, A., Green, T., Figurnov, M., Ronneberger, O., Tunyasuvunakool, K., Bates, R., Žídek, A., Potapenko, A., et al. (2021). Highly accurate protein structure prediction with AlphaFold. Nature *596*, 583–589. https://doi.org/10.1038/s41586-021-03819-2.
8. Groß, S., Panter, F., Pogorevc, D., Seyfert, C.E., Deckarm, S., Bader, C.D., Herrmann, J., and Müller, R. (2021). Improved broad-spectrum antibiotics against Gram-negative pathogens via darobactin biosynthetic pathway engineering. Chem. Sci. *35*, 11882–11893. https://doi.org/10.1039/D1SC02725E.
9. Wang, M., Carver, J.J., Phelan, V.V., Sanchez, L.M., Garg, N., Peng, Y., Nguyen, D.D., Watrous, J., Kapono, C.A., Luzzatto-Knaan, T., et al. (2016). Sharing and community curation of mass spectrometry data with Global Natural Products Social Molecular Networking. Nat. Biotechnol. *34*, 828–837. https://doi.org/10.1038/nbt.3597.
10. Nishihara, K., Kanemori, M., Kitagawa, M., Yanagi, H., and Yura, T. (1998). Chaperone coexpression plasmids: differential and synergistic roles of DnaK-DnaJ-GrpE and GroEL-GroES in assisting folding of an allergen of Japanese cedar pollen, Cryj2, in Escherichia coli. Appl. Environ. Microbiol. *64*, 1694–1699. https://doi.org/10.1128/AEM.64.5.1694-1699.1998.
11. Nguyen, H., Made Kresna, I.D., Böhringer, N., Ruel, J., Mora, E.d.l., Kramer, J.-C., Lewis, K., Nicolet, Y., Schäberle, T.F., and Yokoyama, K. (2022). Characterization of a Radical SAM Oxygenase for the Ether Crosslinking in Darobactin Biosynthesis. J. Am. Chem. Soc. *144*, 18876–18886. https://doi.org/10.1021/jacs.2c05565.
12. Böhringer, N., Green, R., Liu, Y., Mettal, U., Marner, M., Modaresi, S.M., Jakob, R.P., Wuisan, Z.G., Maier, T., Iinishi, A., et al. (2021). Mutasynthetic Production and Antimicrobial Characterization of Darobactin Analogs. Microbiol. Spectr. *3*, e0153521. https://doi.org/10.1128/spectrum.01535-21.
13. Ojha, S., Meng, E.C., and Babbitt, P.C. (2007). Evolution of function in the "two dinucleotide binding domains" flavoproteins. PLoS Comput. Biol. *3*, e121. https://doi.org/10.1371/journal.pcbi.0030121.
14. Podzelinska, K., Latimer, R., Bhattacharya, A., Vining, L.C., Zechel, D.L., and Jia, Z. (2010). Chloramphenicol biosynthesis: the structure of CmlS, a flavin-dependent halogenase showing a covalent flavin-aspartate bond. J. Mol. Biol. *397*, 316–331. https://doi.org/10.1016/j.jmb.2010.01.020.
15. Buedenbender, S., Rachid, S., Müller, R., and Schulz, G.E. (2009). Structure and action of the myxobacterial chondrochloren halogenase CndH: a new variant of FAD-dependent halogenases. J. Mol. Biol. *385*, 520–530. https://doi.org/10.1016/j.jmb.2008.10.057.
16. Mirdita, M., Schütze, K., Moriwaki, Y., Heo, L., Ovchinnikov, S., and Steinegger, M. (2022). ColabFold: making protein folding accessible to all. Nat. Methods *19*, 679–682. https://doi.org/10.1038/s41592-022-01488-1.

17. Holm, L. (2020). DALI and the persistence of protein shape. Protein Sci. *1*, 128–140. https://doi.org/10.1002/pro.3749.

18. Zallot, R., Oberg, N., and Gerlt, J.A. (2019). The EFI Web Resource for Genomic Enzymology Tools: Leveraging Protein, Genome, and Metagenome Databases to Discover Novel Enzymes and Metabolic Pathways. Biochemistry *58*, 4169–4182. https://doi.org/10.1021/acs.biochem.9b00735.

19. Chánique, A.M., Polidori, N., Sovic, L., Kracher, D., Assil-Companioni, L., Galuska, P., Parra, L.P., Gruber, K., and Kourist, R. (2023). A Cold-Active Flavin-Dependent Monooxygenase from Janthinobacterium svalbardensis Unlocks Applications of Baeyer-Villiger Monooxygenases at Low Temperature. ACS Catal. *6*, 3549–3562. https://doi.org/10.1021/acscatal.2c05160.

20. Halgren, T. (2007). New method for fast and accurate binding-site identification and analysis. Chem. Biol. Drug Des. *69*, 146–148. https://doi.org/10.1111/j.1747-0285.2007.00483.x.

21. Halgren, T.A. (2009). Identifying and characterizing binding sites and assessing druggability. J. Chem. Inf. Model. *49*, 377–389. https://doi.org/10.1021/ci800324m.

22. (2021). SiteMap (New York: Schrödinger, LLC).

23. Dong, C., Flecks, S., Unversucht, S., Haupt, C., van Pée, K.H., and Naismith, J.H. (2005). Tryptophan 7-halogenase (PrnA) structure suggests a mechanism for regioselective chlorination. Science (New York, N.Y.) *309*, 2216–2219. https://doi.org/10.1126/science.1116510.

24. Gkotsi, D.S., Dhaliwal, J., McLachlan, M.M., Mulholand, K.R., and Goss, R.J. (2018). Halogenases: powerful tools for biocatalysis (mechanisms applications and scope). Curr. Opin. Chem. Biol. *43*, 119–126. https://doi.org/10.1016/j.cbpa.2018.01.002.

25. Ortega, M.A., Cogan, D.P., Mukherjee, S., Garg, N., Li, B., Thibodeaux, G.N., Maffioli, S.I., Donadio, S., Sosio, M., Escano, J., et al. (2017). Two Flavoenzymes Catalyze the Post-Translational Generation of 5-Chlorotryptophan and 2-Aminovinyl-Cysteine during NAI-107 Biosynthesis. ACS Chem. Biol. *12*, 548–557. https://doi.org/10.1021/acschembio.6b01031.

26. Nguyen, N.A., Lin, Z., Mohanty, I., Garg, N., Schmidt, E.W., and Agarwal, V. (2021). An Obligate Peptidyl Brominase Underlies the Discovery of Highly Distributed Biosynthetic Gene Clusters in Marine Sponge Microbiomes. J. Am. Chem. Soc. *143*, 10221–10231. https://doi.org/10.1021/jacs.1c03474.

27. Sharma, S.V., Tong, X., Pubill-Ulldemolins, C., Cartmell, C., Bogosyan, E.J.A., Rackham, E.J., Marelli, E., Hamed, R.B., and Goss, R.J.M. (2017). Living GenoChemetics by hyphenating synthetic biology and synthetic chemistry in vivo. Nat. Commun. *8*, 229. https://doi.org/10.1038/s41467-017-00194-3.

28. Runguphan, W., and O'Connor, S.E. (2013). Diversification of monoterpene indole alkaloid analogs through cross-coupling. Org. Lett. *15*, 2850–2853. https://doi.org/10.1021/ol401179k.

29. Agarwal, V., El Gamal, A.A., Yamanaka, K., Poth, D., Kersten, R.D., Schorn, M., Allen, E.E., and Moore, B.S. (2014). Biosynthesis of polybrominated aromatic organic compounds by marine bacteria. Nat. Chem. Biol. *10*, 640–647. https://doi.org/10.1038/nchembio.1564.

30. (2021). Enzymatic halogenation: enzyme mining, mechanisms, and implementation in reaction cascades. In Amino Acids, Peptides and Proteins, *44*, S. Dachwitz, C. Widmann, M. Frese, H.H. Niemann, and N. Sewald, eds. *(Royal Society of Chemistry). https://doi.org/10.1039/9781788017008-00001*.

31. Minges, H., and Sewald, N. (2020). Recent Advances in Synthetic Application and Engineering of Halogenases. ChemCatChem *12*, 4450–4470. https://doi.org/10.1002/cctc.202000531.

32. Nesic, M., Ryffel, D.B., Maturano, J., Shevlin, M., Pollack, S.R., Gauthier, D.R., Trigo-Mouriño, P., Zhang, L.-K., Schultz, D.M., McCabe Dunn, J.M., et al. (2022). Total Synthesis of Darobactin A. J. Am. Chem. Soc. *144*, 14026–14030. https://doi.org/10.1021/jacs.2c05891.

33. Lin, Y.-C., Schneider, F., Eberle, K.J., Chiodi, D., Nakamura, H., Reisberg, S.H., Chen, J., saito, m., and Baran, P.S. (2022). Atroposelective Total Synthesis of Darobactin A. J. Am. Chem. Soc. *144*, 14458–14462. https://doi.org/10.1021/jacs.2c05892.

34. Vynne, N.G., Mansson, M., and Gram, L. (2012). Gene sequence based clustering assists in dereplication of Pseudoalteromonas luteoviolacea strains with identical inhibitory activity and antibiotic production. Mar. Drugs *10*, 1729–1740. https://doi.org/10.3390/md10081729.

35. Gibson, D.G., Young, L., Chuang, R.-Y., Venter, J.C., Hutchison, C.A., and Smith, H.O. (2009). Enzymatic assembly of DNA molecules up to several hundred kilobases. Nat. Methods *6*, 343–345. https://doi.org/10.1038/nmeth.1318.

36. Kresna, I.D.M., Linares-Otoya, L., Milzarek, T., Duell, E.R., Mir Mohseni, M., Mettal, U., König, G.M., Gulder, T.A.M., and Schäberle, T.F. (2021). In vitro characterization of 3-chloro-4-hydroxybenzoic acid building block formation in ambigol biosynthesis. Org. Biomol. Chem. *19*, 2302–2311. https://doi.org/10.1039/D0OB02372H.

37. Zehner, S., Kotzsch, A., Bister, B., Süssmuth, R.D., Méndez, C., Salas, J.A., and van Pée, K.H. (2005). A regioselective tryptophan 5-halogenase is involved in pyrroindomycin biosynthesis in Streptomyces rugosporus LL-42D005. Chem. Biol. *12*, 445–452. https://doi.org/10.1016/j.chembiol.2005.02.005.

38. Tamura, K., Stecher, G., and Kumar, S. (2021). MEGA11: Molecular Evolutionary Genetics Analysis Version 11. Mol. Biol. Evol. *38*, 3022–3027. https://doi.org/10.1093/molbev/msab120.

39. Shannon, P., Markiel, A., Ozier, O., Baliga, N.S., Wang, J.T., Ramage, D., Amin, N., Schwikowski, B., and Ideker, T. (2003). Cytoscape: a software environment for integrated models of biomolecular interaction networks. Genome Res. *13*, 2498–2504. https://doi.org/10.1101/gr.1239303.

40. Emsley, P., Lohkamp, B., Scott, W.G., and Cowtan, K. (2010). Features and development of Coot. Acta crystallographica. Section D, Biological crystallography *66*, 486–501. https://doi.org/10.1107/S0907444910007493.

41. Gottlieb, H.E., Kotlyar, V., and Nudelman, A. (1997). NMR Chemical Shifts of Common Laboratory Solvents as Trace Impurities. J. Org. Chem. *62*, 7512–7515. https://doi.org/10.1021/jo971176v.

42. Sastry, G.M., Adzhigirey, M., Day, T., Annabhimoju, R., and Sherman, W. (2013). Protein and ligand preparation: parameters, protocols, and influence on virtual screening enrichments. J. Comput. Aided Mol. Des. *27*, 221–234. https://doi.org/10.1007/s10822-013-9644-8.

43. Friesner, R.A., Banks, J.L., Murphy, R.B., Halgren, T.A., Klicic, J.J., Mainz, D.T., Repasky, M.P., Knoll, E.H., Shelley, M., Perry, J.K., et al. (2004). Glide: a new approach for rapid, accurate docking and scoring. 1. Method and assessment of docking accuracy. J. Med. Chem. *47*, 1739–1749. https://doi.org/10.1021/jm0306430.

44. (2021). LigPrep (New York, NY: Schrödinger, LLC).

45. (2021). Glide (New York, NY: Schrödinger, LLC).

Please cite this article in press as: Böhringer et al., Genome- and metabolome-guided discovery of marine BamA inhibitors revealed a dedicated darobactin halogenase, Cell Chemical Biology (2023), https://doi.org/10.1016/j.chembiol.2023.06.011

STAR★METHODS

KEY RESOURCES TABLE

REAGENT or RESOURCE	SOURCE	IDENTIFIER
Bacterial and virus strains		
Pseudoalteromonas luteoviolacea H33	Vynne et al.[33]	NCBI:txid1365251
Pseudoalteromonas luteoviolacea H33S	Vynne et al.[33]	NCBI:txid1365252
Escherichia coli 1532	ATCC	ATCC 35218
Escherichia coli	ATCC	25922
Escherichia coli NRZ14408	Biomedizinisches Forschungszentrum Seltersberg (BFS)	NRZ14408
Escherichia coli K0416	BFS	K0416
Escherichia coli Survcare 052	BFS	Survcare 052
Escherichia coli MMGI1	BFS	MMGI1
Pseudomonas aeruginosa PAO 1	Fraunhofer-IME strain collection	PAO 1
Pseudomonas aeruginosa PAO 750	Fraunhofer-IME strain collection	PAO 750
Klebsiella pneumoniae subsp. *pneumoniae*	DSMZ	DSM 30104
Acinetobacter baumannii	ATCC	ATCC 19606
Salmonella enterica subsp. *enterica* serovar *Enteritidis*	ATCC	ATCC 13076
Escherichia coli Top10	Invitrogen™	Cat#C404050
Escherichia coli Bap1(DarR)	Wuisan et al.[2]	N/A
Escherichia coli Bap1(DarR) + pGro7	This paper	N/A
Escherichia coli Bap1(DarR) + pLP02	This paper	N/A
Escherichia coli Bap1(DarR) + pLP03	This paper	N/A
Escherichia coli Bap1(DarR) + pJK6.1	This paper	N/A
Escherichia coli Bap1(DarR) + pGro7 + pLP02	This paper	N/A
Escherichia coli Bap1(DarR) + pGro7 + pLP03	This paper	N/A
Escherichia coli Bap1(DarR) + pGro7 + pJK6.1	This paper	N/A
Escherichia coli Bap1(DarR) + pGro7 + pJK9.1	This paper	N/A
Critical commercial assays		
TRANSIL PPB Binding Kit	Sovicell	TPB-0212-2096
Oligonucleotides		
Primers for this study, see Table S2	This paper	N/A
Recombinant DNA		
pLP02	This paper	N/A
pLP03	This paper	N/A
pJK6.1	This paper	N/A
pJK9.1	This paper	N/A
pET28A + FRE	Kresna et al.[36]	N/A
pGro7	Takara	Cat#3340
pZW-ADC9	Wuisan et al.[2]	N/A
Software and algorithms		
AlphaFold	Mirdita et al.[16]	https://deepmind.com/research/highlighted-research/alphafold
Protein Preparation Wizard	Sastry et al.[42]	https://schrodinger.com/science-articles/protein-preparation-wizard
SiteMap	Halgren, Schrödinger[20–22]	https://schrodinger.com/products/sitemap
LigPrep	Schrödinger[44]	https://schrodinger.com/products/ligprep

(*Continued on next page*)

Please cite this article in press as: Böhringer et al., Genome- and metabolome-guided discovery of marine BamA inhibitors revealed a dedicated darobactin halogenase, Cell Chemical Biology (2023), https://doi.org/10.1016/j.chembiol.2023.06.011

Continued

REAGENT or RESOURCE	SOURCE	IDENTIFIER
Glide	Friesner et al.,[43] Schrödinger[45]	https://schrodinger.com/products/glide
Other		
Composition OSMAC media M1-M10, see table in method details	This paper	N/A

RESOURCE AVAILABILITY

Lead contact

Further information and requests for resources and reagents should be directed to and will be fulfilled by the lead contact, Prof. Dr. Till F. Schäberle (Till.F.Schaeberle@agrar.uni-giessen.de).

Materials availability

Plasmids generated in this study are not commercially available. For questions regarding structure elucidation and chemical synthesis, please contact UM; for questions about cloning and *in vitro* work contact TFS.

Data and code availability

- All data reported in this paper will be shared by the lead contact upon request.
- This paper does not report original code.
- Any additional information required to reanalyze the data reported in this paper is available from the lead contact upon request.
- For bromodarobactin A and dehydrodarobactin A production *Pseudoalteromonas luteoviolacea* H33 and *Pseudoalteromonas luteoviolacea* H33S[34] was cultivated in M2 medium for 3 days at 30°C and 180 rpm.
- E. coli ATCC35218, E. coli NRZ14408, E. coli K0416, E. coli Survcare 052, E. coli MMGI1, Pseudomonas aeruginosa PAO 1, Pseudomonas aeruginosa PAO 750, Klebsiella pneumoniae DSM30104, Acinetobacter baumannii ATCC19606, and Salmonella enterica subsp. enterica serovar Enteritidis ATCC13076 were cultivated at 37°C and 180 rpm in Mueller Hinton 2 broth to obtain an overnight culture for the MIC assays.
- *E. coli* Top10 and *E. coli* Bap1(DarR) were cultivated over night in lysogeny broth (LB) medium at 37°C and 180 rpm. If the strains harbor a plasmid the respective antibiotic was added to the medium (kanamycin 50 μg/mL, chloramphenicol 25 μg/mL). To heterologously express darobactin A, bromodarobactin A or darH the cells were grown at 30°C or 18°C after inducing with IPTG for three days in case of darobactin A/bromodarobactin A and over night for the production of darH.

METHOD DETAILS

Detection of bromodarobactin A, dehydrobromodarobactin A and dehydrodarobactin A by UPLC-HRMS

In order to detect novel darobactin analogs from *Pseudoalteromonas* strains, a quasi OSMAC approach was performed. Eleven media (marine broth (Carl Roth, Karlsruhe, Germany) and M1 – M10; media composition in table below) were inoculated from overnight cultures in marine broth (MB) and grown for 3 days. Subsequently, the cells were removed by centrifugation and the supernatant was concentrated as described previously,[12] using a 0.5 g C_{18} SPE column and consecutive evaporation in a GeneVac centrifugal concentrator (SPScientific, Ipswitch, UK). The concentrate was dissolved in 200 μL H_2O + 0.1% formic acid and the crude extracts were subjected to UPLC-HRMS for GNPS molecular networking analysis.[9]

UPLC-HRMS measurements were performed using an instrumental setup consisting of an Agilent Infinity 1290 UPLC system coupled to a DAD detector and a micrOTOFQ II mass spectrometer (Bruker Daltonics, Bremen, Germany) with an electrospray ionization source. For high(er) accuracy measurements a UPLC system of the aforementioned type coupled to DAD and ELSD detectors and a maXis II ESI-qTOF-UHRMS (Bruker Daltonics, Bremen, Germany) was used. The stationary phase of the UPLC system consisted in both cases of an Acquity UPLC BEH C18 1.7 μm (2.1 × 100 mm) column and an Acquity UPLC BEH C18 1.7 μm VanGuard Pre-Column (2.1 × 5 mm; both columns purchased from Waters, Eschborn, Germany). The LC system coupled to the micrOTOFQ II instrument was operated using the following gradient (A: H_2O, 0.1% formic acid; B: MeCN, 0.1% formic acid): 0 min: 95% A; 0.80 min: 95% A; 18.70 min: 4.75% A; 18.80 min: 0% A; 23.00 min: 0% A; 23.10 min: 95% A; 25.00 min: 95% A. The gradient of the LC system coupled to the maXis II ESI-qTOF-UHRMS instrument was as follows (A: H_2O, 0.1% formic acid; B: MeCN, 0.1% formic acid): 0 min: 95% A; 0.30 min: 95% A; 18.00 min: 4.75% A; 18.10 min: 0% A; 22.50 min: 0% A; 22.60 min: 95% A; 25.00 min: 95% A. For both systems the flow rate was set to 600 μL/min and the column oven temperature was maintained at 45°C. A 10 mM sodium formate solution in $H_2O/^iPrOH$ (1:1) served as internal standard for the calibration of mass spectra. Recorded spectra were analyzed with Compass DataAnalysis 4.2 and 5.3 (Bruker), converted to .mzXML and uploaded to the GNPS server. GNPS molecular networking was performed by defining empty media as one group, semi-purified

Please cite this article in press as: Böhringer et al., Genome- and metabolome-guided discovery of marine BamA inhibitors revealed a dedicated darobactin halogenase, Cell Chemical Biology (2023), https://doi.org/10.1016/j.chembiol.2023.06.011

darobactin A (**1**) from a previous experiment as another. *Pseudoalteromonas* crude extracts were then distributed to the other groups based on the respective medium they were grown in. Molecular networking was run under standard conditions and subsequently rerun under relaxed conditions by setting the number of matching fragments to 2 (Standard: 6). GNPS molecular networks[9] were analyzed using CytoScape (ISB, Seattle, USA).

Media composition of OSMAC media M1 - M10. ASW = artificial seawater*. MOPS = 3-(*N*-morpholino)-propane sulphonic acid.

M1	M2	M3	M4	M5	M6	M7	M8	M9	M10
ASW	ASW	ASW	ASW	ASW	ASW	ASW	ASW	ASW	ASW
40 mM MOPS	40 mM MOPS	40 mM MOPS	40 mM MOPS	40 mM MOPS	40 mM MOPS	40 mM MOPS	40 mM MOPS	40 mM MOPS	40 mM MOPS
3 g/L Glycerin	3 g/L Glucose	3 g/L Glucose	3 g/L Glucose	3 g/L Glucose	3 g/L Glucose	3 g/L Starch	3 g/L Glucose	3 g/L Mannitol	3 g/L Soy flour
5 g/L Casein	5 g/L Casein	5 g/L Casein	5 g/L Casein	5 g/L Casein	5 g/L Casein	5 g/L Peptone	5 g/L Malt extract	2.5 g/L Peptone	2.5 g/L Peptone
		Urea 1 g/L	Ammonium acetate 1 g/L	Ammonium chloride 1 g/L	Glutamic acid 1 g/L				

*ASW composition KBr (0.1 g L^{-1}), $MgCl_2 \cdot 6\,H_2O$ (10.61 g L^{-1}), $CaCl_2 \cdot 2\,H_2O$ (1.47 g L^{-1}), KCl (0.66 g L^{-1}), $SrCl_2 \cdot 6\,H_2O$ (0.04 g L^{-1}), Na_2SO_4 (3.92 g L^{-1}), $NaHCO_3$ (0.19 g L^{-1}) and H_3BO_3 (0.03 g L^{-1}).

Isolation of darobactin derivatives

Bromodarobactin A (**2**) and dehydrobromodarobactin A (**4**) were isolated using a modified protocol from Imai et al.[1] Therefore, *P. luteoviolacea* H33 was cultivated in M2 medium for 3 days at 30°C and 180 rpm. Cleared supernatant was incubated with 10% v/v XAD-16N resin and the resin was subsequently washed with H_2O. Compounds were eluted with 80% MeOH +0.1% FA and the MeOH was evaporated using a rotary evaporator. The MeOH free elution fraction was loaded to an SP Sepharose XL strong ion exchange column (220 mL bed volume, GE healthcare, Chalfont St Giles, UK) and subsequently eluted with 10 column volumes (CV) 50 mM NH_4OAc with pH 3 – pH 11. Darobactin analog containing fractions were pooled, lyophilized and purified by HPLC (Shimadzu Deutschland GmbH, Duisburg, Germany), using a gradient (A: H_2O, 0.1% formic acid; B: MeCN, 0.1% formic acid; 0 min–5 min 15% B, 5 min–25 min 15%–25% B, 25 min–30 min 25%–60% B, 30 min–39 min 60%–100% B). Darobactin analogs were collected as pure compounds in a subsequent HPLC run using a gradient of 0 min–5 min 10% B, 5 min–31 min 10%–23.5% B, 31 min–38 min 100% B and weight out in glass vials. In both cases, the flow rate was set to 3 mL/min and the column oven temperature was maintained at 40°C.

Determination of MIC values of darobactin A and darobactin analogs

The test panel for the determination of MIC values for darobactin derivatives consisted of *E. coli* ATCC35218, *E. coli* NRZ14408, *E. coli* K0416, *E. coli* Survcare 052, *E. coli* MMGI1, *Pseudomonas aeruginosa* PAO 1, *Pseudomonas aeruginosa* PAO 750, *Klebsiella pneumoniae* DSM30104, *Acinetobacter baumannii* ATCC19606, and *Salmonella enterica* subsp. *enterica* serovar *enteritidis* ATCC13076. The antibiogram and the resistance determinants for the clinical *E. coli* isolates are given in Data S18 and S19. The MICs were determined by microbroth dilution assays in round bottom 96-well plates. Overnight cultures of *E. coli* ATCC35218 and the clinical isolates *E. coli* NRZ14408, *E. coli* K0416, *E. coli* Survcare 052, *E.* coli MMGI1; *A. baumannii* ATCC19606, *K. pneumoniae* ATCC30104, and *S. enterica* ATCC13076 were adjusted to McFarland Standard of 1.0 and subsequently diluted to 5 x 10^5 cells mL^{-1} in cation adjusted Mueller Hinton 2 broth (CAMHII). Darobactins were screened in 12 concentrations ranging from 64 to 0.03 μg mL^{-1} in triplicate. The same concentrations were tested for rifampicin, tetracycline and gentamicin as positive controls. For tetracycline resistant *E. coli* strains (NRZ14408, K0416 and MMGI1) as well as for *E. coli* Survcare 052 tetracycline was substituted with a colistin dilution series (16–0.007 μg mL^{-1}).

Bacteria suspension without supplemented standard antibiotics or darobactin was used as negative control. After incubation (18 h, 180 rpm, 37°C, 85% relative humidity), cell growth was determined by measuring the turbidity with a microplate spectrophotometer at 600 nm. The MIC was defined as the minimum concentration where at least 85% growth inhibition relative to the negative control was measured. Relative inhibition was calculated as rel. inh. % = 100 * [1- (AU sample - AU Low)/(AU High - AU Low)]. Results are shown in Data S17.

AU: absorption unit; Low: medium blank; High: negative control of maximal growth.

Plasma protein binding assay

The plasma protein binding assay was performed by using the TRANSIL PPB Binding Kit (Sovicell, Leipzig, Germany) according to manufacturer's manual. The TRANSIL PPB Binding Kit consists of a 96-well plate, where each column has eight wells for measurement of the plasma protein binding strength of one compound – two wells act as references and six wells contain increasing

Please cite this article in press as: Böhringer et al., Genome- and metabolome-guided discovery of marine BamA inhibitors revealed a dedicated darobactin halogenase, Cell Chemical Biology (2023), https://doi.org/10.1016/j.chembiol.2023.06.011

concentrations of human serum albumin (HSA) and α_1-acid glycoprotein (AGP) in physiological mixture, immobilized to beads. 16x stock solutions of darobactin A (**1**), bromodarobactin A (**2**), and dehydrobromodarobactin A (**4**) were prepared in phosphate-buffered saline (PBS) containing 32% DMSO. To each well 15 μL of compound stock were added. Hence, the final assay concentration was 5 μM with 2% DMSO. The plate was incubated for 12 minutes at room temperature with 1200 rpm shaking, before a centrifugation step at 750 x *g* for 10 minutes was performed in order to separate the beads from the supernatant containing unbound compounds. The supernatant was analyzed by UPLC-HRMS and the area under the curve of the extracted ion chromatogram of each compound was entered into the data analysis spreadsheet provided by Sovicell to calculate the bound fraction (f_b) of darobactin A, bromodarobactin A, and dehydrobromodarobactin A. Warfarin was included as control.

HRMS/MS analysis

MS/MS fragmentation analysis was performed on the instrumentation mentioned above, using the auto-MSMS setting. Mass spectra were analyzed with Compass DataAnalysis and fragments of darobactin derivates were compared to fragmentation of an authentic darobactin A (**1**) standard.

Heterologous production of bromodarobactin A

Plasmid DNA was isolated using the innuPREP plasmid mini kit 2.0 (AnalytikJena, Jena, Germany) according to the manufacturer's protocol. Genomic DNA was extracted using the innuPREP bacteriaDNA kit (AnalytikJena, Jena, Germany). *E. coli* cells for cloning were grown in lysogeny broth (LB) medium using appropriate antibiotics in commonly used concentrations. DNA fragments were amplified by PCR using Q5 polymerase according to the supplied manual and gel purified using 1% TRIS-agarose-EDTA (TAE) gels. Bands of the correct sizes were excised and the DNA was eluted using the Zymoclean large fragment DNA recovery kit. DNA fragments were fused using self-prepared isothermal assembly reactions.[35] Codon optimized *darA*$_{Pse}$, *darE*$_{Pse}$ and *darH*$_{Pse}$ were synthesized by Eurofins Genomics (Ebersberg, Germany). For creation of pLP02, carrying *darA*$_{Pse}$ and *darE*$_{Pse}$, pRSFDuett-1 was amplified using the primer pair 5′-TGTATATCTCCTTCTTATACTTAACTAATATACTAAGATGGG-3′ and 5′-GCT GCTGCCACCGCTGAGCA-3′, and synthesized *darA*$_{Pse}$ and *darE*$_{Pse}$ were amplified using the primers 5′-GTATAAGAAGGAGATATA CAATGATCGTTGAAGCTCCGAA-3′/5′-TGCAGCTA CCTCCTTAGAAAGATTTAGACCAGTTCCAAGCG-3′ and 5′-CTTTCTAAGGAG GTAGCTGCAATGCTGGGTGACATCTCTGT-3′/5′-TGCTCAGCGGTGGCAGCAGCTTAGATAGATTCTTCGATAACTTTCAGCAG-3′, respectively. All fragments were fused by isothermal assembly. Plasmid pLP03, carrying *darA*$_{Pse}$, *darE*$_{Pse}$ and *darH*$_{Pse}$ was created by amplification of pRSFDuett-1 using the primer pair 5′-TGTATATCTCCTTCTTATACTTAACTAATATACTAAGATGGG-3′/5‘-GCTG CTGCCACCGCTGAGCA-3’, synthesized *darA*$_{Pse}$, *darE*$_{Pse}$ and *darH*$_{Pse}$ were amplified using the primers 5′-GTATAAGAAGGAGATA TACAATGATCGTTGAAGCTCCGAA-3′/5′-TGCAGCTA CCTCCTTAGAAAGATTTAGACCAGTTCCAAGCG-3′, 5′-CTTTCTAAGGAG GTAGCTGCAATGCTGGGTGACATCTCTGT-3′/5′-GCTGACAACCTCCTTAGATAGATTCTTCGATAACTTTCAGCAG-3′ and 5′-TAT CTAAGGAGGTTGTCAGCATGGAATCTAACCACCAGGT-3′/5′-TGCTCAGCGGTGGCAGCAGCTTAGATTTCGAACTGAGAGGTCA GG-3′, respectively. All fragments were fused by isothermal assembly. pJK6.1 carrying *darA*$_{Pho}$, *darE*$_{Pho}$ and *darH*$_{Pse}$ was created by amplification of pZW-ADC9[2] using the primers 5′-TGCATGCACCTCCTTACGCCGCGATGGTTTGTTTTA-3′/5′-GCTGCTGCCA CCGCTGAG-3′ and synthesized *darH*$_{Pse}$ using the primers 5′-CTCAGCGGTGGCAGCAGCTTAGATTTCGAACTGAGAGGTCA-3′/ 5′-CGTAAGGAGGTGCATGCAATGGAATCTAACCACCAGGT-3′ and subsequent isothermal assembly. After isothermal assembly, *E. coli* Top10 was transformed with the respective plasmids and selected on LB_{Kan} agar (Kan = kanamycin). Single colonies were picked and correct assembly was corroborated by test restriction and subsequent sequencing. For heterologous production of bromodarobactin A, darobactin resistant *E. coli* Bap1(DarR)[2] and *E. coli* Bap1(DarR) + pGro7 were transformed with pLP02, pLP03 and pJK6.1 and selected on LB_{Kan} and $LB_{Kan/Ca}$ agar (Kan = kanamycin; Ca = chloramphenicol), respectively. For heterologous expression, 30 mL LB_{Kan} and $LB_{Kan/Ca}$, supplemented with the respective halide salts were inoculated with *E. coli* Bap1(DarR) + pLP02, *E. coli* Bap1(DarR) + pLP03, *E. coli* Bap1(DarR) + pJK6.1 and *E. coli* Bap1(DarR) + pGro7 + pLP02, *E. coli* Bap1(DarR) + pGro7 + pLP03, *E. coli* Bap1(DarR) + pGro7 + pJK6.1 from over-night cultures, respectively, and incubated at 37°C. At an optical density (OD_{600}) of ~0.5, expression of the darobactin biosynthetic genes was induced by adding 1:1000 IPTG (1 M). Incubation was continued for 3 days at 30°C and 18°C, respectively. Samples were prepared for UPLC-HRMS measurements using C_{18} stage tips. Stage tips were washed with 200 μL 100% MeOH and equilibrated using 200 μL 95:5 H_2O/MeCN +0.1% FA and centrifugation at 3000 rcf. Subsequently, 400–500 μL of cleared supernatant were applied to the stage tips and the C_{18} matrix was washed with 30 μL 95:5 H_2O/MeCN +0.1% FA to remove salts. Finally, the samples were eluted using two times 30 μL 20:80 H_2O/MeCN +0.1% FA and 5 μL of eluate were injected for measurement. Recorded spectra were analyzed with Compass DataAnalysis (Bruker).

DarH$_{Pse}$ expression and purification

pJK9.1 carrying 6xHis-*darH*$_{Pse}$ was created by amplification of pRSFDuett-1 using the primers 5′-CCTTCCCTCGATCTGGCTGT-3′/ 5′-CGAATTCGAGCTCGGCGCGC-3′ and amplification of codon-optimized *darH*$_{Pse}$, using 5′-GCGCGCCGAGCTCGAATTCGTTA GATTTCGAACTGAGAGGTC-3′/5′-ACCATCATCACCACAGCCAGATCGAGGGAAGGATGGAATCTAACCACCAGGT-3′ and subsequent isothermal assembly. After isothermal assembly, *E. coli* Top10 cells were transformed with the respective plasmids and selected on LB_{Kan} agar. Single colonies were picked, correct assembly was corroborated by sequencing and *E. coli* Bap1(DarR) was transformed with pJK9.1. For expressing the His-tagged *darH*$_{Pse}$, 100 mL of LB medium supplemented with chloramphenicol and kanamycin were inoculated with 1 mL of *E. coli* BAP1(DarR) + pGro7 + pJK9.1 overnight culture. When an OD_{600} of ~0.5 was reached, the culture was induced 1:1000 with IPTG (1 M) and incubated at 30°C and 180 rpm overnight. On the next day, the cells

Please cite this article in press as: Böhringer et al., Genome- and metabolome-guided discovery of marine BamA inhibitors revealed a dedicated darobactin halogenase, Cell Chemical Biology (2023), https://doi.org/10.1016/j.chembiol.2023.06.011

were harvested by centrifugation at 9391 rcf for 3 min at 4°C. The following steps were carried out on ice and with precooled buffers. The obtained pellet was resuspended in 4 mL lysis buffer (50 mM $NaH_2PO_4 \cdot 2\ H_2O$, 300 mM NaCl, 10 mM imidazole, pH adjusted to 8 with NaOH). The cells were lysed using ultrasound (70% power, cycle 7, 4 × 35 s with 35 s break between the sonification steps). All further purification steps were carried out according to the manufacturer's protocol (Qiagen, Hilden, Germany). Expression and purification of the flavin reductase for the *in vitro* assay was performed likewise, using *E. coli* BAP1(DarR) + pET28A + FRE.[36] Purified proteins were stored in 10% glycerol at −20°C. Samples of the lysate, the flow through, washing steps and elution steps were collected and stored with 1x SDS-PAGE sample buffer at −20°C until further usage. Analysis of the purification steps was achieved by SDS-PAGE. Two 16% separating gels were prepared by mixing 6 mL ROTIPHORESE Gel 30 (37.5:1) (Carl Roth, Karlsruhe, Germany), 5.1 mL 3x tricine gel buffer (363 g/L tris, 45 mL/L conc. HCl, 3 g/L SDS, pH adjusted to 8.45 with HCl and filtered), 1.5 mL 80% glycerol, 2.4 mL ddH_2O, 60 μL 10% APS and 6 μL TEMED. After casting the gel, it was overlaid with 100% isopropanol and polymerized for 45 min. When completely polymerized, the isopropanol was removed and the separating gel was overlaid with a 4% sample gel (900 μL ROTIPHORESE Gel 30 (37.5:1), 2.3 mL 3x tricine gel buffer, 5.9 mL ddH_2O, 75 μL 10% APS, 7.5 μL TEMED). The gel was allowed to polymerize for 30 min and afterward electrophoresis was performed using the PowerPACTM Basic Power Supply (Bio-Rad Laboratories GmbH, Feldkirchen, Germany) in 1x cathode buffer (60.5 g/L tris, 89.5 g/L tricine, 5 g/L SDS, pH adjusted to 8.25) and 1x anode buffer (60.5 g/L tris, 5 mL HCl, pH adjusted to 8.9) at 60 V until the samples left the sample gel. The electrophoresis was continued with 100 V for about 2 h. Afterward, the gel was stained with Roti-Blue (Carl Roth, Karlsruhe, Germany) according to the manufacturer's protocol.

In vitro halogenation assays

Purified darH (100 μL) was incubated with 10 μL purified flavin reductase, 10 μM FAD, 2.4 mM NADH, 25 mM KBr, 0.15 mM substrate (darobactin A, darobactin B or linear heptapeptide) and 10 mM potassium phosphate buffer (pH 7.2) in a total volume of 300 μL.[37] Reaction controls were performed without the halogenase. The reaction was incubated 24 h at 18°C and stopped by adding an equal amount of methanol before LC-MS analysis.

DarH activity assay with darobactin

His-PlDarH (100 μM) was aerobically incubated with darobactin A (100 μM) in the presence of sodium bromide (25 mM), NAD(P)H (1.0 mM), FAD (10 μM), and flavin reductase (10 μM) in 50 μL buffer H (20 mM HEPES pH 8.0) for 3 h at room temperature. The reaction was initiated by adding darobactin A. After 3 h of incubation, the reaction was diluted twice and boil-quenched at 100°C for 5 min. After removal of precipitation by centrifugation, an aliquot (60 μL) of the supernatant was injected to HPLC equipped with an XSelect Peptide CSH C18 column (Waters) equilibrated in 0.1% TFA in water (Solvent A). The elution was achieved with a flow rate of 1.0 mL/min using solvent A and solvent B (0.1% TFA in MeCN): 10–40% B for 0–20 min. Chromatography was monitored by the L-2455 diode array detector. Another aliquot (5 μL) was analyzed by LC-HRMS. HRMS (ESI-TOF) calcd. for bromo-darobactin ($C_{47}H_{54}N_{11}O_{12}Br$, z = +2) 522.6646, found 522.6645.

DarH timecourse assay with darobactin

His-PlDarH (20 μM) was aerobically incubated with darobactin A (100 μM) in the presence of sodium bromide (25 mM), NAD(P)H (1.0 mM), FAD (5.0 μM) in 200 μL buffer H (20 mM HEPES pH 8.0) for 2 h at room temperature. The reaction was initiated by adding darobactin A. Aliquots of 25 μL were taken out from the master reaction and immediately boil-quenched after 16, 30, 60, and 120 min. Each aliquot was diluted twice and centrifuged to remove precipitation. An aliquot (40 μL) of the supernatant was injected to HPLC equipped with an XSelect Peptide CSH C18 column (Waters) equilibrated in 0.1% TFA in water (Solvent A). The elution was achieved with a flow rate of 1.0 mL/min using solvent A and solvent B (0.1% TFA in MeCN): 10–40% B for 0–20 min. Chromatography was monitored by the L-2455 diode array detector.

DarH activity assay with DarA with ether and C-C crosslinks (P2)

His-PlDarH (20 μM) was aerobically incubated with P2 (30 μM) in the presence of sodium bromide (25 mM), NAD(P)H (1.0 mM), FAD (10 μM) in 20 μL buffer H (20 mM HEPES pH 8.0) for 3 h at room temperature. The reaction was initiated by adding P2. After 3 h of incubation, the reaction was diluted twice and boil-quenched at 100°C for 5 min. After removal of precipitation by centrifugation, the supernatant was treated with proteinase K (100 ng) and an addition of 40 μL buffer K (50 mM Tris-HCl pH 8.0 and 5.0 mM $CaCl_2$) for one hour at 37°C. The reaction mixture was then boil-quenched at 100°C for 5 min. Precipitation was removed, and an aliquot (5 μL) was analyzed by LC-HRMS.

Sequences and structures analysis

BLAST search was performed with *P. luteoviolacea* darobactin halogenase protein sequence as target in the NCBI-BLAST+ database to identify homolog sequences. Independent searches were performed against databases containing structural models and against all publicly available protein sequences in UniprotKB and SwissProt. Multiple sequence alignment (MSA) and maximum likelihood phylogenetic tree, calculated with the bootstrap method and 500 repetitions, were obtained and visualized in MEGA 11.[38] Sequence similarity network (SSN) analysis over the Pfam family 13738 was performed with the Enzyme Function Initiative-Enzyme Similarity Tool (EFI-EST) server,[18] using the 54,603 sequences deposited in Uniprot. The selected SSN was generated with an alignment score threshold of 100 and 40% sequence identity, was visualized in Cytoscape.[39] Structural homologs were visualized, compared, and analyzed in Coot.[40]

Please cite this article in press as: Böhringer et al., Genome- and metabolome-guided discovery of marine BamA inhibitors revealed a dedicated darobactin halogenase, Cell Chemical Biology (2023), https://doi.org/10.1016/j.chembiol.2023.06.011

Synthesis of the heptapeptide by SPPS

The linear heptapeptide was synthesized based on standard Fmoc solid phase chemistry. Fmoc-Phe-Wang resin was chosen as starting material, to which Fmoc-Ser(^{t}Bu)-OH, Fmoc-Lys(Boc)-OH, Fmoc-Ser(^{t}Bu)-OH, Fmoc-Trp(Boc)-OH, Fmoc-Asn(Trt)-OH, Fmoc-Trp(Boc)-OH were coupled respectively. All amino acids, the resin, and the coupling reagent were purchased from Merck Chemicals GmbH (Darmstadt, Germany). Solvents and additional chemicals were purchased from Sigma-Aldrich (Taufkirchen, Germany), TCI Deutschland GmbH (Eschborn, Germany), Fisher Scientific GmbH (Schwerte, Germany), VWR (Darmstadt, Germany), and Carl Roth GmbH+Co. KG (Karlsruhe, Germany). A 5 mL syringe equipped with a PE frit and a Luer cap served as peptide synthesis reactor (Carl Roth GmbH+Co. KG, Karlsruhe, Germany). Agitation was achieved by an IKA-VIBRAX-VXR shaker (IKA, Staufen, Germany).

First the Fmoc-Phe-Wang resin (334.0 mg, 0.64 mmol/g, 0.214 mmol) was was swollen in CH_2Cl_2 (2 mL) for 30 min and then washed with DMF (3 x 2 mL). For every Fmoc cleavage the resin was treated twice for 20–30 min with a 25% piperidine solution in DMF (2 mL for each treatment). Afterward the resin was washed with DMF (4 x 2 mL). In order to control that deprotection was complete, a small sample of the resin was treated with 3 drops DIPEA (10% in DMF) and 3 drops TNBS (1% in DMF), with red beads indicating complete Fmoc removal. For each coupling step 2.5 eq of the amino acid, 2.5 eq HBTU, 2.5 eq HOBt, and 5 eq DIPEA were used. The respective amino acid was mixed with HBTU and HOBt in DMF (2 mL). Then DIPEA was added and the mixture was pre-activated for 10 min before adding the resulting solution to the resin. Each coupling was repeated once, with coupling times ranging from 30 to 40 min. Afterward the resin was washed (3 x 2 mL DMF, 3 x 2 mL CH_2Cl_2, 3 x 2 mL DMF). The coupling was controlled by the above described TNBS-test, with colorless resin beads indicating complete coupling. After completion of the final deprotection, the resin was washed (4 x 2 mL DMF, 6 x 2 mL CH_2Cl_2/MeOH (1:1), 6 x 2 mL Et_2O) and dried overnight by lyophilization. In order to remove the side chain protecting groups and cleave the product from the solid support, the resin was treated for 30 min each with a cleavage mix (4 x 1 mL) consisting of 95% TFA, 2.5% H_2O, and 2.5% triisopropylsilane. After each treatment, the resin was rinsed with 1 mL of the cleavage mix. A total volume of 6 mL filtrate was obtained. The filtrate was divided into two portions of 3 mL each. Under cooling in an ice bath the filtrate (2 x 3 mL) was added dropwise to a Falcon tube containing cold Et_2O (2 x 40 mL) to precipitate the product. When precipitation was complete, the samples were centrifuged (16°C, 4000 rpm, 10 min) and the supernatant was removed. The obtained solid was washed with cold Et_2O (20 mL each), centrifuged again (16°C, 4000 rpm, 10 min) and the supernatant was removed. After drying the resulting solid overnight by lyophilization, a gray crude product was obtained (196.0 mg, 0.205 mmol, 95.8%). The crude product was subsequently purified by HPLC (instrument: Hewlett Packard Series 1100, column: Nucleodur C18 Gravity SB (3 μm, 10 × 250 mm), solvents: A: H_2O + 0.1% formic acid, B: MeCN +0.1% formic acid, flow rate: 2 mL/min, column temperature: rt, gradient: 0 min: 5% B, 0–3 min: 5%–15% B, 3–43 min: 15%–30% B, 43–44 min: 30%–95% B, 44–49 min: 95% B, 49–49.5 min: 95% - 5% B, 49.5–54.5 min: 5% B), yielding the product as an off-white solid. The integral ratio of the ^{1}H-NMR suggested, that the heptapeptide formed a salt with 2 eq formic acid, so that the final product yield amounts to 21.4% (47.8 mg, 0.046 mmol).

HRMS (ESI+, Data S49 and S50): *m/z* calculated for $[C_{47}H_{59}N_{11}O_{11}+H]^+$: 954.4468, found: 954.4465; *m/z* calculated for $[C_{47}H_{59}N_{11}O_{11}+2H]^{2+}$: 477.7271, found: 477.7277.

The MS/MS fragmentation analysis is provided in Data S51.

^{1}H-NMR (400 MHz, DMSO-d_6, Data S20–S23): δ [ppm] = 10.88 (s, 1H), 10.78 (s, 1H), 8.52 (br s, 1H), 8.42 (d, *J* = 7.4 Hz, 1H), 8.16 (d, *J* = 7.7 Hz, 1H), 8.10 (d, *J* = 7.7 Hz, 1H), 7.80 (d, *J* = 7.7 Hz, 1H), 7.59 (t, *J* = 7.4 Hz, 2H), 7.48 (s, 1H), 7.34 (d, *J* = 8.1 Hz, 1H), 7.29 (d, *J* = 8.1 Hz, 2H), 7.22–7.15 (m, 3H), 7.15–7.09 (m, 3H), 7.09–6.99 (m, 3H), 6.95 (t, *J* = 7.4 Hz, 2H), 4.60–4.49 (m, 2H), 4.37 (q, *J* = 6.9 Hz, 1H), 4.30 (q, *J* = 6.3 Hz, 1H), 4.14 (q, *J* = 6.1 Hz, 1H), 4.04 (q, *J* = 6.0 Hz, 1H), 3.67 (dd, *J* = 4.0 Hz, 8.9 Hz, overlayed with H_2O), 3.57 (d, *J* = 5.4 Hz, overlayed with H_2O), 3.21 (d, *J* = 4.4 Hz, 1H), 3.18 (d, *J* = 4.0 Hz, 1H), 3.12 (dd, *J* = 3.8 Hz, 14.5 Hz, 2H), 3.02 (dd, *J* = 5.6 Hz, 13.2 Hz, 2H), 2.98–2.92 (obscr. dd, 1H), 2.88 (dd, *J* = 5.6 Hz, 13.2 Hz, 2H), 2.77 (dd, *J* = 9.3 Hz, 14.5 Hz, 1H), 2.70–2.64 (m, 2H), 2.58–2.52 (obscr. dd, 1H), 2.48–2.41 (obscr. dd, 1H), 1.73–1.60 (m, 1H), 1.57–1.37 (m, 3H), 1.36–1.18 (m, 2H).

^{13}C-NMR (100 MHz, DMSO-d_6, Data S24): δ [ppm] = 173.0, 171.9, 171.34, 171.30, 170.7, 169.4, 168.7, 138.5, 136.3, 136.0, 129.6, 127.7, 127.4, 127.2, 125.8, 124.4, 123.7, 121.0, 120.8, 118.5, 118.4, 118.3, 118.2, 111.4, 111.2, 110.0, 109.1, 61.74, 61.68, 56.9, 55.5, 55.3, 54.1, 53.6, 52.4, 49.6, 38.3, 37.4, 37.3, 32.1, 29.3, 27.32, 27.27, 21.9.

^{1}H-NMR (400 MHz, D_2O, Data S28–S31): δ [ppm] = 8.35 (s, 2H), 7.63–7.59 (m, 1H), 7.51 (d, *J* = 8.0 Hz, 1H), 7.45 (d, *J* = 8.2 Hz, 1H, 7.36–7.33 (m, 1H), 7.31 (d, *J* = 7.4 Hz, 2H), 7.29–7.25 (m, 2H), 7.24–7.19 (m, 3H), 7.17–7.13 (m, 2H), 7.07 (t, *J* = 7.2 Hz, 1H), 6.90 (s, 1H), 4.65 (t, *J* = 6.92 Hz, 1H), 4.53 (pseudo-t, *J* = 7.0 Hz, 1H), 4.46 (dd, *J* = 5.3 Hz, 7.5 Hz, 1H), 4.38 (t, *J* = 5.5 Hz, 1H), 4.30, (t, *J* = 5.5 Hz, 1H), 4.23 (dd, *J* = 6.1 Hz, 8.1 Hz, 1H), 4.18 (t, *J* = 7.2 Hz, 1H), 3.77 (d, *J* = 5.5 Hz, 2H), 3.74 (dd, *J* = 5.9 Hz, 11.7 Hz, 1H), 3.67 (dd, *J* = 5.2 Hz, 11.7 Hz, 1H), 3.28 (dd, *J* = 6.2 Hz, 14.7 Hz, 1J), 3.23–3.15 (obscr. dd, 1H), 3.18–3.11 (obscr. dd, 1H), 3.06 (p, *J* = 7.7 Hz, 2H), 2.98 (dd, *J* = 7.5 Hz, 13.8 Hz, 1H), 2.89 (pseudo-t, *J* = 7.5 Hz, 2H, 2.69 (dd, *J* = 6.5 Hz, 15.6 Hz, 1H), 2.57 (dd, *J* = 7.3 Hz, 15.6 Hz, 1H), 1.80–1.69 (m, 1H), 1.69–1.56 (m, 3H), 1.36–1.26 (m, 2H).

^{13}C-NMR (100 MHz, D_2O): δ [ppm] = 174.8, 174.02, 173.95, 171.9, 171.7, 170.9, 138.1, 136.8, 130.0, 129.1, 127.4, 127.1, 125.6, 125.2, 122.7, 122.6, 120.0, 119.9, 118.8, 118.7, 112.6, 109.2, 107.1, 61.8, 61.7, 56.9, 56.1, 54.2, 54.0, 50.7, 39.8, 38.1, 36.9, 31.0, 27.3, 26.9, 22.5. Some signals are only detectable in the spectrum measured without the addition of MeOH as a standard, due to the better signal intensity (Data S32). But also for the spectrum in Data S32 some peaks are obscured by other signals as apparent from the 2D data.

Please cite this article in press as: Böhringer et al., Genome- and metabolome-guided discovery of marine BamA inhibitors revealed a dedicated darobactin halogenase, Cell Chemical Biology (2023), https://doi.org/10.1016/j.chembiol.2023.06.011

The structure was verified by COSY (Data S25 for measurement in DMSO-d_6, Data S34–S37 for measurement in D_2O), HSQC (Data S26 for measurement in DMSO-d_6, Data S38–S41 for measurement in D_2O) and HMBC (Data S27 for measurement in DMSO-d_6, Data S42–S48 for measurement in D_2O) spectra.

IR (ATR, Data S52): ν [cm^{-1}] = 3281 (w), 2202 (w), 2172 (w), 2051 (w), 1977 (w), 1622 (s), 1537 (s), 1392 (w), 1201 (w), 738 (w).

Optical rotation (c = 0.44% w/v, DMSO): $[\alpha]_D^{28} = -10.39$.

IR spectroscopy

IR spectra were recorded using the attenuated total reflection (ATR) technique on an ALPHA IR spectrometer (Bruker Optics, Ettlingen, Germany). The intensities of the bands are indicated as follows: s = strong, m = medium, w = weak.

Polarimetry

Specific optical rotation was measured on a Jasco P-2000 polarimeter (JASCO Deutschland GmbH, Pfungstadt, Germany) at 589 nm in DMSO (Uvasol, Merck KGaA, Darmstadt, Germany).

NMR spectroscopy

Samples of biosynthetic darobactin A derivatives were dissolved in DMSO-d_6, while samples of the synthetic heptapeptide were measured in D_2O as well as in DMSO-d_6. The spectra of dehydrodarobactin A on the other hand were recorded in a mixture of D_2O/MeCN-d_3 (2:1). NMR spectra of darobactin A (**1**), bromodarobactin A (**2**), dehydrobromodarobactin A (**4**), and the linear heptapeptide were acquired on Bruker Avance III HD 600 MHz (^{1}H: 600.05 MHz; ^{13}C: 150.88 MHz), Bruker Avance III HD 400 MHz (^{1}H: 400.25 MHz; ^{13}C: 100.64 MHz), and Bruker Avance II 400 MHz (^{1}H: 400.13 MHz; ^{13}C: 100.61 MHz) NMR spectrometers (Bruker BioSpin GmbH, Ettlingen, Germany). The spectra of dehydrodarobactin A (**3**) were recorded at 300 K on a Bruker AVANCE *NEO* 700 spectrometer (^{1}H: 700.13 MHz; ^{13}C: 176.05 MHz) equipped with a 5 mm TCI cryo probe. For bromodarobactin A and dehydrobromodarobactin A ^{1}H-NMR spectra were additionally measured with double solvent suppression and COSY spectra were recorded with multiple solvent suppression and ^{13}C-decoupling in order to improve the signal to noise ratio. The HSQC spectrum of bromodarobactin A was measured on the 400 MHz NMR spectrometer, because this instrument was equipped with a more sensitive inverse probe. Due to the low sample amounts of biosynthetic darobactins, ^{13}C shifts were obtained from the respective HSQC spectra. The obtained spectra were referenced to the residual solvent signal (DMSO-d_6: δ_H = 2.50 ppm, δ_C = 39.52 ppm, D_2O: δ_H = 4.79 ppm, MeCN-d_3: δ_H = 1.94 ppm, δ_C = 1.32 ppm).[41] For calibration of ^{13}C spectra recorded in D_2O a drop of methanol (δ_C = 49.50 ppm) was added as an internal standard prior to measurement.[41] Yet, as the addition of MeOH impaired the signal intensity both ^{13}C spectra, with (Data S33) and without (Data S32) addition of MeOH, are shown. Analysis of NMR spectra was accomplished using the software TopSpin 3.6.0 and TopSpin 4.1.1 (Bruker BioSpin GmbH, Ettlingen, Germany). Chemical shifts are given in ppm and coupling constants in Hz. Prediction of ^{13}C shifts was carried out using ChemDraw 16.0 Professional (PerkinElmer, Waltham, USA).

Binding site calculation and molecular docking

AlphaFold (AF)[16] was used to generate a 3D model from the DarH$_{Pse}$ sequence. We then built hydrogen atoms and the protonation states and the geometry were optimized with the Protein Preparation Wizard.[42] The putative binding sites in the protein were calculated using the SiteMap program from the Schrödinger Suite.[20–22] To dock the FAD in the DarH$_{Pse}$ AF model, we calculated a receptor grid using the points that define binding site 1 (part where the FAD of YpdA fitted, see Figure S12). The FAD ligand was prepared with LigPrep and was docked on the receptor grid using the SP and XP procedures in Glide.[43–45] The pose with the top XP score (−13.6) is shown in Figure S13A. Attempts to dock the NAD(P), using a grid generated from the part of binding site 1 where the NAD(P) binding motif (Figure S13A) was identified, did not succeed. This is most probably due to the fact, contrary to the one recognizing FAD, that the NAD(P) binding motif is relatively small and thus all other residue sidechains in this part of the cavity might be misplaced by AF which prevented us from obtaining a reasonable pose for NAD(P) docking.

QUANTIFICATION AND STATISTICAL ANALYSIS

One- and two-dimensional NMR spectroscopy as well as LC-HRMS/MS analysis were employed for qualitative substance characterization. A quantitative determination of substance amount/purity was not carried out.

Manuscript 2: Functional *in vitro* and *in vivo* analysis of biosynthetic genes by heterologous expression in *E. coli*

Status: published on 09/15/2023

Author's contributions: study design, experiments, data analysis, manuscript writing, figure design.

STAR Protocols

CellPress
OPEN ACCESS

Protocol

Functional *in vitro* and *in vivo* analysis of biosynthetic genes by heterologous expression in *E. coli*

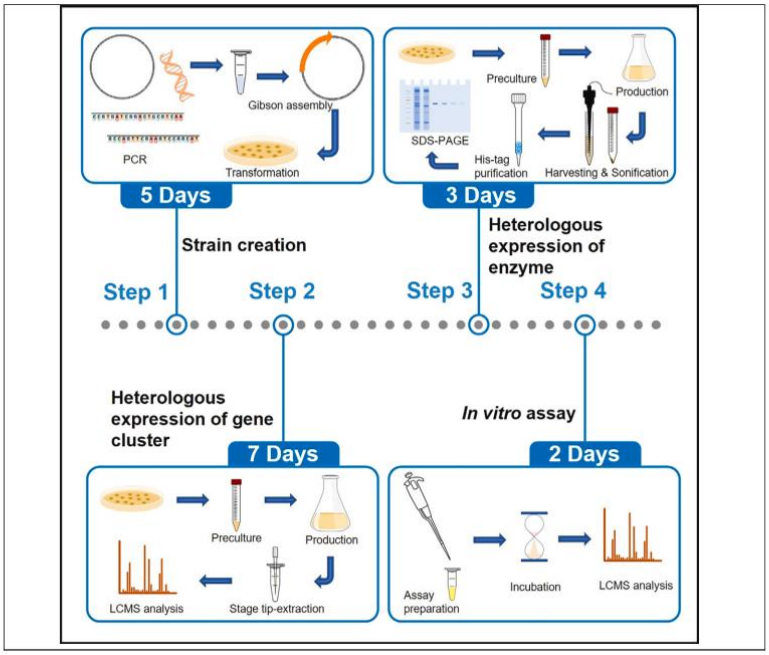

Biosynthetic gene clusters of natural products often harbor genes of unknown function, which are difficult to characterize. Here, we present a protocol for the functional analysis *in vitro* and *in vivo* of these biosynthetic genes by heterologous expression in *E. coli*. We describe steps for the expression of genes of interest in an established *E. coli* strain optimized to heterologously express natural products. We then detail the expression of a His-tagged gene to deduce the specific function of the protein.

Publisher's note: Undertaking any experimental protocol requires adherence to local institutional guidelines for laboratory safety and ethics.

Jil-Christine Kramer, Nils Böhringer, Ute Mettal, Till F. Schäberle

ute.mettal@chemie.uni-giessen.de (U.M.)
till.schaeberle@ime.fraunhofer.de (T.F.S.)

Highlights

Explanation of primer design to clone a gene of interest by Gibson assembly

Heterologous expression of cloned genes of interest

Purification of new proteins with unknown function by His-tag affinity chromatography

In vitro assay to test the activity of the expressed protein *in vitro*

Kramer et al., STAR Protocols 4, 102531
September 15, 2023 © 2023 The Author(s).
https://doi.org/10.1016/j.xpro.2023.102531

STAR Protocols

CellPress
OPEN ACCESS

Protocol

Functional *in vitro* and *in vivo* analysis of biosynthetic genes by heterologous expression in *E. coli*

Jil-Christine Kramer,[1,4] Nils Böhringer,[1,2] Ute Mettal,[1,*] and Till F. Schäberle[1,2,3,5,*]

[1]Institute for Insect Biotechnology, Division for Natural Product Research; Justus-Liebig-University Giessen, Ohlebergsweg 12, 35392 Giessen, Germany

[2]German Center for Infection Research (DZIF); Partner Site Giessen-Marburg-Langen, Ohlebergsweg 12, 35392 Giessen, Germany

[3]Natural Product Department; Fraunhofer-Institute for Molecular Biology and Applied Ecology (IME), Ohlebergsweg 12, 35392 Giessen, Germany

[4]Technical contact: jil-christine.kramer@agrar.uni-giessen.de

[5]Lead contact

*Correspondence: ute.mettal@chemie.uni-giessen.de (U.M.), till.schaeberle@ime.fraunhofer.de (T.F.S.)
https://doi.org/10.1016/j.xpro.2023.102531

SUMMARY

Biosynthetic gene clusters of natural products often harbor genes of unknown function, which are difficult to characterize. Here, we present a protocol for the functional analysis *in vitro* and *in vivo* of these biosynthetic genes by heterologous expression in *E. coli*. We describe steps for the expression of genes of interest in an established *E. coli* strain optimized to heterologously express natural products. We then detail the expression of a His-tagged gene to deduce the specific function of the protein.

For complete details on the use and execution of this protocol, please refer to Böhringer et al.[1]

BEFORE YOU BEGIN

The protocol below describes the specific steps for the heterologous expression of genes of interest that putatively encode unknown functionalities in an *E. coli* K12 strain. By adjusting cultivation conditions this protocol can be used for the heterologous expression in every *E. coli* strain.

General preparation

1. Autoclave the equipment for the work with bacteria (e.g., pipette tips, flasks).
2. Produce and autoclave liquid and solid LB medium according to the recipe in the materials and equipment.
3. Prepare stock solutions as described in materials and equipment.
4. Prepare buffers according to the materials and equipment section.

⚠ CRITICAL: When working with DNA or proteins, gloves should be worn to prevent contaminations with DNases or proteases. When handling bacteria or bacterial cultures the work should be performed under a sterile bench or at least next to a flame and gloves should be used. Every material or liquid that was in contact with bacteria should be autoclaved before disposal and liquids that include solvents should be discarded properly.

Preparation of electrocompetent *E. coli* Top10 and *E. coli* Bap1(Dar^R)/pGro7 cells

Timing: 2 days

5. Inoculate the precultures.
   a. Inoculate 4 mL LB medium with *E. coli* Top10 cells in a 15 mL falcon tube and 4 mL LB medium containing chloramphenicol with *E. coli* Bap1(Dar^R)/pGro7 cells.
   b. Incubate overnight at 180 rpm and 37°C.
6. Inoculation of the main culture.
   a. On the next day transfer 1 mL of each preculture in 20 mL fresh LB medium with or without chloramphenicol, respectively.
   b. Incubate at 180 rpm and 37°C until the culture reaches an OD_{600} value of 0.5.
      i. Measure the OD_{600} for the first time 30 min after inoculation.
      ii. Use a 20 min doubling time for *E. coli* to calculate the estimated time until the culture reaches the planned OD_{600}.

Note: The OD_{600} value should be measured in regular intervals, even before reaching the estimated end point to check whether the calculated time is correct. If the cells are overgrown, restart the experiment using 1 mL of the remaining overnight culture. An OD_{600} in the range of 0.48 up to 0.6 is acceptable.

7. After reaching an OD_{600} value of 0.5, wash the cells with sterile and ice cold 10% glycerol.
   a. The following steps have to be carried out on ice.
   b. Harvest the cell pellet by centrifugation at 10.000 × *g* and 4°C for 3 min.
   c. Decant the supernatant and resuspend the pellet in 2 mL 10% glycerol.
   d. Wash the cells by centrifugation at 10.000 × *g* and 4°C for 3 min.
   e. Repeat the washing step.
   f. Discard the supernatant and resuspend the pellet in 1 mL 10% glycerol.
   g. Prepare aliquots of 50 µL.
   h. Cells can be directly used for the transformation or stored at −80°C for approx. 3 months.

Ordering of codon optimized genes of interest

Timing: 1 h

8. Codon optimize your region of interest with an online tool.
   a. For the codon optimization you can either use a web-based tool (e.g., JCat[2]) or the tool provided by the supplier of DNA.
   b. Follow instructions given by the software.
9. Before ordering the codon optimized sequence it is useful to attach a ribosomal binding site to your gene.
   a. Attach upstream of your gene of interest the ribosomal binding site (e.g., GGAGG) followed by a spacer consisting of eight random bases before the start codon of the gene of interest.

Note: You also have the option to introduce the ribosomal binding site by PCR.

Design of primers

Timing: 1–3 h

10. Design a forward and a reverse primer binding to your gene of interest with overlaps to the plasmid sequence using a suitable cloning software, e.g., SnapGene (see Figure 1).[3]
    a. Select 18–21 bp on both sides of your gene of interest.
       i. Shorten the primer (not less than 18 bp) if the melting temperature is above 70°C.

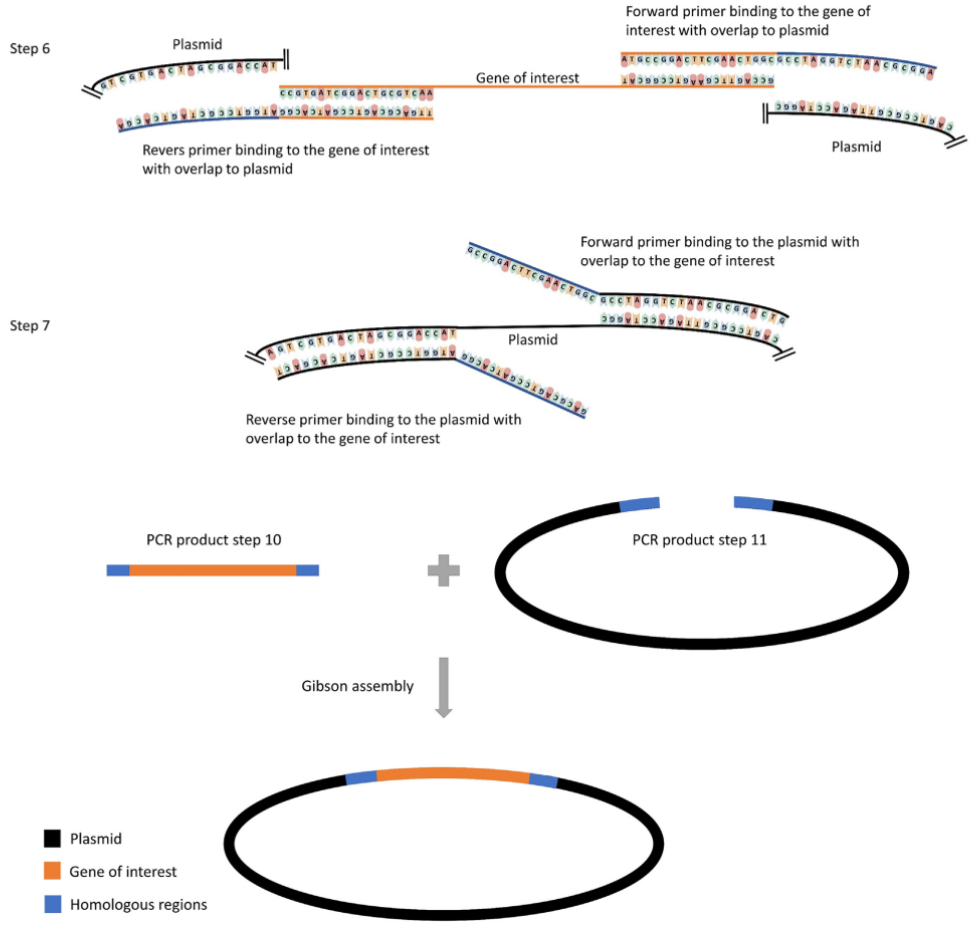

Figure 1. Scheme of primer design and Gibson assembly strategy for the heterologous expression of a gene of interest

Top: Visualization of the primer design (step 10 and 11). Step 10 indicates the binding sites and heterologous regions of the forward and reverse primers for the amplification of the gene of interest and step 11 shows the forward and reverse primers for the amplification of the plasmid backbone (shown in black). These primers carry a region homologous to the primers of step 10 (indicated in blue). Bottom: Gibson assembly components and the finished plasmid carrying the gene of interest (orange).

b. Copy the sequences left and right of the insertion point (18–21 bp, the melting temperature of this primer part should not be noticeably higher than 50°C because of the Gibson assembly) on your plasmid and attach them, according to the orientation of your gene, to the bases selected on your gene of interest.

Optional: Include the ribosomal binding site and the eight base spacer upstream of the gene of interest (between the binding site of the gene of interest and the plasmid sequence).

11. Design forward and reverse primers for the amplification of the plasmid with overlaps to the gene of interest (see Figure 1).
    a. Select the sequence located on the plasmid from step 10b to create the forward and reverse primers.
    b. Copy the sequence of the forward and reverse primers of the gene of interest (step 10a) and attach it to the primer homologous to the plasmid.
12. As a control perform a virtual Gibson assembly[4] using SnapGene.[3]
13. Check whether the gene is inserted in the correct position and orientation.
14. Order the primers at your standard supplier.

KEY RESOURCES TABLE

REAGENT or RESOURCE	SOURCE	IDENTIFIER
Bacterial and virus strains		
Escherichia coli Top10	Invitrogen	Cat#C404050
Escherichia coli Bap1(Dar^R)	Wuisan et al.[5]	N/A
Escherichia coli Bap1(Dar^R)/pGro7	This paper	N/A
Escherichia coli Top10/pJK6.1	This paper	N/A
Escherichia coli Top10/pJK9.1	This paper	N/A
Escherichia coli Bap1(Dar^R)/pGro7/pJK6.1	This paper	N/A
Escherichia coli Bap1(Dar^R)/pGro7/pJK9.1	This paper	N/A
Oligonucleotides		
Primer: JCK7_pRSF_Gib_rv for constructing pJK6.1 binding pZW-ADC9; reverse: TGCA TGCACCTCCTTACGCCGCGATGGTTTGTTTTA	This paper	N/A
Primer: JCK8_pRSF_Gib_fw for constructing pJK6.1 binding pZW-ADC9; forward: GCTG CTGCCACCGCTGAG	This paper	N/A
Primer: JCK13_FAD_pRSF_Gib_rv for constructing pJK6.1 binding *darH*; reverse: CTCAGCGGTGGC AGCAGCTTAGATTTCGAACTGAGAGGTCA	This paper	N/A
Primer: JCK12_FAD_pRSF_Gib_fw for constructing pJK6.1 binding *darH*; forward: CGTAAGGAGGTG CATGCAATGGAATCTAACCACCAGGT	This paper	N/A
Primer: JCK28_pRSF_duet_His.XA_Gib_rv for constructing pJK9.1 binding pRSFDuett-1; reverse: CCTTCCCTCGATCTGGCTGT	This paper	N/A
Primer: JCK27_pRSF_duet_His.Xa_Gib_fw for constructing pJK9.1 binding pRSFDuett-1; forward: CGAATTCGAGCTCGGCGCGC	This paper	N/A
Primer: JCK26_FAD_His-tag_Gib_rv for constructing pJK9.1 binding *darH*; reverse: GCGCGCCGAGCTCGAATTCGTTAGATTT CGAACTGAGAGGTC	This paper	N/A
Primer: JCK25_FAD_His-tag_Gib_fw for constructing pJK9.1 binding *darH*; forward: ACCATCATCACCACAGCCAGATCGAGG GAAGGATGGAATCTAACCACCAGGT	This paper	N/A
Recombinant DNA		
pJK6.1	This paper	N/A
pJK9.1	This paper	N/A
pGro7	Takara	Cat#3340
pZW-ADC9	Wuisan et al.[5]	N/A
pRSFDuett-1	Novagen	Cat#71341
Software and algorithms		
SnapGene	GSL Biotech LLC[3]	https://www.snapgene.com/

MATERIALS AND EQUIPMENT

Lysogeny broth (LB medium)	
Reagent	Amount
Tryptone	10 g/L
Yeast extract	5 g/L
Sodium chloride (NaCl)	5 g/L
Adjust pH to 7.0	
Store at room temperature. Can be stored for a year.	

Antibiotics and supplements		
Reagent	Stock solution	Working concentration
Chloramphenicol	20 mg/mL	20 μg/mL
Isopropyl-β-D-thiogalactopyranoside (IPTG)	1 M	1 mM
Kanamycin	50 mg/mL	50 μg/mL
Potassium bromide (KBr)	100 mg/mL	100 μg/mL
Aliquots of the stock solutions can be stored at −20°C for a year.		

⚠ CRITICAL: Chloramphenicol, kanamycin, and potassium bromide are hazardous substances. When handling them personal safety equipment should be used.

TAE buffer 50× (1 L)		
Reagent	Final concentration	Amount
Tris base	2 M	242 g
Acetic acid	1 M	57.1 mL
EDTA disodium salt	0.05 M	18.612 g
Store at room temperature for up to a year.		

⚠ CRITICAL: Acetic acid is a corrosive and flammable substance and should be handled under a fume hood. EDTA is hazardous and should just like acetic acid be handled with personal safety equipment.

QIAGEN lysis buffer[6] (1 L)		
Reagent	Final concentration	Amount
$NaH_2PO_4 \times H_2O$	50 mM	6.90 g
NaCl	300 mM	17.54 g
Imidazole	10 mM	0.68 g
Adjust pH to 8.0 with NaOH		
Store at 4°C for a year.		

QIAGEN wash buffer[6] (1 L)		
Reagent	Final concentration	Amount
$NaH_2PO_4 \times H_2O$	50 mM	6.90 g
NaCl	300 mM	17.54 g
Imidazole	20 mM	1.36 g
Adjust pH to 8.0 with NaOH		
Store at 4°C for a year.		

QIAGEN elution buffer[6] (1 L)		
Reagent	Final concentration	Amount
$NaH_2PO_4 \times H_2O$	50 mM	6.90 g
NaCl	300 mM	17.54 g
Imidazole	250 mM	17.00 g
Adjust pH to 8.0 with NaOH		
Store at 4°C for a year.		

⚠ CRITICAL: Imidazole is a hazardous, corrosive substance and should be handled with personal safety equipment.

- 10% glycerol: Add 5 mL glycerol to 45 mL ddH_2O. Autoclave before usage. Store at room temperature for up to a year.
- Eluent 1: Add 50 mL acetonitrile to 950 mL ddH_2O and 1 mL formic acid. Can be stored for a year at room temperature
- Eluent 2: Add 200 mL acetonitrile to 800 mL ddH_2O and 1 mL formic acid. Can be stored for a year at room temperature
- Potassium phosphate buffer pH 7.2: Dissolve 10.73 g K_2HPO_4 and 5.23 g KH_2PO_4 in 800 mL ddH_2O. Then adjust to a final volume of 1 L with ddH_2O. Can be stored for 2 years at room temperature.

⚠ CRITICAL: Acetonitrile is a flammable and harmful substance and formic acid is a toxic, corrosive and flammable substance. When working with both of them personal safety equipment should be used and they should be handled under the fume hood.

STEP-BY-STEP METHOD DETAILS

Strain construction

Timing: 5 days

This step describes how the plasmids and strains for the heterologous expression of the biosynthetic gene cluster as well as for the expression of the His-tagged protein are constructed.

1. Perform PCRs of the Gibson assembly fragments.
   a. Mix the components of the PCR reactions according to the table providing the PCR reaction master mix.

Note: Sequences of the primers can be found in the key resources table.

PCR reactions			
Primer	Construct	Binding site	Length
JCK7_pRSF_Gib_rv JCK8_pRSF_Gib_fw	pJK6.1	pZW-ADC9[5]	5704 bp
JCK13_FAD_pRSF_Gib_rv JCK12_FAD_pRSF_Gib_fw	pJK6.1	*darH*	1555 bp
JCK28_pRSF_duet_His.XA_Gib_rv JCK27_pRSF_duet_His.Xa_Gib_fw	pJK9.1	pRSFDuett-1	3838 bp
JCK26_FAD_His-tag_Gib_rv JCK25_FAD_His-tag_Gib_fw	pJK9.1	*darH*	1570 bp

Note: Primer JCK28_pRSF_duet_His.XA_Gib_rv binds to an already in pRSFDuett-1 included factor XA cutting site.

PCR reaction master mix	
Reagent	Amount
Q5 reaction buffer (5×)	5 μL
dNTP mix (10 mM each)	0.5 μL
Primer 1 (10 pmol/μL)	0.625 μL
Primer 2 (10 pmol/μL)	0.625 μL
Q5 Polymerase (2 U/μL)	0.125 μL
Template DNA (10–15 ng/μL)	1 μL
ddH_2O	17.125 μL

b. Calculate the correct extension time for the length of your fragment.
   i. For Q5 polymerase use an extension time of 45 s per 1 kb for complex, GC-rich templates.
   ii. Run the PCR with the protocol outlined in the PCR cycling conditions table. (The table shows the extension time for *darH* in pJK6.1.)

PCR cycling conditions			
Steps	Temperature	Time	Cycles
Initial Denaturation	95°C	3 min	1
Denaturation	95°C	30 s	35 cycles
Annealing	50°C	30 s	
Extension	72°C	1 min 10 s	
Final extension	72°C	5 min	1
Hold	10°C	10 min	1
Final Hold	4°C	Forever	

Pause point: The PCR reaction can be stored overnight at 4°C prior to agarose gel electrophoresis and DNA purification.

2. Perform agarose gel electrophoresis for checking the PCR results.
   a. Prepare a 1% agarose gel.
      i. Place the gel tray in a gel caster to seal the edges of the gel tray and put a comb with an appropriate number of wells in the comb guide of the gel tray.
      ii. Weigh in 0.4 g agarose and suspend it in 40 mL 1× TAE buffer. Heat the suspension in a microwave to dissolve the agarose.
      iii. After the agarose is completely dissolved add 4 μL SYBR safe.
      iv. Pour the gel into the gel tray and let it polymerize for approx. 20 min.
   b. Loading and running the gel.
      i. Prepare the electrophoresis chamber by filling in 1× TAE buffer.
      ii. Place the gel in the electrophoresis chamber
      iii. Prepare a small strip of parafilm.
      iv. Take out 3 μL of 6× loading dye and divide it in two drops on the parafilm (one drop per PCR sample).
      v. Use 3 μL of each PCR reaction and mix it with the loading dye drop on the parafilm (be careful to keep the drops separated) and load the mixture into the wells of the gel starting with the second well.
      vi. Add 10 μL of DNA Ladder into the first well and run the gel for 30 min at 120 V.
   c. Analyze the gel under UV light.
   d. PCR reactions yielding signals of the correct size (see Figure 2) can be purified by a PCR purification kit (troubleshooting).

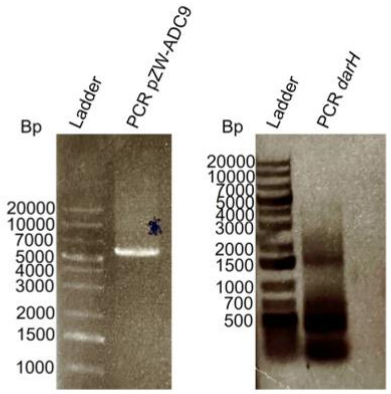

Figure 2. Agarose gel of the PCR reactions for the construction of pJK6.1

Left: Agarose gel of the amplification of pZW-ADC9 with JCK7 and JCK8. A signal at the expected size of 5704 bp can be observed. The PCR reaction can be purified with a PCR purification kit and used for Gibson assembly. Right: Agarose gel of the PCR reaction of *darH* with JCK12 and JCK13. A signal at the expected size of 1555 bp can be detected. However, since there are other unspecific signals it is recommended to purify this signal from the gel before using it for a Gibson assembly.

Optional: After amplification of the plasmid backbone the sample can be treated with DpnI to get rid of template plasmid DNA to avoid false positives in the Gibson assembly.

Note: If the PCR shows unspecific signals (i.e., fragments not showing the desired size in the agarose gel analysis), it is more suitable to purify the desired fragment by cutting the correct signal from the gel.

Pause point: Unpurified PCR reactions can be stored at 4°C or −20°C until next day. Purified DNA should be stored at −20°C until further usage.

3. Perform a Gibson assembly using the PCR fragments (see Figure 1).
   a. For 2–3 fragments use 0.02–0.5 pmol of DNA.
      i. For calculating the required amount of the fragments use the following equation: $pmol = (weight\ in\ ng) \times \frac{1000}{(base\ pairs \times 650\ daltions)}$ or the NEBioCalculator tool.[7,8]
      ii. Add the calculated volume of DNA to the Gibson assembly master mix[4] and adjust the volume to 20 µL with ddH_2O.
      iii. Incubate the mixture for 1 h at 50°C in a thermocycler.
   b. Remove the salts from the assembled plasmid.
      i. Fill a Petri dish (Ø94 mm) approx. three quarters with ultrapure water.
      ii. Place a MF-Millipore 0.025 µm MCE Membrane filter (13 mm) on the water surface.
      iii. Carefully pipette the Gibson assembly mixture on the filter and incubate it with closed lid for 1 h.
      iv. After incubation carefully transfer the Gibson assembly mixture into an Eppendorf tube.

⚠ CRITICAL: When placing the membrane filter disk on the water do not touch it with your hands. Use a forceps to carefully take it from the packing and wear gloves.

4. Transform the assembled plasmid with *E. coli* Top10.
   a. Thaw the competent cells on ice (when freshly prepared skip this step).
   b. Add 5 µL of the salt free Gibson assembly mix from step 3b.
   c. Transfer the mixture into an electroporation cuvette (0.2 cm gap) and make sure the liquid is at the bottom of the cuvette and free from air bubbles.
   d. Place the cuvette in an electroporator (MicroPulser; Bio-Rad) and apply a voltage of 2.5 kV (bacteria Ec2). (A typical time constant is ~5 ms.)

e. Immediately add 800 μL LB medium and mix gently by pipetting up and down.
f. Transfer the culture into a 2 mL Eppendorf tube and incubate for 1 h at 37°C.
g. After incubation centrifuge the culture for 4 min at 3000 × *g*.
h. Decant the supernatant until only approx. 200 μL are left.
i. Resuspend the cell pellet in the remainder of the supernatant and spread it on an LB agarose plate containing kanamycin.
j. Incubate the agar plate overnight at 37°C (troubleshooting).

5. Verify the correct assembly of the plasmid.
   a. Pick colonies and plate them on a fresh LB agar plate containing kanamycin. Simultaneously, use the same colonies to inoculate 4 mL liquid LB medium containing kanamycin in a 15 mL falcon tube.
      i. Mark fields on a Petri dish and number them. Add liquid LB agar containing kanamycin and allow the agar to solidify. Fill three 15 mL flacon tubes with 4 mL LB medium supplemented with kanamycin and number them from one to three.
      ii. Use an autoclaved toothpick to pick up one colony, streak it in field number 1 and transfer the toothpick into the liquid medium of falcon tube number one.
      iii. Repeat this step with two more colonies.
      iv. Plate 10 to 15 more colonies without inoculation in liquid medium in case you want to test more colonies later on.
      v. Incubate the agar plate at 37°C and the liquid cultures at 180 rpm and 37°C overnight.
   b. On the next day isolate the plasmids using a bacterial plasmid isolation kit and wrap the agar plate in parafilm for long-term storage at 4°C.

Pause point: Purified plasmids are stable for months if they are stored at −20°C.

   c. Perform a restriction digest with the three isolated plasmids.
      i. Choose a restriction enzyme that preferably has a cutting site in your plasmid and in the newly inserted fragment, for example EcoRI for pJK6.1 and *Sma*I for pJK9.1.
      ii. Measure the plasmid concentration with a NanoDrop.
      iii. Calculate the volume needed for an amount of 1000 ng of plasmid.
      iv. The volume of the restriction digest mix should be approx. 2.5× bigger than the plasmid volume. Calculate the ingredients as it can be seen in the table for the restriction digest reaction mix.
      v. Prepare the restriction digest reaction mix by combining the ingredients in the calculated amounts and incubate for 1 h. The incubation temperature needs to be chosen according to the specific incubation temperature of the selected restriction enzyme.
      vi. Perform an agarose gel electrophoresis as described in step 2 by adding the appropriate amount of 6× loading dye and loading the whole reaction mix to the wells of the gel.
      vii. In case the correct restriction pattern appears on the gel the plasmid should be sent for sequencing with primers covering the overlapping part of the plasmid to the insert from both sides (see Figure 3).

Restriction digest reaction mix		
11.76 μL Plasmid 1 (85 ng/μL)	10 μL Plasmid 2 (100 ng/μL)	12.5 μL Plasmid 3 (80 ng/μL)
1 μL Restriction enzyme	1 μL Restriction enzyme	1 μL Restriction enzyme
3 μL Buffer	2.5 μL Buffer	3.1 μL Buffer
14.24 μL ddH_2O	11.5 μL ddH_2O	13.4 μL ddH_2O
Total 30 μL	Total 25 μL	Total 31 μL

6. Compare the sequence of the theoretical construct in SnapGene[3] with the experimentally obtained sequence to verify the assembled plasmid.

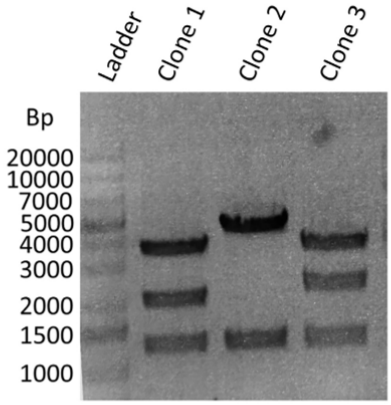

Figure 3. Agarose gel of the restriction digest of three pJK6.1 plasmids isolated from three different colonies using *Eco*RI

Expected is a pattern with signals at 3536 bp, 2257 bp, 1251 bp, and 177 bp. Clones 1 and 3 show the correct pattern (177 bp not shown due to low signal intensity). The Gibson assembly of these two plasmids was most likely successful and they can be sent for a final sequencing check.

7. Transform a mutation free and correctly assembled plasmid with competent *E. coli* Bap1(Dar^R)/pGro7 cells as described in step 4 (but using kanamycin and chloramphenicol) to create the production strain.
8. Create glycerol stocks of the Top10 and Bap1 strains for long-term storage at −80°C.
   a. Inoculate 4 mL LB medium supplemented with kanamycin with the colony from the stored *E. coli* Top10 plate that possesses the correct plasmid. Likewise, inoculate 4 mL LB medium containing kanamycin and chloramphenicol with a colony of the *E. coli* Bap1/pGro7 strain created in step 7. Both cultures are prepared in 15 mL falcon tubes.
   b. Incubate them overnight at 37°C and 180 rpm.
   c. The next day take 600 µL from the culture and add them to a cryotube containing 600 µL sterile 50% glycerol.
   d. Carefully mix by pipetting up and down and store the tube at −80°C.

Heterologous expression of the gene cluster

Timing: 7 days

In this section, the whole gene cluster of the natural product containing the gene of unknown function is expressed using the strain *E. coli* Bap1/pGro7/pJK6.1, whose construction is outlined in the section "strain construction".

9. Inoculate 4 mL LB medium supplemented with chloramphenicol and kanamycin with *E. coli* Bap1/pGro7/pJK6.1 in a 15 mL falcon tube and incubate it overnight at 37°C and 180 rpm.
10. On the following day inoculate 20 mL LB medium containing kanamycin and chloramphenicol with 1 mL of the overnight culture in a 100 mL flask. Incubate at 37°C and 180 rpm.
11. Incubate the cells until an OD_{600} value of 0.5 is reached, as described in the section preparation of electrocompetent *E. coli* Top10 and *E. coli* Bap1(Dar^R)/pGro^7 cells.

Note: If the cells are overgrown, restart the experiment using 1 mL of the remaining overnight culture. An OD_{600} value in the range of 0.48 up to 0.6 is acceptable.

12. Induce the production by adding IPTG to the culture as well as KBr (materials and equipment) and continue incubation for 3 days at 18°C and 180 rpm.

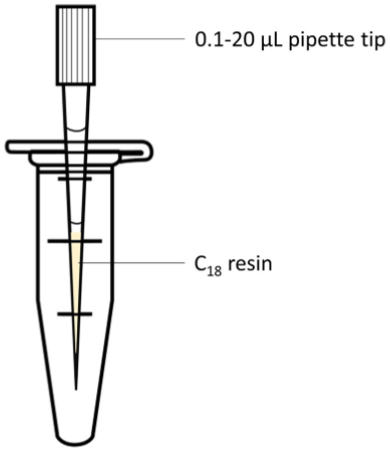

Figure 4. C_{18} stage tip column set up

13. After 3 days of incubation take a sample and prepare it for LCMS measurement.
    a. Take a 500 µL sample from the culture and centrifuge it at 15.000 × *g* for 4 min. The supernatant will be added to the tip column later, as described in step 13f.
    b. During centrifugation prepare a stage tip column as it can be seen in Figure 4.
        i. Heat a hex wrench with a Bunsen burner and use it to pierce a hole into the lid of a 2 mL Eppendorf tube.
        ii. Use a cannula to punch out two pieces (approx. 1 mm in diameter) of an Empore Octadecyl C18 47 mm extraction disk and push it into the tip of a pipette tip.

    Note: When pushing the C_{18} sorbent into the tip, do not use too much force to pack the sorbent too tightly. The sorbent should fit into the tip, but must not be pushed deeply into it.

    c. Equilibrate the column with 200 µL methanol by centrifugation at 3000 × *g* and 4°C for 4 min.
    d. Remove the flowthrough and add 200 µL eluent 1 (5% acetonitrile with 0.1% formic acid, see also materials and equipment).
    e. Centrifugate for 4 min at 3000 × *g* and 4°C.
    f. Discard the flowthrough and add 200 µL of the sample supernatant.
    g. Centrifugate for 4 min at 3000 × *g* and 4°C.

    ⚠ CRITICAL: Methanol is a flammable, toxic and hazardous substance. Methanol should be handled carefully with personal safety equipment and it should be handled and under the fume hood.

    Note: The sample should pass through the column completely. If this is not the case after 4 min the centrifugation time can be increased. If prolonging the centrifugation time is not sufficient, the speed can be increased up to 4000 × *g*.

    h. After the sample has passed through the column another 200 µL can be added and the centrifugation step is repeated.
    i. Wash the column with 30 µL eluent 1 by centrifugation at 3000 × *g* and 4°C for 4 min.
    j. Elute the column by adding 30 µL eluent 2 (20% acetonitrile with 0.1% formic acid, see also materials and equipment).

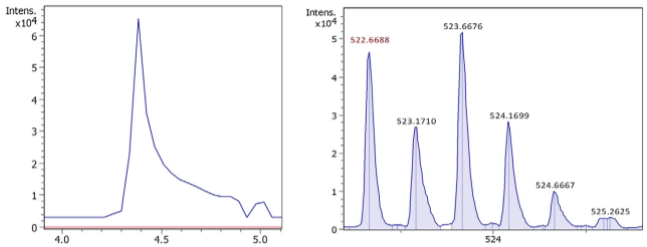

Figure 5. Extracted ion chromatogram (EIC, calc. $[M + 2H]^{2+} \pm 0.01$ Da) and mass spectrum of bromodarobactin A ($C_{47}H_{54}N_{11}O_{12}Br$, 522.6641 *m/z*)

Left: Extracted ion chromatograms of bromodarobactin A of the control sample (pZW-ADC9, without *darH*, *red*) and of a pJK6.1 sample (blue). A peak is present in the pJK6.1 sample, but not in the control. Right: Mass spectrum of bromodarobactin A displaying the typical isotopic pattern of a brominated compound.

k. Centrifugate for 4 min at 3000 × *g* and 4°C.
l. Repeat the elution step.
m. Transfer the sample to a LCMS vial, submit the sample to LCMS measurement and analyze the obtained data (Figure 5, troubleshooting).

⚠ CRITICAL: Eluent 1 and 2 should be handled with personal safety equipment and under the fume hood.

Heterologous expression of the His-tagged enzyme

Timing: 3 days

14. Inoculate 4 mL LB medium supplemented with chloramphenicol and kanamycin with *E. coli* Bap1/pGro7/pJK9.1 in a 15 mL falcon tube. Incubate overnight at 37°C and 180 rpm.
15. The next day inoculate 100 mL LB medium containing kanamycin and chloramphenicol with 1 mL of the overnight culture in a 300 mL flask. Incubate at 37°C and 180 rpm.
16. Incubate the cells until an OD_{600} value of 0.5 is reached as described in the section preparation of electrocompetent *E. coli* Top10 and *E. coli* Bap1(Dar^R)/$pGro^7$ cells.

Note: If the cells are overgrown, restart the experiment using 1 mL of the remaining overnight culture. An OD_{600} value in the range of 0.48 up to 0.6 is acceptable.

17. Induce the production by adding IPTG (materials and equipment) to the culture and continue incubation overnight at 18°C and 180 rpm.
18. The following steps have to be carried out on ice. Harvest the cells by centrifugation for 10 min at 10.000 × *g* and 4°C.
19. Decant the supernatant and resuspend the pellet in 4 mL cool QIAGEN lysis buffer (materials and equipment).

Pause point: Without lysis buffer the cell pellet can be stored at −20°C or −80°C for a few months.

20. Open the cells by sonication.
    a. Sonicate for 35 s using the settings cycle 7 and 70%.
    b. Pause for 35 s.

c. Repeat steps a and b three times.

Note: Cells can also be opened enzymatically.

21. Pellet the cell debris by centrifugation at 4°C and 10.000 × *g* for 30 min.

Pause point: The cleared supernatant can be store at −20°C for 2 weeks.

Optional: If the lysate was frozen, thaw it on ice.

22. Add 5 µL 4× NuPage LDS sample buffer to 20 µL of the cleared lysate obtained in step 21 and store the mixture at −20°C until it is used for SDS-PAGE analysis.
23. Purify the protein with a Ni-NTA column (QIAGEN).
    a. Pipette 1 mL of the Ni-NTA slurry into a polypropylene column and drain the storage liquid.
    b. Add the 4 mL of lysate obtained in step 21 on the column and let it slowly elute.
    c. Take a 20 µL sample from the flowthrough, add 5 µL 4× NuPage LDS sample buffer and store the mixture at −20°C until it is used for SDS-PAGE analysis.
    d. Wash the column twice with 2.5 mL of QIAGEN wash buffer (materials and equipment).
    e. Collect the washing fractions, mix 20 µL of each washing fraction with 5 µL 4× NuPage LDS sample buffer and store at −20°C until it is used for SDS-PAGE analysis.
    f. Elute the column four times with 0.5 mL QIAGEN elution buffer (materials and equipment).
    g. Take a sample of 20 µL from each elution fraction and add 5 µL of 4× NuPage LDS sample buffer and store the mixture at −20°C until it is used for SDS-PAGE analysis.
    h. Elution fractions should be stored with 10% glycerol.

⚠ CRITICAL: Buffers for the protein purification contain imidazole and should be handled with personal safety equipment.

Pause point: SDS-PAGE samples can be stored at −20°C for weeks. Stability of the purified protein varies, but DarH is stable for at least 6 months at −20°C.

24. Perform an SDS-PAGE analysis of the samples collected during purification.
    a. Take out a Mini-PROTEAN TGX Stain-Free gel from the package and remove the green tape form the bottom.
    b. Assemble the Mini-PROTEAN tetra cell and add 1× running buffer (ROTIPHORESE 10× SDS-PAGE) into the inner and outer chamber.
    c. Load the samples and the 10 µL of the PageRuler Prestained Protein Ladder into the wells of the gel and run the gel at 200 V until the dye reaches the bottom of the gel (approx. 30 min).
    d. Use the opening lever at the marked positions to open the gel cassette.
    e. Stain the gel with ROTIBlue staining solution.
        i. Shake the staining solution.
        ii. Mix 10 mL ROTIBlue, 30 mL ddH_2O, and 10 mL methanol in a 50 mL flacon tube.
        iii. Incubate the gel shaking in the staining solution for 2 h up to overnight.
        iv. If incubated overnight destain the gel in water for 2 h on the next day.
        v. Use a camera to document the gel (Figure 6, troubleshooting).

⚠ CRITICAL: ROTIBlue, and methanol are hazardous substances and they should only be handled with personal safety equipment and under the fume hoot.

In vitro assay

Timing: 2 days

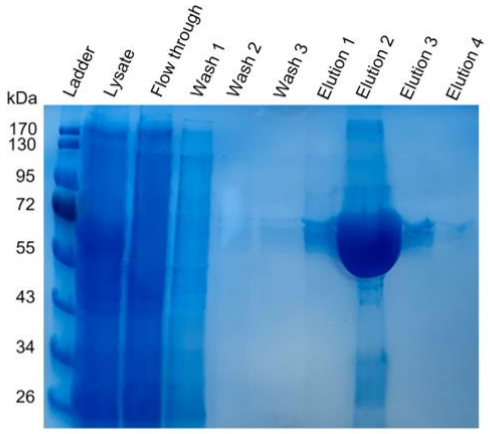

Figure 6. SDS-PAGE gel of the His-tag purification of DarH using pJK9.1
Elution fractions 1,2, and 3 show a signal with the expected protein size of 58 kDa. Only faint signals of this size are visible in the washing fractions, which indicates that most of the product is bound to the column but it is nearly saturated. Elution fraction 2 can be used for an *in vitro* assay.

25. The *in vitro* halogenation assay is performed according to a modified protocol by Zehner et al.[9] by preparing the halogenase *in vitro* assay mix and incubating it at 18°C for 24 h.

Halogenase *in vitro* assay mix	
Reagent	Amount
Darobactin A (1 mg/mL)	43.27 µL
KBr (100 mg/mL)	9 µL
NADH (100 mg/mL)	4.8 µL
FAD (10 mg/mL)	2.4 µL
Potassium phosphate buffer pH 7.2	140 µL
DarH	100 µL
Total	300 µL

26. The reaction is stopped after incubation by adding an equal amount of methanol.
27. After centrifugation for 5 min at 15.000 × *g* the supernatant is transferred to a LCMS vial and subjected to LCMS measurement (Figure 7).

⚠ CRITICAL: Adding the methanol to stop the reaction should be performed with personal safety equipment and under the fume hood.

EXPECTED OUTCOMES

Construction of the strain for the heterologous expression of the gene cluster and the experssion of the His-tagged enzyme.

Heterologous expression of the gene cluster.

Heterologous expression of the His-tagged enzyme.

In vitro assay with the purified enzyme to prove catalytic function.

LIMITATIONS

The protocol represents a stable method for the heterologous expression of natural products and enzymes of a natural product gene cluster. However, *E. coli* might not always be the right choice as heterologous expression host. Depending on the original producer the protocol might be adapted to a more closely related model organism.

TROUBLESHOOTING

Poblem 1: Amplification of gene not possible

- There is no PCR product visible on the agarose gel.

Potential solution

- Try different PCR conditions as described in the table PCR reaction master mix with supplements and / or try an annealing temperature gradient PCR.

PCR reaction master mix with supplements

Reagent	Amount	Amount	Amount
Q5 reaction buffer (5×)	5 µL	5 µL	5 µL
dNTP mix (10 mM each)	0.5 µL	0.5 µL	0.5 µL
Primer 1 (10 pmol/µL)	0.625 µL	0.625 µL	0.625 µL
Primer 2 (10 pmol/µL)	0.625 µL	0.625 µL	0.625 µL
Q5 Polymerase	0.125 µL	0.125 µL	0.125 µL
Template DNA (10–15 µg/µL)	1 µL	1 µL	1 µL
DMSO	0.75 µL		0.75 µL
GC-enhancer		5 µL	5 µL
ddH_2O	16.374 µL	12.125 µL	11.374 µL

Problem 2: Transformation failed

- There are no colonies growing on the plate after incubation overnight.

Potential solution

- Your cells might not be competent or transformation efficiency is low.
  - o Transform your competent cells with a control plasmid.
- The plasmid was not assembled in the Gibson assembly.
  - o Perform an agarose gel electrophoresis with a unincubated and incubated Gibson assembly.
  - o Check the unincubated sample for signals of the plasmid and fragment.
    - Eventually increase amount of fragment and/or plasmid.
  - o Check the incubated sample for assembly of the plasmid.
    - Increase the incubation time up to 2 h.
    - Repeat the fragment PCR with different conditions and generate new fragment DNA.

Problem 3: Product is not produced or only on low amounts

- In the LCMS data the expected product cannot be detected or only with low intensity.

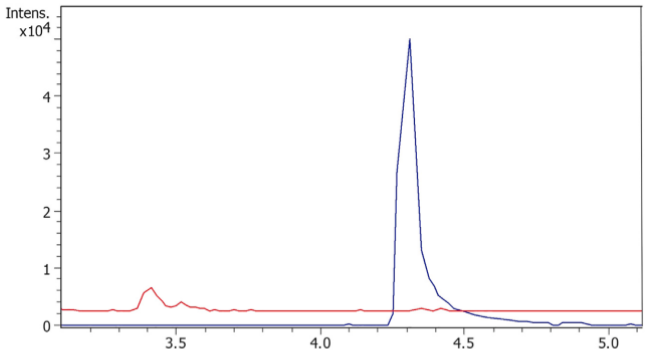

Figure 7. Extracted ion chromatogram (EIC, calc. $[M + 2H]^{2+} \pm 0.05$ Da) of bromodarobactin A ($C_{47}H_{54}N_{11}O_{12}Br$, 522.6641 *m/z*, blue) and extracted ion chromatogram (EIC, calc. $[M + 2H]^{2+} \pm 0.05$ Da) of darobactin A ($C_{47}H_{55}N_{11}O_{12}$, 483.7089 *m/z*, red)

After 24 h of incubation nearly all darobactin A (peak at approx. 3.5 min retention time, red) is converted to bromodarobactin A (peak at approx. 4.4 min retention time, blue).

Potential solution

- Try different incubation temperatures for the strain after induction with IPTG.
- Increase incubation time up to 5 days.
- Use different colonies for the production.
- Create a freshly transformed strain by transforming the production strain again with the plasmid and inoculate the preculture directly from the plate.

Problem 4: Protein is not expressed

- There are no signals of the expected size detectable on the SDS-PAGE gel.

Potential solution

- Try different incubation temperatures for the protein expression (overnight 30°C, overnight room temperature, 4 h 37°C).
- Use different colonies of the production strain.
- Create a freshly transformed strain by transforming the production strain again with the plasmid and inoculate the preculture directly from the plate.

Problem 5: Protein purification is not possible

- There are no signals of the expected size detectable in the elution fractions but in the lysate and washing fractions.

Potential solution

- Perform a western blot to check if the His-tag is accessible/still present.
- Presence of the protein in the washing fraction might be a sign of column saturation.
    - oElute the column using higher concentrations of imidazole.

RESOURCE AVAILABILITY

Lead contact

Further information and requests for resources and reagents should be directed to and will be fulfilled by the lead contact, Till F. Schäberle (Till.F.Schaeberle@agrar.uni-giessen.de).

Materials availability

Plasmids and strains generated in this study are not commercially available.

Data and code availability

All data reported in this study will be shared by the lead contact upon request.

ACKNOWLEDGMENTS

This work was supported by the State Ministry of Higher Education, Research and Arts of the state Hesse through the LOEWE program for the Center for Insect Biotechnology and Bioresources, and the German Federal Ministry of Education and Research (BMBF, via grant GBi2S and DZIF TTU 09.918).

AUTHOR CONTRIBUTIONS

Conceptualization and methodology, N.B., J.-C.K., and T.F.S.; investigation (biological experiments), J.-C.K.; investigation (LCMS), U.M.; data analysis, J.-C.K.; writing – original draft, J.-C.K., T.F.S.; writing – review and editing, U.M.; visualization, J.-C.K.; supervision, T.F.S.; project administration, T.F.S.; and funding acquisition, T.F.S.

DECLARATION OF INTERESTS

The authors declare no competing interests.

REFERENCES

1. Böhringer, N., Kramer, J.-C., de La Mora, E., Padva, L., Wuisan, Z.G., Liu, Y., Kurz, M., Marner, M., Nguyen, H., Amara, P., et al. (2023). Genome- and metabolome-guided discovery of marine BamA inhibitors revealed a dedicated darobactin halogenase. Cell Chem. Biol. Published Online: Jul. 3, 2023. https://doi.org/10.1016/j.chembiol.2023.06.011.

2. Grote, A., Hiller, K., Scheer, M., Münch, R., Nörtemann, B., Hempel, D.C., and Jahn, D. (2005). JCat: a novel tool to adapt codon usage of a target gene to its potential expression host. Nucleic acids research. Web Server issue *33*, W526–W531. https://doi.org/10.1093/nar/gki376.

3. Dotmatics. SnapGene; GSL Biotech LLC.

4. Gibson, D.G., Young, L., Chuang, R.-Y., Venter, J.C., Hutchison, C.A., and Smith, H.O. (2009). Enzymatic assembly of DNA molecules up to several hundred kilobases. Nat. Methods *6*, 343–345. Published Online: Apr. 12, 2009. https://doi.org/10.1038/nmeth.1318.

5. Wuisan, Z.G., Kresna, I.D.M., Böhringer, N., Lewis, K., and Schäberle, T.F. (2021). Optimization of heterologous Darobactin A expression and identification of the minimal biosynthetic gene cluster. Metab. Eng. *66*, 123–136. Published Online: Apr. 16, 2021. https://doi.org/10.1016/j.ymben.2021.04.007.

6. Qiagen (2003). The QIAexpressionist: A Handbook for High-Level Expression and Puridication of 6xHis-Tagged Proteins.

7. New England BioLabs. Gibson Assembly® Protocol (E5510). https://international.neb.com/protocols/2012/12/11/gibson-assembly-protocol-e5510.

8. New England BioLabs. NEBioCalculator. https://nebiocalculator.neb.com/#!/ligation.

9. Zehner, S., Kotzsch, A., Bister, B., Süssmuth, R.D., Méndez, C., Salas, J.A., and van Pée, K.H. (2005). A regioselective tryptophan 5-halogenase is involved in pyrroindomycin biosynthesis in Streptomyces rugosporus LL-42D005. Chem. Biol. *12*, 445–452. https://doi.org/10.1016/j.chembiol.2005.02.005.

3. Chapter 2: Derivatization of DAR by introducing non-canonical amino acids

Using DAR A as a lead structure, many promising new derivatives with increased activity or improved drug-like properties have been developed. However, with the exception of a few experiments in one study (Seyfert *et al.*, 2023b), all attempts focused on derivatization by exchanging the amino acids with other natural amino acids (Imai *et al.*, 2019; Groß *et al.*, 2021; Marner *et al.*, 2023; Seyfert *et al.*, 2023b; Seyfert *et al.*, 2023a; Böhringer *et al.*, 2024). Therefore, the aim of the following study was to develop a targeted approach for the integration of non-canonical amino acids into DAR (Kramer *et al.*, 2025). This was achieved by adapting the amber stop codon suppression technique for the heterologous expression of DAR A in *E. coli*. An altered aminoacyl-tRNA synthase capable of recognizing a non-canonical amino acid was used in combination with a tRNA that recognizes a nonsense codon. This nonsense codon is integrated into *darA* by mutating the codon of the desired integration site of the non-canonical amino acid. The non-canonical amino acid of choice is then added to the culture broth (Young and Schultz, 2010; Wang *et al.*, 2012; Kramer *et al.*, 2025). Using this technique, four new DAR A derivatives were produced: DAR A F7I with an iodination at the *para* position of F^7 in the DAR A heptapeptide, DAR A $F7F_5$ with aromatic perfluorination of F^7, DAR A F7OMe with a methoxy group attached to the *para* position of F^7 and DAR A F7F with a fluorination at the *para* position of F^7. The latter was purified and characterized by NMR experiments. In minimum inhibitory concentration studies, DAR A F7F showed an activity similar to DAR A (Kramer *et al.*, 2025).

Manuscript 3: Expanding the Range of Darobactin Derivatives by Amber Stop Codon Suppression To Introduce Non-canonical Amino Acids

Status: accepted on 04/07/2025, published online on 04/30/2025

Author's contributions: study design, method development, main contribution to all experiments, data analysis, manuscript writing, figure design.

ACS OMEGA

Open Access

http://pubs.acs.org/journal/acsodf

Article

Expanding the Range of Darobactin Derivatives by Amber Stop Codon Suppression To Introduce Non-canonical Amino Acids

Jil-Christine Kramer, Zerlina G. Wuisan, Ute Mettal, Michael Marner, and Till F. Schäberle*

Cite This: https://doi.org/10.1021/acsomega.4c10307

Read Online

ACCESS | Metrics & More | Article Recommendations | Supporting Information

ABSTRACT: The ribosomally synthesized and post-translationally modified peptide (RiPP) darobactin A is a promising new antibiotic candidate with anti-Gram-negative activity inflicted by the inhibition of the novel target BamA. Genome mining revealed many putative darobactin producer strains, but a limited number of compound modification options. In this study, the amber stop codon suppression technique was used to integrate non-canonical amino acids into the bicyclic heptapeptide, creating new darobactin derivatives. The C-terminal phenylalanine was replaced by non-canonical phenylalanine derivatives with different substituents. Darobactin A F7F, featuring a fluorine atom in the para position of the C-terminal phenylalanine, was purified to enable structure validation by NMR. Activity assays revealed antimicrobial potency against selected Gram-negative strains comparable to darobactin A.

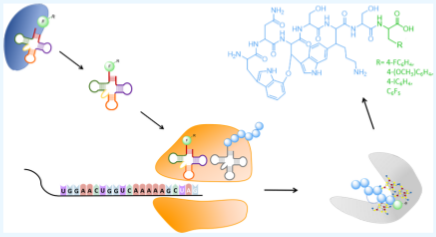

INTRODUCTION

Darobactin A (DAR A) is a ribosomally synthesized and post-translationally modified peptide (RiPP) that consists of seven amino acids (i.e., WNWSKSF). It has a bicyclic structure originating from an ether bridge between W^1 and W^3, plus an aryl bridge between W^3 and K^5. The natural product was first discovered in *Photorhabdus* species and was observed to possess anti-Gram-negative activity based on a novel mode of action. The compound inhibits the functionality of BamA, an essential part of the outer membrane β-barrel assembly machinery (BAM) complex of Gram-negative bacteria. BamA catalyzes the folding and insertion of outer membrane (OM) proteins like lipoproteins or lipopolysaccharides, with transport, virulence or multidrug resistance function.[1−3] BamA exists in two major conformations, the lateral-open and the lateral-closed state.[4−6] As shown by Haysom *et al.*, darobactin B (DAR B)[7] stabilizes the lateral-closed state of BamA, preventing the release of OM proteins from the cytoplasm.[8] Since OM proteins are essential for cell maintenance, BamA, the essential part of the BAM complex, represents an interesting drug target.[2] During in vitro studies, DAR A and its derivatives showed promising activity against various Gram-negative bacteria, including multidrug-resistant clinical isolates.[1,9,10] Furthermore, DAR A and B showed efficacy against resistant *Escherichia coli*, *Klebsiella pneumoniae*, and *Pseudomonas aeruginosa* in mouse models.[1,11] The biosynthetic gene cluster (BGC) consists of the precursor peptide encoded by *darA*, the *darB-D* genes encoding an ABC transporter and the radical SAM (rSAM) enzyme encoded by *darE*.[1] DarE was proven to catalyze both intramolecular ring closures.[12] Heterologous expression studies showed that only *darA* and *darE* are essential for the expression and constitute the minimal BGC.[1,13] In silico analysis of publicly available genome data showed that homologous BGCs are present in many strains from different genera, such as *Yersinia* or *Vibrio*.[1,14] Variations of the seven core amino acids within the gene sequence of the respective *darA* of these BGCs indicate putative existence of natural analogues, and although several groups described the generation of new analogues by genetic engineering of heterologous producer strains, modifications beyond canonical amino acids are so far limited.[7,11,15,16] To the best of our knowledge, the only enzyme that was experimentally investigated in this regard is DarH. The halogenase DarH was discovered in marine *Pseudoalteromonas luteoviolaceae* strains and was shown to catalyze bromination or iodination of the C-8 carbon of W^1.[1,10] Another successful attempt to introduce non-canonical amino acids (ncAAs) into the bicyclic heptapeptide was reported by Seyfert *et al.* In this study, feeding assays with non-canonical tryptophane analogues were performed. When feeding chlorinated tryptophane, either W^3 or W^7 was modified, and when feeding fluorinated tryptophan, either W^1, W^7, or both were fluorinated.[16] Hence, the position of the modification could not be predicted due to the presence of multiple

Received: November 13, 2024
Revised: April 4, 2025
Accepted: April 7, 2025

tryptophan residues in the bicyclic heptapeptide (positions 1, 3, and 7). Therefore, in this study, we adapted the amber stop codon suppression technique to conduct targeted introduction of ncAAs into DAR A to improve the drug-like properties of the compound.[17,18] The system adapted in this study uses a pyrrolysyl-tRNA synthase-$tRNA^{Pyl}_{CUA}$ pair from *M. mazei*, which was specifically engineered by Wang *et al.* to accept phenylalanine derivatives with large substituents in the *para* position. Hence, the encoding triplet has to be replaced by the amber stop codon to be recognized by the $tRNA^{Pyl}_{CUA}$. Heterologous expression of the modified gene in the presence of the pyrrolysyl-tRNA synthase-$tRNA^{Pyl}_{CUA}$ pair, should result in the incorporation of a ncAA at the respective position.[19] Next to this system, there are also different orthogonal translation systems (OTS) derived from other organisms. These systems can not only be used to improve the biological activity of a peptide, but also to introduce spectroscopic probes, add ligands for several chemical reactions, add linkers, or obtain new-to-nature protein properties.[18] In theory, the strain carrying the amber stop codon could be used to produce multiple derivatives of the desired peptide, since the pyrrolysyl-tRNA synthase can accept various ncAAs depending on which phenylalanine derivative is supplemented to the medium.[19]

RESULTS AND DISCUSSION

In this study, the triplet encoding for the C-terminal phenylalanine F^7 in the core peptide region of the native *darA* was mutated to the amber stop codon TAG (Figure 1). We coexpressed the modified *darA* plus *darE* on one plasmid and the pyrrolysyl-tRNA synthase-$tRNA^{Pyl}_{CUA}$ pair on a second plasmid in *E. coli* BL21.

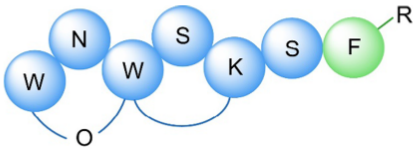

Orig. 5′ TGG AAC TGG TCA AAA AGC TTC 3′
Mod. 5′ TGG AAC TGG TCA AAA AGC TAG 3′

Figure 1. Scheme of DAR A F7-R and the DNA sequence of the DAR A core peptide before and after modification. Blue circles represent natural amino acids of DAR A, while the non-canonical phenylalanine (F) at position seven is displayed in green. The −R represents any desired phenylalanine substituent. The original (Orig.) sequence encoding the DAR A core peptide and the modified version (Mod., marked in green) carrying the amber stop codon are shown below.

The cultivation was done in minimal medium supplemented with the respective non-canonical phenylalanine (in the absence of canonical phenylalanine). This work resulted in the biosynthesis of new DAR A derivatives with an altered F^7 residue (Figure 2).

Initially, we cultivated the expression strain in the presence of 4-fluoro-L-phenylalanine (4−F-F) and subsequently analyzed the culture extract by UPLC-HRMS. Interestingly, we could detect a clear peak corresponding to the sum formula $C_{47}H_{54}N_{11}O_{12}F$ $[M+2H]^{2+}$ with 492.7056 m/z (calcd 492.7041 m/z) at a retention time of 3.7 min (Figures 3A, S1 and S2). This peak was not present in samples obtained

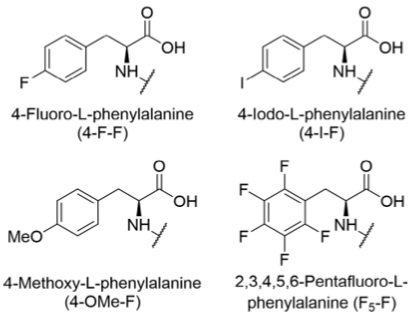

Figure 2. Structures of the non-canonical phenylalanine derivatives successfully integrated in DAR A.

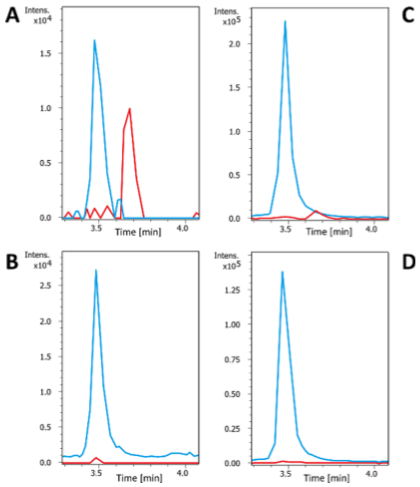

Figure 3. LCMS analysis of the heterologous expression of DAR A F7F and the control strain. Extracted ion chromatograms (EIC, calcd $[M + 2H]^{2+}$ ± 0.01 Da) of DAR A F7F are shown in red ($C_{47}H_{54}N_{11}O_{12}F$; 492.7041 m/z) and the extracted ion chromatograms (EIC, calcd $[M + 2H]^{2+}$ ± 0.01 Da) of DAR A are shown in blue ($C_{47}H_{55}N_{11}O_{12}$; 483.7089 m/z). The intensity (Intens.) is plotted on the *y*-axis and the retention time in minutes (min) is plotted on the *x*-axis. Samples are dissolved in 20:80 H_2O/MeCN + 0.1% FA. (A) Analysis of the heterologous expression of *E. coli* BL21/pEVOL-pylT-N346A/C348A/pJK64 with 4−F-F addition. (B) Analysis of the heterologous expression with *E. coli* BL21/pEVOL-pylT-N346A/C348A/pJK64 without 4−F-F addition. (C) Analysis of the control strain *E. coli* BL21/pEVOL-pylT-N346A/C348A/pZW-ADC9 with 4−F-F addition. (D) Analysis of the control strain *E. coli* BL21/pEVOL-pylT-N346A/C348A/pZW-ADC9 without 4−F-F addition.

from cultivations without 4−F-F (Figures 3B and S3). This compound was named darobactin A F7F (DAR A F7F), due to the fluorination of the phenylalanine at position seven (F^7). In addition, a peak corresponding to the unmodified DAR A could be detected in all cultivations (sum formula $C_{47}H_{55}N_{11}O_{12}$ $[M + 2H]^{2+}$ with 483.7101 m/z at a retention time of 3.5 min, Figure 3A,B, S3 and S4). When expressing the unmodified minimal BGC, DAR A was produced in the sample

https://doi.org/10.1021/acsomega.4c10307
ACS Omega XXXX, XXX, XXX−XXX

with and without 4−F-F, while DAR A F7F could only be detected when the phenylalanine derivative was added (Figures 3C,D, S5 and S6). Although the expression strain was cultivated in minimal medium, *E. coli* is able to synthesize phenylalanine via the shikimate pathway, because it is required for bacterial growth.[20] The presence of both DAR A and DAR A F7F in the same sample suggests that the natural and the mutant aminoacyl-tRNA synthase (aaRS) accept both, 4−F-F and phenylalanine as substrates. The DAR A F7F to DAR A expression ratio is approximately 1:23 in the strain without modification of *darA* on the plasmid, but 1:1.6 in the strain carrying the plasmid with the amber stop codon mutation. The production rate was observed to shift even further towards the new derivative DAR A F7F (ratio ∼1:0.3) when cultivation was performed in a larger volumes (Figure S7).

Structural Analysis. HRMS/MS fragmentation of DAR A F7F revealed the same fragments as DAR A (Figures 4, S8 and S9): N-terminal b_2* with 300.0979 m/z (W^1−N^2), the fragment containing the carbon−carbon bridge between W^3 and K^5 with 398.1823 m/z (W^3−S^4−K^5), and the b_5* W^1−N^2−W^3−S^4−K^5 with 697.2729 m/z. For DAR A, C-terminal fragments y_2 with 253.1183 m/z (S^6−F^7) and y_5 with 650.2933 m/z (W^3−S^4−K^5−S^6−F^7) were detected. On the other hand, for DAR A F7F, the y_2 fragment was observed at 271.1086 m/z (S^6−F_F^7, calcd 271.1089), while the y_5 fragment was found at 668.2832 m/z (W^3−S^4−K^5−S^6−F_F^7, calcd 668.2844 m/z) (Figure 4). The observed mass differences between the two sets of signature fragments are indicative of the fluorine substituent, suggesting the successful heterologous expression of DAR A F7F. To allow further characterization, DAR A F7F was produced and purified on larger scale.

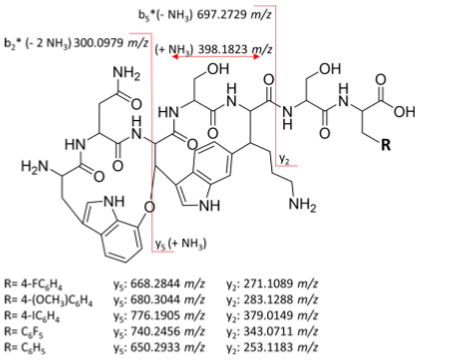

Figure 4. General structure of DAR A derivatives with signature fragment ions detectable in UPLC-HRMS/MS measurements. The mass/charge ratio of the y_2 and y_5 fragments depends on the residue −R and therefore on the substituent attached to the phenyl ring of phenylalanine F^7.

For this purpose, 30 L of culture was fermented and DAR A F7F was purified using an Amberlite XAD-16N column followed by ion exchange chromatography on SP Sepharose XL, flash chromatography, and HPLC, thereupon yielding a total amount of 1.2 mg.

Confirmation of the structure hypothesis derived from the MS/MS analysis was established by 1- and 2-dimensional NMR analysis (for key correlations cf. Figure 5b−d). The core structure of DAR A F7F matched well with the reference data of DAR A, as apparent from the comparison of the corresponding ^{1}H NMR spectra (Figures S21−S22). Furthermore, HMBC correlations between H-17 and C-6, H-21 and C-31, and H-23 and C-31 confirmed the characteristic ring closures (W^1−W^3 C−O−C ether bond and W^3−K^5 C−C bond) of the darobactin scaffold. The incorporation of 4−F-F at the C-terminal end of the molecule was verified by the HMBC correlation between H-39 and C-38. As expected, the 4−F-F residue shows additional line splitting due to coupling of the fluorine nucleus with protons H-42,42' and H-43,43' as well as with carbon atoms C-42,42', C-43,43', and C-44. Consequently, for each of the aforementioned carbon atoms, a doublet signal is detected. The observed ^{13}C chemical shifts as well as the values of the C−F coupling constants (C-42,42': 131.1 ppm, $^3J_{C,F}$ = 8.2 Hz; C-43,43': 115.1 ppm, $^2J_{C,F}$ = 21.3 Hz; C-44:161.7 ppm, $^1J_{C,F}$ = 241.5 Hz) are typical for monofluorinated aromatic rings and match well with literature data.[21−23] Likewise, the observed ^{19}F NMR shift of −117.94 ppm is in good agreement with the value reported for 4−F-F.[24] The multiplicity observed in the ^{19}F NMR spectrum also shows resemblance to literature data for 4−F-F,[25] even though the resolution is not sufficient to determine coupling constants.

Activity Assay. The antimicrobial activity of purified DAR A F7F was investigated by determination of the minimum inhibitory concentrations (MIC) against a panel of Gram-negative and Gram-positive control strains (Tables 1 and S3). In general, the potency and the antimicrobial spectrum of DAR A F7F are similar to the parent compound DAR A, while DAR B showed stronger activity against *E. coli*, *K. pneumoniae*, and *P. aeruginosa* strains. Initially, we tested the new compound against *E. coli* MG1655 bamA6ΔbamB, an engineered strain which is highly susceptible to BamA inhibitors,[26] and detected intriguing activity (0.125 μg/mL). In further assays, DAR A F7F inhibited the growth of *K. pneumoniae* and *E. coli* strains at 8−4 μg/mL (including mcr-1 positive clinical isolate NRZ14408). The potency is comparable to the parent compound DAR A (one dilution step difference), while the reference compound DAR B inhibited the same *E. coli* and *K. pneumoniae* strains at 2−0.5 μg/mL. We could not observe any meaningful growth inhibitory effects of DAR A F7F and DAR A against *P. aeruginosa* ATCC27853, PA103, and the clinical isolate *P. aeruginosa* EXT111762. In contrast, the moderately virulent laboratory strain PAO1[27] and the efflux deficient variant PAO750[28] were inhibited by the new and the parent compound at 8 μg/mL (DAR A F7F) and 4−2 μg/mL (DAR A). Similarly, the activity of DAR A F7F was identical against *E. coli* ATCC25922 and the ΔTolC mutant (8−4 μg/mL), indicating that drug-efflux might not be of primary concern during further optimization of darobactin-type compounds. No activity was observed against *S. aureus* and *A. baumannii* ATCC19606 in the selected concentration range.

Heterologous Expression with Further Phenylalanine Derivatives. Next, we investigated whether further novel DAR A derivatives can be produced using the amber stop codon technique. Hence, the heterologous production strain was cultivated in minimal media supplemented with different phenylalanine analogues, for which the literature indicated good integration efficiencies. Although it has to be kept in mind that variations in the literature data can be observed and that Young *et al.* used a different OTS.[19,29] We decided to use 4-chloro-L-phenylalanine (4−Cl-F), 4-trifluoromethyl-L-phenylalanine (4-CF_3−F), 4-azido-L-phenylalanine (4-N_3−F), 4-

https://doi.org/10.1021/acsomega.4c10307
ACS Omega XXXX, XXX, XXX−XXX

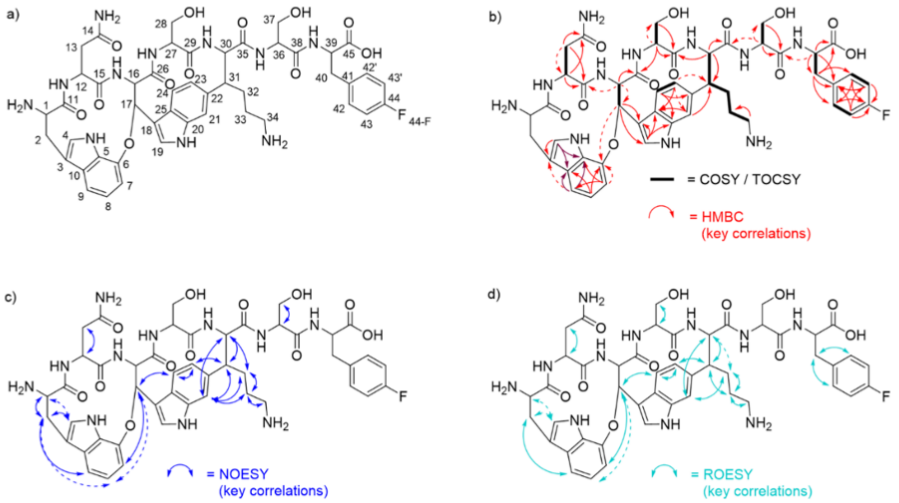

Figure 5. (a) Structure of DAR A F7F, including the atom numbering used for NMR structure elucidation. (b) COSY, TOCSY, and key HMBC correlations of DAR A F7F. (HMBC correlations to C-5 and C-10 could not be distinguished due to the proximity of the respective signals, indicated by dark red arrows.) (c) Key NOESY correlations of DAR A F7F. (d) Key ROESY correlations of DAR A F7F. Dashed arrows indicate weak correlation signals.

Table 1. MIC values of DAR A, DAR B and DAR A F7F (F7F) against *Escherichia coli* (Ec), *Pseudomonas aeruginosa* (Pa), *Klebsiella pneumoniae* (Kp), *Acinetobacter baumannii* (Ab), and *Staphylococcus aureus* (Sa)[a]

	organism and test strain	MIC μg/mL		
		DAR B	DAR A	F7F
Ec	MG1655 bamA6ΔbamB	n.d.	<0.03	0.125
	ATCC25922	1−0.5	n.d.	8−4
	ATCC25922 ΔTolC	0.5−0.25	n.d.	8−4
	NRZ14408 mcr-1	1−0.5[7]	4[7]	8
Pa	PAO1	2−1[9]	4−2[7]	8
	PAO750	0.5	4	8
	PA103	8[11]	n.d.	64
	ATCC27853	8 [9]	>64	>64
	EXT111762	2−1[9]	>64	64
Ab	ATCC19606	32[7]	>64	>64
Kp	DSM30104	2−1[7]	4	8
	ATCC700603	2−1[11]	n.d.	16−8
Sa	ATCC33592	>64	>64	>64

[a]Experiments were done in triplicate, and values are given in μg/mL.

nitro-L-phenylalanine (4-NO_2−F), 4-methoxy-L-phenylalanine (4-OMe-F), 4-bromo-L-phenylalanine (4−Br-F), 4-iodo-L-phenylalanine (4−I-F), 3,4-dihydroxy-L-phenylalanine (3,4-OH-F) and 2,3,4,5,6-pentafluoro-L-phenylalanine (F_5−F) as respective supplements.

In samples generated by heterologous expression in the presence of 4-OMe-F, 4−I−F, and F_5−F (Figure 2), we detected by UPLC-HRMS peaks matching the expected mass to charge ratios of the respective DAR A derivatives at retention times between 3.7 and 4.9 min (Figure 6). In all samples, the characteristic fragments of DAR A were detected, except fragment b_5*, which was only present for the DAR A F7F and darobactin A F7F_5 (DAR A F7F_5) derivatives.

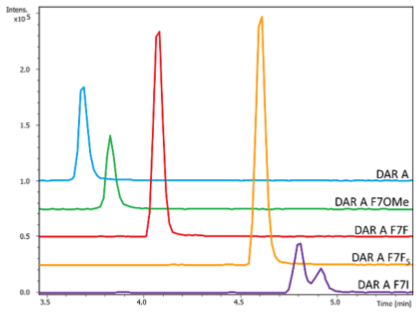

Figure 6. Extracted ion chromatograms (EIC, calcd $[M + 2H]^{2+}$ ± 0.01 Da) of DAR A F7I in purple ($C_{47}H_{54}N_{11}O_{12}I$; 546.6572 *m*/*z*), DAR A F7F_5 in yellow ($C_{47}H_{50}N_{11}O_{12}F_5$; 528.6853 *m*/*z*), DAR A F7F in red ($C_{47}H_{54}N_{11}O_{12}F$; 492.7041 *m*/*z*), DAR A F7OMe in green ($C_{48}H_{57}N_{11}O_{13}$; 498.7141 *m*/*z*) and DAR A in blue ($C_{47}H_{55}N_{11}O_{12}$; 483.7089 *m*/*z*) from the heterologous expression of *E. coli* BL21/pEVOL-pylT-N346A/C348A/pJK64 with the respective non-canonical phenylalanine derivatives. Samples were dissolved in 50:50 H_2O/MeOH. The intensity (Intens.) is plotted on the *y*-axis and the retention time in minutes (min) on the *x*-axis.

However, due to the modification of the phenylalanine in position seven, fragments y_2 and y_5 differ from the fragmentation signature of the native compound. When cultivating in the presence of 4-OMe-F the signals at 283.1296 *m*/*z* and 680.3050 *m*/*z* correspond to the calculated y_2 and y_5 fragments of darobactin A F7OMe (DAR A F7OMe) of calculated 283.1288 *m*/*z* (y_2, S^6−$F_{OMe}{}^7$) and 680.3044 *m*/*z* (y_5, W^3−S^4−K^5−S^6−$F_{OMe}{}^7$), indicating the successful heterologous expression of this derivative (Figures 4 and S12−S14). Similar results were achieved when cultivating in the presence

https://doi.org/10.1021/acsomega.4c10307
ACS Omega XXXX, XXX, XXX−XXX

of 4−I-F. Mass to charge ratios of 379.0146 m/z and 776.1906 m/z corresponding to the y_2 ($S^6-F_1^7$, calcd 379.0149 m/z) and y_5 ($W^3-S^4-K^5-S^6-F_1^7$, calcd 776.1905 m/z) fragments of darobactin A F7I (DAR A F7I) could be detected (Figure 4 and S15−S17). For the heterologous expression with F_5−F, the y_2 fragment of 343.0720 m/z ($S^6-F_{F5}^7$, calcd 343.0711 m/z) and the y_5 fragment of 740.2463 m/z ($W^3-S^4-K^5-S^6-F_{F5}^7$, calcd 740.2456 m/z) were present, demonstrating the production of DAR A F7F_5 (Figure 4 and S18−S20).

The heterologous expression supplemented with either 4−Cl-F or 4-CF_3−F, 4-N_3−F, 4-NO_2−F, 4−Br−F, or 3,4-OH-F did not lead to the detection of the expected derivative. Also, the newly engineered DAR A derivatives exhibit varying production levels (Figure 6). One reason could be different integration rates of the phenylalanine derivatives, which was already observed for other RiPPs in the literature as well as shown for DAR A in this study. For example, only for Wang *et al.* postulated low yields of brominated phenylalanine is integration, while other studies indicated good efficiencies.[19,29,30] In our study described herein, the attempts to include 4-BR-F into DAR A were unsuccessful.[19] This indicates that integration efficiencies may be specific for each RiPP product. Another possibility could be a reduced interaction rate of the altered linear heptapeptide with the rSAM enzyme to introduce the two rings.[12,19,29] The linear heptapeptides might have been produced but subsequently degraded by unspecific proteases, because the intramolecular ring closures are not introduced to stabilize the compound. Since the mechanism of how the rings are introduced is not understood in detail, it can only be hypothesized that some of the newly introduced phenylalanine residues might have disturbed interactions with the enzyme.[12]

In this study, we successfully adapted the amber stop codon suppression for targeted introduction of ncAAs in DAR A. We were able to detect four new derivatives, DAR A F7F, DAR A F7OMe, DAR A F7I, and DAR A F7F_5. The first one, DAR A F7F, was isolated and characterized by NMR. In MIC studies, the compound showed similar activities compared to DAR A. In general, the method developed in this study provides a solid tool for the biotechnological modification of darobactins.

MATERIAL AND METHODS

Plasmid Construction. The plasmids were constructed by a self-prepared isothermal assembly reaction.[31] The plasmid pJK63, carrying the DAR A precursor peptide, the gene for the rSAM enzyme, both from *Photorhabdus khanii* DSM3369, and the gene for the tRNA with the CUA anticodon,[19] were generated from pZW-ADC9[13] and pEVOL-pylT-N346A/C348A.[19] The expression vector pJK64 was cloned by amplifying pJK63 to exchange the phenylalanine triplet of the core peptide with the triplet TAG. Primer sequences and further information are provided in Tables S1 and S2. To generate the production strain, *E. coli* BL21 was transformed with the plasmids pJK64 and pEVOL-pylT-N346A/C348A.[31]

Heterologous Expression of the DAR A Derivatives. For the heterologous expression of target derivatives, a preculture of the production strain *E. coli* BL21+ pJK64+ pEVOL-pylT-N346A/C348A was prepared in LB_{Kan+Ca} and used to inoculate $DAR49^*_{Kan+Ca}$. The culture was incubated at 37 °C and 200 rpm until an optical density (OD_{600}) of 1.0, cooled for 15 min at 4 °C and the production was induced by adding 1 mM IPTG (isopropyl-β-D-thiogalactopyranoside), 0.2% arabinose, and 2 mM of the respective phenylalanine analogue (dissolved in 1 M NaOH just before use). Incubation was performed for 3 days at 30 °C and 200 rpm.

UPLC-HRMS and HRMS/MS Sample Preparation and Measurement. UPLC-HRMS samples were prepared by using C_{18} stage tips or C_{18} SPE columns. For the C_{18} stage tip purification, the column was prepared as described previously.[32] The stage tip was washed with 200 mL of 100% MeOH and afterward equilibrated using 200 mL of 95:5 H_2O/acetonitrile (MeCN) + 0.1% formic acid (FA) by centrifugation at 3000 rpm and 4 °C for ∼4 min. Cleared supernatant of the cultivation (400−500 μL) was applied to the stage tip by repeating the centrifugation step twice. To remove salts, the C_{18} matrix was washed with 30 mL 95:5 H_2O/MeCN + 0.1% FA. Afterward, the sample was eluted twice using 30 mL 20:80 H_2O/MeCN + 0.1% FA for each elution. For the C_{18} SPE extraction, a SPE column, CHROMABOND C18 ec f, 100 μm, 6 mL/1000 mg (Macherey- Nagel, Düren, Germany) was washed twice with 6 mL MeOH and afterward twice with 6 mL ddH_2O. The column was loaded with 50 mL culture supernatant (1 mL/min) and subsequently washed with 6 mL ddH_2O. Afterward, the column was left under vacuum for 15 min to dry completely. The product was eluted with three times 6 mL 50:50 H_2O/MeOH + 0.1% FA, followed by 6 mL MeOH + 0.1% FA, three times 6 mL 20:80 H_2O/MeCN + 0.1% FA, and 6 mL MeCN + 0.1% FA. The samples were dried and redissolved in 100 μL 50:50 H_2O/MeOH. UPLC-HRMS measurements were carried out with an Agilent Infinity 1290 UPLC system coupled to a DAD detector and a micrOTOFQ II mass spectrometer (Bruker Daltonics, Bremen, Germany) with an electrospray ionization source. Measurements with high accuracy were done on a UPLC system of the same type coupled to DAD and ELSD detectors and a maXis II ESI-qTOF-UHRMS (Bruker Daltonics, Bremen, Germany). In both cases, the stationary phase of the UPLC system was an Acquity UPLC BEH C18, 130 Å, 1.7 μm (2.1 mm × 100 mm) column and an Acquity UPLC BEH C18, 130 Å, 1.7 μm VanGuard Pre-Column (2.1 mm × 5 mm; Waters, Eschborn, Germany). The following gradient was used for the LC system coupled to micrOTOFQ II: 0 min: 95% A; 0.80 min: 95% A; 18.70 min: 4.75% A; 18.80 min: 0% A; 23.00 min: 0% A; 23.10 min: 95% A; 25.00 min: 95% A (A: H_2O, 0.1% FA; B: MeCN, 0.1% FA). For the LC system coupled to the maXis II ESI-qTOF-UHRMS instrument, a gradient of 0 min: 95% A; 0.30 min: 95% A; 18.00 min: 4.75% A; 18.10 min: 0% A; 22.50 min: 0% A; 22.60 min: 95% A; 25.00 min: 95% A (A: H_2O, 0.1% FA; B: MeCN, 0.1% FA) was used. A flow rate of 600 μL/min and a column oven temperature of 45 °C were used for both systems. The internal standard for mass spectra calibration was a 10 mM sodium formate solution in H_2O/^{i}PrOH (1:1). A sample volume of 5 μL was injected. For MS/MS fragmentation analysis, auto-MSMS settings were used. The recorded spectra were analyzed using Compass DataAnalysis version 4.2 and 5.3 (Bruker).

Purification of the DAR A F7F. DAR A F7F was isolated according to a modified protocol from Imai et al.[1] *E. coli* BL21+ pJK64 + pEVOL-pylT-N346A/C348A was cultivated as described above, and the culture broth was lyophilized after 3 days of cultivation. The compound was extracted from the lyophilized culture broth using 50:50 H_2O/MeOH. The concentrated extract was incubated with 10% v/v Amberlite XAD-16N resin (20−60 mesh, Sigma Life Science [Merck KGaA], Darmstadt, Germany) and the resin was subsequently washed with two column volumes (CV) of H_2O + 0.1% FA.

https://doi.org/10.1021/acsomega.4c10307
ACS Omega XXXX, XXX, XXX−XXX

The compound was eluted with 3 CV 50:50 H_2O/MeOH + 0.1% FA, and the MeOH was removed using a rotary evaporator. Afterward, the elution fraction was loaded onto a SP Sepharose XL strong ion exchange column (220 mL bed volume, GE Healthcare, Uppsala, Sweden) and washed with 10 CV H_2O+ 0.1% FA. Elution was done with 50 mM NH_4OAc pH adjusted to 5, 7, 9, and 11 using 10 CV each. The compound containing elution fraction with pH 7 was further purified by reversed-phase flash chromatography using a Puriflash 4125 chromatography system (Interchim, Montluçon, France) with a puriFlash C18-AQ 30 μm F0120 flash column (Interchim) as follows: 0−20 min: 5% D; 20−60 min: 5−100% D; 60−90 min: 100% D (C: H_2O, 0.1% FA, D: MeOH, 0.1% FA), with a flow rate of 30 mL/min. DAR A F7F containing fractions were combined and dried in a GeneVac centrifugal concentrator (SPScientific, Ipswich, UK). Dry weight was determined, and fractions were subjected to HPLC (Shimadzu Deutschland GmbH, Duisburg, Germany) purification with a NUCLEODUR C18 Gravity-SB 3 μm (Macherey-Nagel, Düren, Germany) using a gradient:

0−5 min: 5% B; 5−7 min: 5−25% B; 7−27 min: 25−50% B; 27−30 min: 50−100% B (A: H_2O, 0.1% FA; B: MeCN, 0.1% FA). The flow rate was set to 2 mL/min, and the column oven temperature was maintained at 40 °C.

NMR Spectroscopy. NMR spectra (^{1}H, ^{13}C, ^{19}F, COSY, ^{1}H,^{1}H-TOCSY, NOESY, ROESY, HSQC, HSQC-TOCSY, and HMBC) were recorded at 298 K on an Avance Neo 700 MHz spectrometer (^{1}H: 700.28 MHz, ^{13}C: 176.09 MHz, ^{19}F: 658.92 MHz; Bruker BioSpin GmbH, Rheinstetten, Germany) equipped with a 5 mm CryoProbe Prodigy TCI (^{1}H, ^{15}N, ^{13}C Z-GRD). All measurements were carried out using D_2O as a solvent. Chemical shifts are given in ppm. ^{1}H spectra were referenced to the residual solvent signal (δ = 4.79 ppm).[33] For ^{13}C measurements, 3-(trimethylsilyl)propionic-2,2,3,3-d_4 acid sodium salt was used as the external standard. For ^{19}F measurements, α,α,α-trifluorotoluene served as an external standard. For a better resolution of the correlation signals, HSQC and HMBC spectra were acquired using nonuniform sampling (NUS). HSQC-TOCSY, ^{1}H,^{1}H-TOCSY, NOESY, and ROESY spectra were measured with H_2O suppression. For ^{1}H, ^{13}C DEPTQ-135, ^{19}F, COSY, HSQC (with NUS sampling), and HMBC experiments, a concentrated sample of DAR A F7F was used, while HSQC (without NUS sampling), HSQC-TOCSY, ^{1}H,^{1}H-TOCSY, NOESY, and ROESY experiments were acquired for a dilute sample. Analysis of NMR spectra was achieved using TopSpin 3.6.0 (Bruker BioSpin GmbH, Rheinstetten, Germany).

Antimicrobial Activity of DAR A F7F. The antimicrobial activity of DAR A F7F was interrogated by determining the minimum inhibitory concentration (MIC) against the following test panel: *E. coli* MG1655 bamA6_bamB, *E. coli* ATCC35218, *E. coli* ATCC25922, *E. coli* ATCC25922 ΔTolC, *E. coli* NRZ14408 mcr-1, *Pseudomonas aeruginosa* PAO1, , *P. aeruginosa* PAO750, *P. aeruginosa* PA103, *P. aeruginosa* ATCC27853, *P. aeruginosa* EXT111762, *A. baumannii* ATCC19606, *K. pneumoniae* DSM30104, *K. pneumoniae* ATCC700603, and *S. aureus* ATCC33592. The antibiogram and the resistance determinants of the clinical isolates *E. coli* NRZ14408 and *P. aeruginosa* EXT111762 can be found in our previous studies.[10,11]

Briefly, the assays were conducted by using the microbroth dilution method in round-bottom 96-well plates. Overnight cultures of the test strains were adjusted to McFarland Standard of 1.0 and subsequently diluted to 5× 10^5 cells mL^{-1} in cation-adjusted Mueller Hinton 2 broth. Darobactins were screened in 12 concentrations ranging from 64 to 0.03 μg mL^{-1} in triplicate. Ceftazidime, ciprofloxacin, and gentamicin were used as standards on each assay plate. Bacterial suspension without supplemented standard antibiotics or darobactin was used as a negative control. After incubation (18 h, 180 rpm, 37 °C, 85% relative humidity), cell growth was determined by measuring the turbidity using a microplate spectrophotometer at 600 nm. The MIC was defined as the minimum concentration at which at least 85% growth inhibition relative to the negative control was measured. Relative inhibition (h) was calculated according to h % = 100 * [1 − (AU sample − AU Low)/(AU High − AU Low)]. AU: absorption unit; Low: medium blank; High: negative control of maximal growth. Results were compared to reference darobactins and are summarized in Table S3.

■ ASSOCIATED CONTENT

Supporting Information

The Supporting Information is available free of charge at https://pubs.acs.org/doi/10.1021/acsomega.4c10307.

Primer sequences, plasmid descriptions, antimicrobial activity assay data, and UPLC-HRMS/MS and NMR data (PDF)

■ AUTHOR INFORMATION

Corresponding Author

Till F. Schäberle − *Natural Product Research Department, Institute for Insect Biotechnology, Justus-Liebig-University Giessen, 35392 Giessen, Germany; Natural Product Department, Fraunhofer-Institute for Molecular Biology and Applied Ecology (IME), 35392 Giessen, Germany; German Center for Infection Research (DZIF), Partner Site Giessen-Marburg-Langen, 35392 Giessen, Germany;* orcid.org/0000-0001-9947-8079; Email: Till.F.Schaeberle@agrar.uni-giessen.de

Authors

Jil-Christine Kramer − *Natural Product Research Department, Institute for Insect Biotechnology, Justus-Liebig-University Giessen, 35392 Giessen, Germany;* orcid.org/0000-0001-6469-3828

Zerlina G. Wuisan − *Natural Product Research Department, Institute for Insect Biotechnology, Justus-Liebig-University Giessen, 35392 Giessen, Germany*

Ute Mettal − *Natural Product Research Department, Institute for Insect Biotechnology, Justus-Liebig-University Giessen, 35392 Giessen, Germany*

Michael Marner − *Natural Product Research Department, Institute for Insect Biotechnology, Justus-Liebig-University Giessen, 35392 Giessen, Germany; Natural Product Department, Fraunhofer-Institute for Molecular Biology and Applied Ecology (IME), 35392 Giessen, Germany;* orcid.org/0000-0002-1024-1567

Complete contact information is available at: https://pubs.acs.org/10.1021/acsomega.4c10307

Notes

The authors declare no competing financial interest.

■ ACKNOWLEDGMENTS

We would like to thank Dr. Heike Hausmann for assisting with the NMR experiments. We acknowledge financial support from the German Federal Ministry of Education and Research (BMBF) via GoBio initial (16LW0251).

■ REFERENCES

(1) Imai, Y.; Meyer, K. J.; Iinishi, A.; Favre-Godal, Q.; Green, R.; Manuse, S.; Caboni, M.; Mori, M.; Niles, S.; Ghiglieri, M.; Honrao, C.; Ma, X.; Guo, J. J.; Makriyannis, A.; Linares-Otoya, L.; Böhringer, N.; Wuisan, Z. G.; Kaur, H.; Wu, R.; Mateus, A.; Typas, A.; Savitski, M. M.; Espinoza, J. L.; O'Rourke, A.; Nelson, K. E.; Hiller, S.; Noinaj, N.; Schäberle, T. F.; D'Onofrio, A.; Lewis, K. A new antibiotic selectively kills Gram-negative pathogens. *Nature* **2019**, *576* (7787), 459−464.

(2) Knowles, T. J.; Scott-Tucker, A.; Overduin, M.; Henderson, I. R. Membrane protein architects: the role of the BAM complex in outer membrane protein assembly. *Nature reviews. Microbiology* **2009**, *7* (3), 206−214.

(3) Pettersson, A.; Poolman, J. T.; van der Ley, P.; Tommassen, J. Response of Neisseria meningitidis to iron limitation. *Antonie van Leeuwenhoek* **1997**, *71* (1−2), 129−136.

(4) Gu, Y.; Li, H.; Dong, H.; Zeng, Y.; Zhang, Z.; Paterson, N. G.; Stansfeld, P. J.; Wang, Z.; Zhang, Y.; Wang, W.; Dong, C. Structural basis of outer membrane protein insertion by the BAM complex. *Nature* **2016**, *531* (7592), 64−69.

(5) Iadanza, M. G.; Higgins, A. J.; Schiffrin, B.; Calabrese, A. N.; Brockwell, D. J.; Ashcroft, A. E.; Radford, S. E.; Ranson, N. A. Lateral opening in the intact β-barrel assembly machinery captured by cryo-EM. *Nat. Commun.* **2016**, *7*, No. 12865.

(6) Wu, R.; Bakelar, J. W.; Lundquist, K.; Zhang, Z.; Kuo, K. M.; Ryoo, D.; Pang, Y. T.; Sun, C.; White, T.; Klose, T.; Jiang, W.; Gumbart, J. C.; Noinaj, N. Plasticity within the barrel domain of BamA mediates a hybrid-barrel mechanism by BAM. *Nat. Commun.* **2021**, *12* (1), 7131.

(7) Böhringer, N.; Green, R.; Liu, Y.; Mettal, U.; Marner, M.; Modaresi, S. M.; Jakob, R. P.; Wuisan, Z. G.; Maier, T.; Iinishi, A.; Hiller, S.; Lewis, K.; Schäberle, T. F. Mutasynthetic Production and Antimicrobial Characterization of Darobactin Analogs. *Microbiol. Spectrum* **2021**, *9* (3), No. e0153521.

(8) Haysom, S. F.; Machin, J.; Whitehouse, J. M.; Horne, J. E.; Fenn, K.; Ma, Y.; El Mkami, H.; Böhringer, N.; Schäberle, T. F.; Ranson, N. A.; Radford, S. E.; Pliotas, C. Darobactin B Stabilises a Lateral-Closed Conformation of the BAM Complex in E. coli Cells. *Angew. Chem., Int. Ed. Engl.* **2023**, *62* (34), No. e202218783.

(9) Marner, M.; Kolberg, L.; Horst, J.; Böhringer, N.; Hübner, J.; Kresna, I. D. M.; Liu, Y.; Mettal, U.; Wang, L.; Meyer-Bühn, M.; Mihajlovic, S.; Kappler, M.; Schäberle, T. F.; von Both, U. Antimicrobial Activity of Ceftazidime-Avibactam, Ceftolozane-Tazobactam, Cefiderocol, and Novel Darobactin Analogs against Multidrug-Resistant Pseudomonas aeruginosa Isolates from Pediatric and Adolescent Cystic Fibrosis Patients. *Microbiol. Spectrum* **2023**, *11* (1), No. e0443722.

(10) Böhringer, N.; Kramer, J.-C.; de La Mora, E.; Padva, L.; Wuisan, Z. G.; Liu, Y.; Kurz, M.; Marner, M.; Nguyen, H.; Amara, P.; Yokoyama, K.; Nicolet, Y.; Mettal, U.; Schäberle, T. F. Genome- and metabolome-guided discovery of marine BamA inhibitors revealed a dedicated darobactin halogenase. *Cell Chem. Biol.* **2023**, *30* (8), 943.e7−952.e7.

(11) Böhringer, N.; Wuisan, Z. G.; Marner, M.; Kresna, I. D. M.; Mettal, U.; Schmitt, S.; Reiter, S.; Liu, Y.; Brinkrolf, K.; Rupp, O.; Schwengers, O.; Findeisen, J.; Herold, S.; Matt, U.; Schäberle, T. F. Nanoliter-scale selection of optimized bioengineered peptide antibiotics that rescue mice with bacterial lung infection. *bioRxiv* **2024**, No. 596569.

(12) Nguyen, H.; Made Kresna, I. D.; Böhringer, N.; Ruel, J.; de La Mora, E.; Kramer, J.-C.; Lewis, K.; Nicolet, Y.; Schäberle, T. F.; Yokoyama, K. Characterization of a Radical SAM Oxygenase for the Ether Crosslinking in Darobactin Biosynthesis. *J. Am. Chem. Soc.* **2022**, *144* (41), 18876−18886.

(13) Wuisan, Z. G.; Kresna, I. D. M.; Böhringer, N.; Lewis, K.; Schäberle, T. F. Optimization of heterologous Darobactin A expression and identification of the minimal biosynthetic gene cluster. *Metabolic engineering* **2021**, *66*, 123−136.

(14) Ma, S.; Xi, W.; Wang, S.; Chen, H.; Guo, S.; Mo, T.; Chen, W.; Deng, Z.; Chen, F.; Ding, W.; Zhang, Q. Substrate-Controlled Catalysis in the Ether Cross-Link-Forming Radical SAM Enzymes. *J. Am. Chem. Soc.* **2023**, *145* (42), 22945−22953.

(15) Seyfert, C. E.; Müller, A. V.; Walsh, D. J.; Birkelbach, J.; Kany, A. M.; Porten, C.; Yuan, B.; Krug, D.; Herrmann, J.; Marlovits, T. C.; Hirsch, A. K. H.; Müller, R. New Genetically Engineered Derivatives of Antibacterial Darobactins Underpin Their Potential for Antibiotic Development. *Journal of medicinal chemistry* **2023**, *66* (23), 16330−16341.

(16) Seyfert, C. E.; Porten, C.; Yuan, B.; Deckarm, S.; Panter, F.; Bader, C. D.; Coetzee, J.; Deschner, F.; Tehrani, K. H. M. E.; Higgins, P. G.; Seifert, H.; Marlovits, T. C.; Herrmann, J.; Müller, R. Darobactins Exhibiting Superior Antibiotic Activity by Cryo-EM Structure Guided Biosynthetic Engineering. *Angew. Chem., Int. Ed. Engl.* **2023**, *62* (2), No. e202214094.

(17) Young, T. S.; Schultz, P. G. Beyond the canonical 20 amino acids: expanding the genetic lexicon. *J. Biol. Chem.* **2010**, *285* (15), 11039−11044.

(18) Koch, N. G.; Budisa, N. Evolution of Pyrrolysyl-tRNA Synthetase: From Methanogenesis to Genetic Code Expansion. *Chem. Rev.* **2024**, *124* (16), 9580−9608.

(19) Wang, Y.-S.; Fang, X.; Wallace, A. L.; Wu, B.; Liu, W. R. A rationally designed pyrrolysyl-tRNA synthetase mutant with a broad substrate spectrum. *J. Am. Chem. Soc.* **2012**, *134* (6), 2950−2953.

(20) Shende, V. V.; Bauman, K. D.; Moore, B. S. The shikimate pathway: gateway to metabolic diversity. *Natural product reports* **2024**, *41* (4), 604−648.

(21) Liu, S.; Yang, Y.; Zhen, X.; Li, J.; He, H.; Feng, J.; Whiting, A. Enhanced reduction of C-N multiple bonds using sodium borohydride and an amorphous nickel catalyst. *Organic & biomolecular chemistry* **2012**, *10* (3), 663−670.

(22) Dolbier, W. R. *Guide to fluorine NMR for organic chemists*, 2nd ed.; Wiley Blackwell, 2016.

(23) Hesse, M.; Meier, H.; Zeeh, B. *Spektroskopische Methoden in der organischen Chemie*, 7, überarb. Aufl.; Thieme, 2005.

(24) SciFinder. *Chemical Abstracts Service: Columbus, OH; 19F NMR spectrum; spectrum ID 12F_2WRA_420.F; CAS No. 51 65 0.* https://scifinder-n.cas.org/.

(25) Pham, L. B. T.; Costantino, A.; Barbieri, L.; Calderone, V.; Luchinat, E.; Banci, L. Direct Expression of Fluorinated Proteins in Human Cells for 19F In-Cell NMR Spectroscopy. *J. Am. Chem. Soc.* **2023**, *145* (2), 1389−1399.

(26) Ruiz, N.; Wu, T.; Kahne, D.; Silhavy, T. J. Probing the barrier function of the outer membrane with chemical conditionality. *ACS Chem. Biol.* **2006**, *1* (6), 385−395.

(27) Lee, D. G.; Urbach, J. M.; Wu, G.; Liberati, N. T.; Feinbaum, R. L.; Miyata, S.; Diggins, L. T.; He, J.; Saucier, M.; Déziel, E.; Friedman, L.; Li, L.; Grills, G.; Montgomery, K.; Kucherlapati, R.; Rahme, L. G.; Ausubel, F. M. Genomic analysis reveals that Pseudomonas aeruginosa virulence is combinatorial. *Genome biology* **2006**, *7* (10), R90.

(28) Kumar, A.; Chua, K.-L.; Schweizer, H. P. Method for regulated expression of single-copy efflux pump genes in a surrogate Pseudomonas aeruginosa strain: identification of the BpeEF-OprC chloramphenicol and trimethoprim efflux pump of Burkholderia pseudomallei 1026b. *Antimicrob. Agents Chemother.* **2006**, *50* (10), 3460−3463.

(29) Young, D. D.; Young, T. S.; Jahnz, M.; Ahmad, I.; Spraggon, G.; Schultz, P. G. An evolved aminoacyl-tRNA synthetase with atypical polysubstrate specificity. *Biochemistry* **2011**, *50* (11), 1894−1900.

https://doi.org/10.1021/acsomega.4c10307
ACS Omega XXXX, XXX, XXX−XXX

(30) Kakkar, N.; Perez, J. G.; Liu, W. R.; Jewett, M. C.; van der Donk, W. A. Incorporation of Nonproteinogenic Amino Acids in Class I and II Lantibiotics. *ACS Chem. Biol.* **2018**, *13* (4), 951−957.
(31) Gibson, D. G.; Young, L.; Chuang, R.-Y.; Venter, J. C.; Hutchison, C. A.; Smith, H. O. Enzymatic assembly of DNA molecules up to several hundred kilobases. *Nat. Methods* **2009**, *6* (5), 343−345.
(32) Kramer, J.-C.; Böhringer, N.; Mettal, U.; Schäberle, T. F. Functional in vitro and in vivo analysis of biosynthetic genes by heterologous expression in E. coli. *STAR protocols* **2023**, *4* (3), No. 102531.
(33) Gottlieb, H. E.; Kotlyar, V.; Nudelman, A. NMR Chemical Shifts of Common Laboratory Solvents as Trace Impurities. *Journal of organic chemistry* **1997**, *62* (21), 7512−7515.

https://doi.org/10.1021/acsomega.4c10307
ACS Omega XXXX, XXX, XXX−XXX

4. Discussion and future perspectives

We are facing an AMR crisis which was fruther exacerbated by the COVID-19 pandemic (O'Neill, 2016; Miethke *et al.*, 2021; Segala *et al.*, 2021; Yang *et al.*, 2024). From 2017 to 2023, only 16 new antibiotics have entered the market, while AMR is increasing. Of these 16 new antibiotics, 13 are traditional antibiotics and ten belong to an existing class of antibiotics with already established resistance mechanisms (WHO, 2023). This numbers highlight the urgent need for new antibiotics, especially against Gram-negative bacteria (WHO, 2024). Next to the inner membrane, these bacteria also possess an OM that acts as an additional barrier to the antibiotic, making the discovery of new Gram-negative active compounds challenging (Nikaido, 2003; Silhavy *et al.*, 2010; Storek *et al.*, 2024). Only six out of the 13 traditional antibiotics that entered the marked between 2017 and 2023 are active against the WHO "critical" Gram-negative pathogens. In addition, only four out of twelve traditional antibiotics entering the clinical pipeline from 2017 to 2023 meet at least one of the WHO innovation criteria and show activity against one of the WHO "critical" Gram-negative pathogens (WHO, 2023). These data show that we do not have enough treatment options for these "critical" pathogens and that the number of future treatment options is limited as well. The fact that large pharmaceutical companies have stopped investing in the antibacterial research, and that most of the development work is handled by small companies that lack money and man power, has led to a future perspective that is forcing us to act (WHO, 2021).

Approximately 60% of all antibiotics that have entered the clinical phases in the last 40 years are derivatives of known NPs or semi-synthetic drugs based on NPs. They have been and remain the most promising source of new antimicrobial drugs (Hutchings *et al.*, 2019; Newman and Cragg, 2020). After the golden age of antibiotic discovery, many of the NPs produced by easy-to-cultivate bacteria had already been discovered, leading to a stagnation in the field (Hutchings *et al.*, 2019). However, sampling in under-explored environments or environments not targeted during this period, can reveal novel antibiotics (Kaltenpoth, 2009; Palaniyandi *et al.*, 2013; Wilson *et al.*, 2014; Hutchings *et al.*, 2019). With the rise of advanced genome sequencing tools, genomic-driven natural product discovery provided new insights into the potential of bacteria as NP producers. The BGC of the NP can be identified by bioinformatic tools and different molecular biological

approaches can be used to produce the NP either in the original producer or in a heterologous expression host (Rutledge and Challis, 2015; Hutchings *et al.*, 2019). In the case of DAR A, insect symbionts were studied, specifically nematophilic bacteria from the genus *Photorhabdus* and *Xenorhabdus* (Imai *et al.*, 2019). These bacteria live association with the nematode gut microbiome and when the nematode invades its prey, these bacteria are released, producing neurotoxins to immobilize the prey and antimicrobials to combat environmental microorganisms (Crawford and Clardy, 2011; Tobias *et al.*, 2018). However, their most abundant competitors probably come from the nematode gut microbiome itself, and these competitors are closely related to common opportunistic human pathogens (Tambong, 2013; Imai *et al.*, 2019). Given that the antimicrobials should not be toxic to eukaryotic organisms such as the nematode, DAR A is a good example of a clever selection of under-explored environments for the discovery of novel antibiotics (Bellows and Fisher, 1999; Imai *et al.*, 2019). The fact that DAR A is active against the "critical" WHO priority pathogens as well as against *P. aeruginosa*, both *in vitro* and *in vivo*, makes DAR A a very important discovery (Imai *et al.*, 2019; WHO, 2024). In addition, the compound meets three out of the four WHO innovation criteria, which is not achieved by any of the 13 traditional antibiotics that entered the market between 2017 and 2023 (WHO, 2023). By targeting Bam A, a part of the BAM complex, the compound acts on a new target and therefore has a new mode of action with no known cross-resistance (Imai *et al.*, 2019; WHO, 2023). Since BamA is located in the OM of Gram-negative bacteria, the problem of having to penetrate this additional barrier to reach the antibiotic target is circumvented (Silhavy *et al.*, 2010; Imai *et al.*, 2019; Tomasek and Kahne, 2021). When DAR A binds to BamA, the closed conformation of the protein is induced and stabilized (Haysom *et al.*, 2023). This binding site is more conserved in Gram-negative bacteria than the binding sites of other BamA inhibitors and therefore the reason for the broad-spectrum activity of Dar A (Imai *et al.*, 2019; Miller *et al.*, 2022; Haysom *et al.*, 2023; Storek *et al.*, 2024).

Furthermore, the biosynthetic machinery of DAR A is of interest. DarE, which introduces the two crosslinks characterizing DAR A as a bicyclic heptapeptide, belongs to a novel class of radical SAM oxygenases and the mechanism has not yet been fully elucidated (Imai *et al.*, 2019; Nguyen *et al.*, 2022). These findings make DAR A a promising new candidate for lead development opening up a promising new class of BamA inhibitors (Imai *et al.*, 2019).

It is therefore not surprising that several studies to improve the potency and pharmacokinetics of the compound were soon initiated, leading to the discovery of new derivatives (Böhringer *et al.*, 2021; Groß *et al.*, 2021; Böhringer *et al.*, 2023; Marner *et al.*, 2023; Seyfert *et al.*, 2023b; Seyfert *et al.*, 2023a; Böhringer *et al.*, 2024). In the majority of the studies, amino acids at one or more positions of the DAR A heptapeptide were exchanged by mutation, the derivatives were heterologously expressed in *E. coli* and purified to obtain the compound for activity studies and NMR experiments (Böhringer *et al.*, 2021; Groß *et al.*, 2021; Marner *et al.*, 2023; Seyfert *et al.*, 2023b; Seyfert *et al.*, 2023a). The most promising candidates published to date are DAR B and DAR B9 (the latter identical to DAR D22) (Marner *et al.*, 2023; Seyfert *et al.*, 2023b). In activity studies using clinical isolates of multidrug-resistant bacteria, these two compounds performed even better against *P. aeruginosa* than recently licensed drugs such as ceftazidime-avibactam and ceftolozane-tazobactam (Marner *et al.*, 2023).

Another study used a broad-spectrum approach, generating a randomized library for heterologous expression. In a first attempt, it was tested whether the size of the two rings or the heptapeptide at the C- or N-terminus could be extended or shortened, which was not the case. Positions W^1, W^3 and K^5 appeared to be highly conserved, while for position F^7 also W^7 is accepted. This is why two libraries were designed: W^1-X^2-W^3-X^4-K^5-X^6-W^7 and W^1-X^2-W^3-X^4-K^5-X^6-F^7, where X represent the randomized amino acids. The screening for active compounds was performed by encapsulating the heterologous expression strain with a fluorescent sensor strain in alginate-based beads. After growth, the beads were analyzed in a flow cytometer to observe the fluorescence level of the sensor strain and thus assess the growth inhibition ability of the produced DAR derivative (Böhringer *et al.*, 2024). The top ten of the most present derivatives included DAR A and DAR 9, which were recovered from the beads three times (Böhringer *et al.*, 2024). Others are DAR B, DAR D38 and the novel derivatives WNWTKHF and WNWTKTF (Groß *et al.*, 2021; Marner *et al.*, 2023; Böhringer *et al.*, 2024). Although the *in vitro* activity of DAR B and DAR B9 is comparable, DAR B showed an advantage over DAR B9 in early ADMET (pharmacokinetics with direct influence on the efficacy of a drug: absorption, distribution, metabolism, excretion, toxicity) and mouse studies (Davis and Riley, 2004; Böhringer *et al.*, 2024).

Several studies, including the two publications in the first chapter of this dissertation, searched in databases for other DAR producers to identify natural

derivatives (Groß *et al.*, 2021; Böhringer *et al.*, 2023; Kramer *et al.*, 2023). Groß *et al.* (2021) found the DAR BGC in *P. luteoviolacea* S4054 and identified two additional genes, named *darF* and *darG*. Both enzymes yielded only hypothetical proteins of unknown function and ABC transporter predictions in database searches. In heterologous expression studies, they appeared to reduce the production level of DAR. While the function of DarG remains unclear, DarF was shown to be a protease that degrades DAR, possibly for self-resistance purposes (Groß *et al.*, 2021).

In the first and second publication of this dissertation, the amino acid sequence of DarE was used for database searches. Thereby a DAR BGC in *P. luteoviolacea* H33 could be identified, which was found to contain three additional genes: *darF*, *darG* and *darH* (Böhringer *et al.*, 2023; Kramer *et al.*, 2023). DarF was not analyzed further as it is expected to be the protease already identified by Groß *et al.* (2021). An OSMAC (one strain many compounds) approach was used to cultivate this strain in the laboratory to identify new DAR derivatives and elucidate the function of the unknown enzymes (Bode *et al.*, 2002; Böhringer *et al.*, 2023). The three new derivatives, bromodarobactin A (Br-DAR A), dehydrodarobactin A (DH-DAR A) and dehydrobromodarobactin A (DH-Br-DAR A), were identified. Br-DAR A has the same structure as DAR A, but the C-8 position of W^1 is brominated. DH-DAR A is also based on DAR A with a double bond located in the K^5 side chain and DH-Br-DAR A has both modifications (Böhringer *et al.*, 2023).
BR-DAR A and DH-Br-DAR A were purified from the original producer and antimicrobial activity was determined. Br-DAR A showed improved activity compared to DAR A against the panel tested (Böhringer *et al.*, 2023). As the indole ring of the W^1 is not involved in the binding of BamA according to the literature, this improved activity of Br-DAR A is hypothesized to be due to an improved membrane permeability as a result of the bromination (Kaur *et al.*, 2021; Böhringer *et al.*, 2023). For DH-Br-DAR A slightly higher MIC values compared to DAR A, could be explained by an increase in rigidity caused by the double bond, thus affecting BamA binding (Böhringer *et al.*, 2023). In order to identify which of the two unknown genes from the BGC is responsible for the post-translational modifications, heterologous expression studies were conducted as described in the second manuscript of this dissertation (Kramer *et al.*, 2023). *DarG* and *darH* were codon optimized, cloned together with the DAR minimal BGC and heterologously

expressed in *E. coli*. After a small scale purification step using a C_{18} column, the culture supernatant was analyzed by HRMS/MS to evaluate the change in the metabolite profile. Expression of the DAR A minimal BGC together with *darG* did not lead to any results other than the DAR A production, and the mechanism for the DH-DAR A production remains unclear. However, when DAR A was expressed in the presence of *darH*, Br-DAR A was observed, leading to the conclusion that DarH is a tryptophan halogenase. To further characterize DarH, it was tested whether other halogens than bromine could be incorporated by this halogenase. Instead of adding potassium bromide to the culture broth, potassium iodide, chloride or fluoride was added respectively. The only other modified DAR A that could be detected was iodinated DAR A (Böhringer *et al.*, 2023; Kramer *et al.*, 2023).

In addition, another construct containing the codon-optimized *darH* gene was cloned to purify the enzyme by His-tag purification. The expression was optimized by testing different cultivation conditions and the successful production could already be judged by the yellow color of the resin used for the His-tag purification (Böhringer *et al.*, 2023; Kramer *et al.*, 2023). This yellow color could be due to co-purified flavin adenine dinucleotide (FAD), which is supported by the fact that screening for homologous enzymes led to the identification of a FAD- and NAD(P)-binding site in DarH (Wink, 1997; Böhringer *et al.*, 2023). Using the purified DarH, an *in vitro* assay was developed and DAR A was successfully transformed into BR-DAR A. Substrate specificity was tested by using DAR B and the linear DAR heptapeptide, only the former could be halogenated (Böhringer *et al.*, 2023).

Screening the UniProtKB and SwissProt databases, the majority of similar enzymes were annotated as FAD-dependent oxidoreductases and none of the 250 enzymes were annotated as flavin-dependent halogenases. The different homologs were widely distributed among bacteria, plants and metazoans. Sequence comparison with the Protein Data Bank revealed only homologues in the family of the FAD/NAD(P)-binding proteins. In a phylogenetic analysis, DarH is grouped with the disulfide reductase YpdA and the flavin-containing putative monooxygenase (pdb id 3d1c), both from *S. aureus* (Hammerstad and Hersleth, 2020; Böhringer *et al.*, 2023). Tryptophan halogenases and MibH, the only flavin-dependent halogenase with sequence similarity, are clustered in an independent group (Ortega *et al.*, 2017; Böhringer *et al.*, 2023). To support the finding that DarH possesses a FAD- and NAD(P)-binding domain, an AlphaFold model was calculated

and overlaid with proteins of varying similarity (Jumper *et al.*, 2021; Böhringer *et al.*, 2023). For MibH, the only significant structural conservation is in the FAD-binding domain with 160 amino acids, while the similarity to YdpA with 323 amino acids in the FAD- and NAD(P)-binding domain is much higher (Ortega *et al.*, 2017; Hammerstad and Hersleth, 2020; Böhringer *et al.*, 2023). These results already suggest how unique DarH is, which is supported by a novel fold in the C-terminal domain that has no similarity to anything in the databases. It is hypothesized that this novel fold is involved in the binding of DAR A (Böhringer *et al.*, 2023). When using SiteMap to calculate putative binding sites, the top-ranked binding sites for FAD and NAD(P) are very similar to those of YpdA and they are common in the literature (Halgren, 2007; Halgren, 2009; Hammerstad and Hersleth, 2020; Böhringer *et al.*, 2023; Schrödinger, 2024). Other binding sites are located in the C-terminal domain, supporting the hypothesized role in binding and positioning of DAR A. Taking all of these findings together, DarH opens up a new class of FAD-dependent oxidoreductases with its novel fold (Böhringer *et al.*, 2023).

In the future, mutation studies would be a good option to understand the mechanism of the halogenation in more detail. DarH mutants can be heterologously expressed, His-tag purified like the wild-type enzyme and used for microscale thermophoresis experiments (MST). In these experiments molecular interactions can be measured, as it has been shown for a protein of the RAS family (Seidel *et al.*, 2013; Jerabek-Willemsen *et al.*, 2014; Welsch *et al.*, 2017). In this study, the potential ligand binding site was validated by mutants showing a reduced binding affinity compared to the wild-type in MST experiments (Welsch *et al.*, 2017). Similar conclusions could be drawn from measurements of the interaction between DAR A and DarH. For example, it was shown for RebH that a specific lysine forms a lysine-halogen intermediate during the halogenation reaction of tryptophan (Yeh *et al.*, 2007). It could be confirmed that DarH is a FDH and acts according to the mechanism of RebH by exchanging the lysine that is predicted to form the lysine-halogen intermediate. If similar binding constants of DAR A to the mutant DarH are observed compared to those of DAR A to the wild-type DarH, but no conversion form DAR A to Br-DAR A takes place during *in vitro* assays, it could be concluded that the transfer of the halogen to DAR A is mediated by this lysine. This may indicate how to modify the enzyme to accept halogens other than bromide and iodide.

The C-terminal domain could also be mutated. If low binding constants and no conversion during *in vitro* assays are observed, this would be another indication that this C-terminal domain is involved in DAR A binding. Binding constants could not only be determined for DAR A and DarH, but also for FAD or NAD(P) and DarH. By measuring the constant for the wild-type and then for a DarH mutant, with mutations in the potential FAD-binding site, the binding site could be validated.
Another option would be to obtain a crystal structure of the enzyme. Also co-crystallization with FAD, NAD(P) or DAR A could confirm the knowledge gained by comparing sequences in databases and performing calculations in AlphaFold and SiteMap. This could be a useful tool, especially for identifying the DAR binding site and confirming the role of the novel C-terminal fold.
It has already been shown that DarH can modify another bicyclic DAR derivative, but not the linear DAR A heptapeptide. Therefore, it was postulated that after translation of the precursor peptide, DarE introduces the rings, yet unidentified proteases cut off the signaling sequences and DarH can only act on the matured DAR (Böhringer *et al.*, 2023). This suggests that the bicyclic structure is important for binding to DarH. Knowledge about the substrate binding site would not only help to understand the mechanism of the enzyme, but would also open up the possibility of broadening the range of accepted substrates and thus halogenating other RiPPs.
Although the activity of Br-DAR A is very similar to that of the most promising DAR candidate DAR B, bringing BR-DAR A to the market would be rather challenging. *In vitro* studies with DAR A and DarH showed a slow conversion rate from DAR A to Br-DAR A and the yield from the heterologous expression of the compound itself in *E. coli* is rather low. Also, purification of the product from the original producer is not of high yield. DarH is an interesting enzyme, but the bromination is not yet suitable for large-scale production. To optimize heterologous expression, the turnover rate could be increased, for example by mutation. This would require detailed knowledge of the enzyme mechanism, which could be obtained through the experiments mentioned above. Another option would be to optimize the cultivation conditions for the original producer. Upscaling the cultivation conditions of either the heterologous expression host or the original producer in fermenters might also be viable routes. However, not only the upstream process should be optimized, but also the downstream process needs further development. Purification protocols should be revised to avoid compound losses in the

purification steps to increase the overall yield. Once production and purification have been optimized, these parameters could be applied to the iodinated DAR A, for which the activity has not yet been determined.

Given the fact that bromination increased the activity of DAR A, introducing halogens or other functional groups into the molecule is an interesting approach. As DarH has been shown to halogenate other DAR derivatives as well, the identification of the enzyme provides a first step towards DAR derivatization other than amino acid exchange (Böhringer *et al.*, 2023; Kramer *et al.*, 2023). This could not only increase the *in vitro* activity of the derivative, but also significantly alter the pharmacokinetics of the compound (Piccionello *et al.*, 2019). This is already indicated by the stronger plasma binding of Br-DAR A compared to DAR A (Böhringer *et al.*, 2023).
In particular, halogenations are widely observed in NPs (Gribble, 2024), but apart from the study in the second chapter of this dissertation, there is only one other study dealing with the halogenation of DAR (Seyfert *et al.*, 2023b; Kramer *et al.*, 2025). In this study, 6-fluoro- and 5-chloro-L-tryptophan were added to the culture broth during heterologous expression of DAR D9 (W^1-N^2-W^3-S^4-K^5-S^6-W^7). This approach led to the discovery of five halogenated DAR D9 compounds, three fluorinated and two chlorinated derivatives. However, this approach shows low selectivity for the position, in which the halogenated amino acid is integrated, because DAR D9 has more than one tryptophan in its structure. For example, when 5-chloro-L-tryptophan was added to the culture broth, a mixture of the substrate either chlorinated at W^3 or W^7 was obtained. This mixture of products and low yields are disadvantages of this technique (Seyfert *et al.*, 2023b).
With the amber stop codon suppression technique described in chapter two of this dissertation the introduction of non-canonical amino acids is targeted (Young and Schultz, 2010; Wang *et al.*, 2012; Kramer *et al.*, 2025). This technique uses a tRNA that recognizes a nonsense codon, together with an aminoacyl-tRNA synthase, mutated to extend the substrate range to non-canonical amino acids. The integration site of the non-canonical amino acid is selected by replacing the original codon at the exchange position in the BGC to the nonsense codon. The modified aminoacyl-tRNA synthase, the tRNA and the modified BGC are heterologously expressed in *E. coli*. The non-canonical amino acid of choice is then supplemented to the culture broth during the heterologous expression (Young and

Schultz, 2010; Wang *et al.*, 2012). In this study, the nonsense codon is located in *darA* at the C-terminal position of the heptapeptide (F^7) (Kramer *et al.*, 2025). This position was chosen on the one hand because the available aminoacyl-tRNA synthase can use non-canonical phenylalanine derivatives as substrates. On the other hand, phenylalanine is the last amino acid in the DAR A heptapeptide and therefore has the greatest distance from the ring closures. As there is no data available for the exact binding of DAR A to DarE, choosing this position reduces the chance of the modification interfering with the DAR maturation process.

For initial tests, it was decided to add 4-fluoro-L-phenylalanine to the culture broth, as the fluorine atom is rather small and the carbon-fluorine bound is strong, theoretically reducing the risk of interfering with the DarE interaction. In small-scale cultivation, the expected mass-to-charge ratio of DAR A F7F with the corresponding fragmentation pattern was observed in HRMS/MS. But the production of DAR A was also observed, and was even higher than the production of DAR A F7F in this small-scale experiment. Furthermore, small amounts of DAR A F7F could be observed in the cultivation without the mutant aminoacyl-tRNA synthase, the specific tRNA and the altered *darA* sequence. This finding indicates that also the wild-type aminoacyl-tRNA synthase can use 4-fluoro-L-phenylalanine as substrate and *vice versa*. However, the amount of DAR A F7F was low in the wild-type cultivation compared to the cultivation of the mutant, suggesting that only feeding of the non-canonical amino acid alone is not sufficient (Kramer *et al.*, 2025). Also in the feeding studies of Seyfert *et al.* (2023b), only one out of the five new halogenated derivatives was produced in a sufficient quantities for NMR studies. Upscaling the production of DAR A F7F resulted in an increase in the production of the target compound, while the production levels of DAR A decreased drastically. DAR A F7F could be purified in sufficient yield for NMR experiments and activity assays. In these activity assays, DAR A F7F showed a similar range of activity compared to DAR A (Kramer *et al.*, 2025). But even if the fluorination does not improve the activity, it could improve pharmacokinetics of the compound. This effect of halogenation has already been observed for other compounds, in particular for the fluorination of NPs (Piccionello *et al.*, 2019). It was also shown that the plasma binding of Br-DAR A was increased compared to DAR A, providing an example of a halogenation altering the pharmacokinetics of DAR (Böhringer *et al.*, 2023). Therefore, pharmacokinetic studies should be performed to further characterize the potential of DAR A F7F.

Next to 4-fluoro-L-phenylalanine, a set of other non-canonical phenylalanine derivatives was tested for integration in small-scale cultivation experiments. This set included the following derivatives: 4-chloro-L-phenylalanine (4-Cl-F), 4-trifluoromethyl-L-phenylalanine (4-CF_3-F), 4-azido-L-phenylalanine (4-N_3-F), 4-nitro-L-phenylalanine (4-NO_2-F), 4-methoxy-L-phenylalanine (4-OMe-F), 4-bromo-L-phenylalanine (4-Br-F), 4-iodo-L-phenylalanine (4-I-F), 3,4-dihydroxy-L-phenylalanine (3,4-OH-F) and 2,3,4,5,6-pentafluoro-L-phenylalanine (F_5-F). From this set, DAR A F7OMe with a methoxy group at the *para* position of F^7, DAR A F7I with an iodination at the *para* position of F^7 and DAR A F7F_5 with aromatic perfluorination of F^7 could be detected by HRMS/MS. Other phenylalanine derivatives of this set did not lead to the production of DAR A derivatives (Kramer *et al.*, 2025). One reason for this could be different integration efficiencies, which have been observed in other studies as well (Young *et al.*, 2011; Wang *et al.*, 2012; Tharp *et al.*, 2014; Kakkar *et al.*, 2018; Kramer *et al.*, 2025). This is supported by the varying yields of the derivatives obtained, the highest being DAR A F7F_5, followed by DAR A F7F, DAR A F7OMe and DAR A F7I (Kramer *et al.*, 2025).

In general, the integration efficiencies observed in the literature partially reflect the observations of this study (Kramer *et al.*, 2025). For example, the integration efficiency for 4-bromo-L-phenylalanine was reported to be very high in most of the studies, only for Wang *et al.* (2012) integration efficiencies were low (Young *et al.*, 2011; Tharp *et al.*, 2014; Kakkar *et al.*, 2018). For 4-iodo-L-phenylalanine, a rather low integration efficiency can be observed in the literature (Wang *et al.*, 2012; Tharp *et al.*, 2014), with the exception of the study by Young *et al.* (2011). However, it should to be noted that Young *et al.* (2011) used a system derived from a different organism. In contrast, in the study presented here, DAR A F7Br was not observed at all and DAR A F7I could be obtained. The analogue 4-chloro-L-phenylalanine could be integrated in Tharp *et al.* (2014), but not in the study of Wang *et al.* (2012) or in the study of this dissertation (Kramer *et al.*, 2025). This suggests that the efficiency may also depend on the peptide. For DAR, low yields together with the slow working DarE could result in production levels below the detection limit (Nguyen *et al.*, 2022; Kramer *et al.*, 2025). In addition, the modification could further slowdown the reaction with DarE. To overcome these problems, a longer fermentation could be

tested. To avoid nutrient depletion in the broth during longer fermentation times, it may be necessary to use fermenters with constant nutrient supply.

Another possible reason for the unsuccessful DAR production with some of the phenylalanine derivatives could be interference of the modified linear heptapeptide with the reaction catalyzed by DarE. With the amber stop codon suppression technique, there is always a risk that the heptapeptide of the derivative is translated, but the peptide cannot be processed by DarE and therefore the ring closures are not integrated and the peptide being degraded by proteases. This risk can be decreased when more detailed information about DarE is available to predict which position can be exchanged and which functional groups attached to the amino acid would not interfere with the reaction. Expression systems derived from other organisms such as the one used in the study by Young *et al.* (2011), could also be tested to obtain the missing variants.

It would also be possible to integrate *darH* into the expression system to obtain Br-DAR A variants with a phenylalanine derivative. Another possibility would be to conduct the DarH *in vitro* assay, developed in the first and second publication of this dissertation, using a DAR A derivative with a non-canonical amino acid as substrate. But, since the production of Br-DAR is rather low, combined with the low yields of the DAR A derivatives containing the non-canonical amino acids, these attempts would still need a lot of optimizations to obtain more than analytical amounts.

For the already existing derivatives upscale experiments should be carried out to obtain enough material to test activity and pharmacokinetics (Kramer *et al.*, 2025). Furthermore, the successfully developed method for the integration of non-canonical amino acids into DAR A, could be adapted to other DAR derivatives, such as the most promising candidate DAR B, in order to further optimize the derivative (Marner *et al.*, 2023; Kramer *et al.*, 2025). At present, this technique is limited to phenylalanine derivatives due to the mutanted aminoacyl-tRNA synthase used in this study. However, it would be possible to mutate other types of aminoacyl-tRNA synthases to accept non-canonical tryptophan derivatives, for example. This would be particularly interesting for DAR, since for Br-DAR A, which has a bromination at the W^1, the activity was increased (Böhringer *et al.*, 2023). But this exchange is likely to be even more problematic, since DarE acts directly on these amino acid (Imai *et al.*, 2019; Nguyen *et al.*, 2022).

Overall, daropeptides represent a promising new compound class for which many optimization techniques have already been applied to improve the activity and pharmacokinetics. However, the three studies of this dissertation show that there is still potential for optimization, especially when it comes to the integration of functional groups. While the production methods for the compounds discussed here still leave room for improvement, the studies provide an example of using DAR A, an antibiotic with a novel mode of action, as a lead structure for compound optimization. The modifications may not always increase the activity itself, but they might have a significant impact on the pharmacokinetics of the compound, potentially making the derivative a more suitable antibiotic drug. Therefore, pharmacokinetic studies and *in vivo* studies should be conducted to evaluate promising candidates. The next steps, especially for further developed compounds such as DAR B, should be in-depth testing of the clinical candidate to provide a dossier to apply for and enter clinical trials to bring the compound to the market and help us tackle the upcoming AMR crisis (Ventola, 2015; O'Neill, 2016; Marner *et al.*, 2023).

5. References

Arnison, P.G., Bibb, M.J., Bierbaum, G., Bowers, A.A., Bugni, T.S., Bulaj, G., *et al.* (2013) Ribosomally synthesized and post-translationally modified peptide natural products: overview and recommendations for a universal nomenclature. *Nat Prod Rep* **30** (1): 108–160.

Bellows, T.S., and Fisher, T.W. (1999) *Handbook of Biological Control: Principles and Applications of Biological Control:* Elsevier.

Blin, K., Shaw, S., Steinke, K., Villebro, R., Ziemert, N., Lee, S.Y., *et al.* (2019) antiSMASH 5.0: updates to the secondary metabolite genome mining pipeline. *Nucleic Acids Res* **47** (W1): W81-W87.

Bode, H.B., Bethe, B., Höfs, R., and Zeeck, A. (2002) Big Effects from Small Changes: Possible Ways to Explore Nature's Chemical Diversity. *ChemBioChem* **3** (7): 619.

Böhringer, N., Green, R., Liu, Y., Mettal, U., Marner, M., Modaresi, S.M., *et al.* (2021) Mutasynthetic Production and Antimicrobial Characterization of Darobactin Analogs. *Microbiol Spectr* **9** (3): e0153521.

Böhringer, N., Kramer, J.-C., La Mora, E.d., Padva, L., Wuisan, Z.G., Liu, Y., *et al.* (2023) Genome- and metabolome-guided discovery of marine BamA inhibitors revealed a dedicated darobactin halogenase. *Cell Chem Biol* **30** (8): 943-952.e7.

Böhringer, N., Wuisan, Z.G., Marner, M., Kresna, I.D.M., Mettal, U., Schmitt, S., *et al.* (2024) *Nanoliter-scale selection of optimized bioengineered peptide antibiotics that rescue mice with bacterial lung infection*.

Breton, R.C., and Reynolds, W.F. (2013) Using NMR to identify and characterize natural products. *Nat Prod Rep* **30** (4): 501–524.

Broberg, A., Menkis, A., and Vasiliauskas, R. (2006) Kutznerides 1-4, depsipeptides from the actinomycete Kutzneria sp. 744 inhabiting mycorrhizal roots of Picea abies seedlings. *J Nat Prod* **69** (1): 97–102.

Butler, A., and Carter-Franklin, J.N. (2004) The role of vanadium bromoperoxidase in the biosynthesis of halogenated marine natural products. *Nat Prod Rep* **21** (1): 180–188.

Celik, E., and Calık, P. (2012) Production of recombinant proteins by yeast cells. *Biotechnol Adv* **30** (5): 1108–1118.

Crawford, J.M., and Clardy, J. (2011) Bacterial symbionts and natural products. *Chem Commun (Camb)* **47** (27): 7559–7566.

Da Ribeiro Cunha, B., Fonseca, L.P., and Calado, C.R.C. (2019) Antibiotic Discovery: Where Have We Come from, Where Do We Go? *Antibiotics (Basel)* **8** (2).

Date, T., and Wickner, W. (1981) Isolation of the Escherichia coli leader peptidase gene and effects of leader peptidase overproduction in vivo. *Proc. Natl. Acad. Sci. U.S.A.* **78** (10): 6106–6110.

Davis, A.M., and Riley, R.J. (2004) Predictive ADMET studies, the challenges and the opportunities. *Curr Opin Chem Biol* **8** (4): 378–386.

Desai, P.N., Shrivastava, N., and Padh, H. (2010) Production of heterologous proteins in plants: strategies for optimal expression. *Biotechnol Adv* **28** (4): 427–435.

Dong, C., Huang, F., Deng, H., Schaffrath, C., Spencer, J.B., O'Hagan, D., and Naismith, J.H. (2004) Crystal structure and mechanism of a bacterial fluorinating enzyme. *Nature* **427** (6974): 561–565.

Driessen, A.J., Manting, E.H., and van der Does, C. (2001) The structural basis of protein targeting and translocation in bacteria. *Nat Struct Biol* **8** (6): 492–498.

Edwards, D.J., Marquez, B.L., Nogle, L.M., McPhail, K., Goeger, D.E., Roberts, M.A., and Gerwick, W.H. (2004) Structure and biosynthesis of the jamaicamides, new mixed polyketide-peptide neurotoxins from the marine cyanobacterium Lyngbya majuscula. *Chem Biol* **11** (6): 817–833.

Eustáquio, A.S., Pojer, F., Noel, J.P., and Moore, B.S. (2008) Discovery and characterization of a marine bacterial SAM-dependent chlorinase. *Nat Chem Biol* **4** (1): 69–74.

Fleming, A. (1929) On the Antibacterial Action of Cultures of a Penicillium, with Special Reference to their Use in the Isolation of B. influenzæ. *Br J Exp Pathol* **10** (3): 226–236.

Gao, Y., Honzatko, R.B., and Peters, R.J. (2012) Terpenoid synthase structures: a so far incomplete view of complex catalysis. *Nat Prod Rep* **29** (10): 1153–1175.

Gavrish, E., Sit, C.S., Cao, S., Kandror, O., Spoering, A., Peoples, A., *et al.* (2014) Lassomycin, a ribosomally synthesized cyclic peptide, kills mycobacterium tuberculosis by targeting the ATP-dependent protease ClpC1P1P2. *Chem Biol* **21** (4): 509–518.

Gelpi, A., Gilbertson, A., and Tucker, J.D. (2015) Magic bullet: Paul Ehrlich, Salvarsan and the birth of venereology. *Sex Transm Infect* **91** (1): 68–69.

Genuth, N.R., and Barna, M. (2018) Heterogeneity and specialized functions of translation machinery: from genes to organisms. *Nat Rev Genet* **19** (7): 431–452.

Gerding, M.A., Ogata, Y., Pecora, N.D., Niki, H., and Boer, P.A.J. de (2007) The trans-envelope Tol-Pal complex is part of the cell division machinery and required for proper outer-membrane invagination during cell constriction in E. coli. *Mol Microbiol* **63** (4): 1008–1025.

Ghequire, M.G.K., Swings, T., Michiels, J., Buchanan, S.K., and Mot, R. de (2018) Hitting with a BAM: Selective Killing by Lectin-Like Bacteriocins. *mBio* **9** (2).

Gribble, G.W. (2024) A Survey of Recently Discovered Naturally Occurring Organohalogen Compounds. *J Nat Prod* **87** (4): 1285–1305.

Groll, M., Huber, R., and Potts, B.C.M. (2006) Crystal structures of Salinosporamide A (NPI-0052) and B (NPI-0047) in complex with the 20S proteasome reveal important consequences of beta-lactone ring opening and a mechanism for irreversible binding. *J Am Chem Soc* **128** (15): 5136–5141.

Groß, S., Panter, F., Pogorevc, D., Seyfert, C.E., Deckarm, S., Bader, C.D., *et al.* (2021) Improved broad-spectrum antibiotics against Gram-negative pathogens via darobactin biosynthetic pathway engineering. *Chem Sci* **12** (35): 11882–11893.

Guo, S., Wang, S., Ma, S., Deng, Z., Ding, W., and Zhang, Q. (2022) Radical SAM-dependent ether crosslink in daropeptide biosynthesis. *Nat Commun* **13** (1): 2361.

Gustafsson, C., Govindarajan, S., and Minshull, J. (2004) Codon bias and heterologous protein expression. *Trends Biotechnol* **22** (7): 346–353.

Hagan, C.L., Kim, S., and Kahne, D. (2010) Reconstitution of outer membrane protein assembly from purified components. *Science* **328** (5980): 890–892.

Hagan, C.L., Wzorek, J.S., and Kahne, D. (2015) Inhibition of the β-barrel assembly machine by a peptide that binds BamD. *Proc. Natl. Acad. Sci. U.S.A.* **112** (7): 2011–2016.

Hager, L.P., Morris, D.R., Brown, F.S., and Eberwein, H. (1966) Chloroperoxidase. *Journal of Biological Chemistry* **241** (8): 1769–1777.

Halgren, T. (2007) New method for fast and accurate binding-site identification and analysis. *Chem Biol Drug Des* **69** (2): 146–148.

Halgren, T.A. (2009) Identifying and characterizing binding sites and assessing druggability. *J Chem Inf Model* **49** (2): 377–389.

Hammerstad, M., and Hersleth, H.-P. (2020) *Bacillithiol Disulfide Reductase Bdr (YpdA) from Staphylococcus aureus*.

Harris, C.M., Kannan, R., Kopecka, H., and Harris, T.M. (1985) The role of the chlorine substituents in the antibiotic vancomycin: preparation and characterization of mono- and didechlorovancomycin. *J Am Chem Soc* **107** (23): 6652–6658.

Hart, E.M., Mitchell, A.M., Konovalova, A., Grabowicz, M., Sheng, J., Han, X., *et al.* (2019) A small-molecule inhibitor of BamA impervious to efflux and the outer membrane permeability barrier. *Proc. Natl. Acad. Sci. U.S.A.* **116** (43): 21748–21757.

Haysom, S.F., Machin, J., Whitehouse, J.M., Horne, J.E., Fenn, K., Ma, Y., *et al.* (2023) Darobactin B Stabilises a Lateral-Closed Conformation of the BAM Complex in E. coli Cells. *Angew Chem Int Ed Engl* **62** (34): e202218783.

Hernandez, I., San-Juan-Rodriguez, A., Good, C.B., and Gellad, W.F. (2020) Changes in List Prices, Net Prices, and Discounts for Branded Drugs in the US, 2007-2018. *JAMA* **323** (9): 854–862.

Hershberg, R., and Petrov, D.A. (2008) Selection on codon bias. *Annu Rev Genet* **42:** 287–299.

Hertweck, C. (2009) The biosynthetic logic of polyketide diversity. *Angew Chem Int Ed Engl* **48** (26): 4688–4716.

Hodgkin, D.C. (1949) The X-ray analysis of the structure of penicillin. *Adv Sci* **6** (22): 85–89.

Hornung, A., Bertazzo, M., Dziarnowski, A., Schneider, K., Welzel, K., Wohlert, S.-E., *et al.* (2007) A genomic screening approach to the structure-guided identification of drug candidates from natural sources. *Chembiochem* **8** (7): 757–766.

Hutchings, M.I., Truman, A.W., and Wilkinson, B. (2019) Antibiotics: past, present and future. *Curr Opin Microbiol* **51:** 72–80.

Iadanza, M.G., Higgins, A.J., Schiffrin, B., Calabrese, A.N., Brockwell, D.J., Ashcroft, A.E., *et al.* (2016) Lateral opening in the intact β-barrel assembly machinery captured by cryo-EM. *Nat Commun* **7:** 12865.

Imai, Y., Meyer, K.J., Iinishi, A., Favre-Godal, Q., Green, R., Manuse, S., *et al.* (2019) A new antibiotic selectively kills Gram-negative pathogens. *Nature* **576** (7787): 459–464.

Jerabek-Willemsen, M., André, T., Wanner, R., Roth, H.M., Duhr, S., Baaske, P., and Breitsprecher, D. (2014) MicroScale Thermophoresis: Interaction analysis and beyond. *Journal of Molecular Structure* **1077:** 101–113.

Jumper, J., Evans, R., Pritzel, A., Green, T., Figurnov, M., Ronneberger, O., *et al.* (2021) Highly accurate protein structure prediction with AlphaFold. *Nature* **596** (7873): 583–589.

Kadjo, A.E., and Eustáquio, A.S. (2023) Bacterial natural product discovery by heterologous expression. *J Ind Microbiol Biotechnol* **50** (1).

Kakkar, N., Perez, J.G., Liu, W.R., Jewett, M.C., and van der Donk, W.A. (2018) Incorporation of Nonproteinogenic Amino Acids in Class I and II Lantibiotics. *ACS Chem Biol* **13** (4): 951–957.

Kaltenpoth, M. (2009) Actinobacteria as mutualists: general healthcare for insects? *Trends Microbiol* **17** (12): 529–535.

Katz, L., and Baltz, R.H. (2016) Natural product discovery: past, present, and future. *J Ind Microbiol Biotechnol* **43** (2-3): 155–176.

Kaur, H., Jakob, R.P., Marzinek, J.K., Green, R., Imai, Y., Bolla, J.R., *et al.* (2021) The antibiotic darobactin mimics a β-strand to inhibit outer membrane insertase. *Nature* **593** (7857): 125–129.

Kawai, K., Wang, G., Okamoto, S., and Ochi, K. (2007) The rare earth, scandium, causes antibiotic overproduction in Streptomyces spp. *FEMS Microbiol Lett* **274** (2): 311–315.

Keller, S., Wage, T., Hohaus, K., Hölzer, M., Eichhorn, E., and van Pée, K.-H. (2000) Purification and Partial Characterization of Tryptophan 7-Halogenase (PrnA) fromPseudomonas fluorescens. *Angew. Chem. Int. Ed.* **39** (13): 2300–2302.

Khaldi, N., Seifuddin, F.T., Turner, G., Haft, D., Nierman, W.C., Wolfe, K.H., and Fedorova, N.D. (2010) SMURF: Genomic mapping of fungal secondary metabolite clusters. *Fungal Genet Biol* **47** (9): 736–741.

Klassen, J.L. (2014) Microbial secondary metabolites and their impacts on insect symbioses. *Curr Opin Insect Sci* **4:** 15–22.

Konovalova, A., Kahne, D.E., and Silhavy, T.J. (2017) Outer Membrane Biogenesis. *Annu Rev Microbiol* **71:** 539–556.

Kramer, J.-C., Böhringer, N., Mettal, U., and Schäberle, T.F. (2023) Functional in vitro and in vivo analysis of biosynthetic genes by heterologous expression in E. coli. *STAR Protoc* **4** (3): 102531.

Kramer, J.-C., Wuisan, Z.G., Mettal, U., Marner, M., and Schäberle, T.F. (2025) Expanding the Range of Darobactin Derivatives by Amber Stop Codon Suppression To Introduce Non-canonical Amino Acids. *ACS Omega*.

Krug, D., and Müller, R. (2014) Secondary metabolomics: the impact of mass spectrometry-based approaches on the discovery and characterization of microbial natural products. *Nat Prod Rep* **31** (6): 768–783.

Kundu, R. (2020) Cationic Amphiphilic Peptides: Synthetic Antimicrobial Agents Inspired by Nature. *ChemMedChem* **15** (20): 1887–1896.

Li, G.-W., Oh, E., and Weissman, J.S. (2012) The anti-Shine-Dalgarno sequence drives translational pausing and codon choice in bacteria. *Nature* **484** (7395): 538–541.

Li, Y., Zhu, X., Zhang, J., Lin, Y., You, X., Chen, M., *et al.* (2020) Identification of a Compound That Inhibits the Growth of Gram-Negative Bacteria by Blocking BamA-BamD Interaction. *Front Microbiol* **11:** 1252.

Lin, S., van Lanen, S.G., and Shen, B. (2007) Regiospecific chlorination of (S)-beta-tyrosyl-S-carrier protein catalyzed by SgcC3 in the biosynthesis of the enediyne antitumor antibiotic C-1027. *J Am Chem Soc* **129** (41): 12432–12438.

Lincke, T., Behnken, S., Ishida, K., Roth, M., and Hertweck, C. (2010) Closthioamide: an unprecedented polythioamide antibiotic from the strictly anaerobic bacterium Clostridium cellulolyticum. *Angew Chem Int Ed Engl* **49** (11): 2011–2013.

Ling, L.L., Schneider, T., Peoples, A.J., Spoering, A.L., Engels, I., Conlon, B.P., *et al.* (2015) A new antibiotic kills pathogens without detectable resistance. *Nature* **517** (7535): 455–459.

Livermore, D.M. (2011) Discovery research: the scientific challenge of finding new antibiotics. *J Antimicrob Chemother* **66** (9): 1941–1944.

Ludewig, H., Molyneux, S., Ferrinho, S., Guo, K., Lynch, R., Gkotsi, D.S., and Goss, R.J. (2020) Halogenases: structures and functions. *Curr Opin Struct Biol* **65:** 51–60.

Luther, A., Urfer, M., Zahn, M., Müller, M., Wang, S.-Y., Mondal, M., *et al.* (2019) Chimeric peptidomimetic antibiotics against Gram-negative bacteria. *Nature* **576** (7787): 452–458.

Marner, M., Kolberg, L., Horst, J., Böhringer, N., Hübner, J., Kresna, I.D.M., *et al.* (2023) Antimicrobial Activity of Ceftazidime-Avibactam, Ceftolozane-Tazobactam, Cefiderocol, and Novel Darobactin Analogs against Multidrug-Resistant Pseudomonas aeruginosa Isolates from Pediatric and Adolescent Cystic Fibrosis Patients. *Microbiol Spectr* **11** (1): e0443722.

Matano, L.M., Coyne, M.J., García-Bayona, L., and Comstock, L.E. (2021) Bacteroidetocins Target the Essential Outer Membrane Protein BamA of Bacteroidales Symbionts and Pathogens. *mBio* **12** (5): e0228521.

Medema, M.H., Blin, K., Cimermancic, P., Jager, V. de, Zakrzewski, P., Fischbach, M.A., *et al.* (2011) antiSMASH: rapid identification, annotation and analysis of secondary metabolite biosynthesis gene clusters in bacterial and fungal genome sequences. *Nucleic Acids Res* **39** (Web Server issue): W339-46.

Medema, M.H., Paalvast, Y., Nguyen, D.D., Melnik, A., Dorrestein, P.C., Takano, E., and Breitling, R. (2014) Pep2Path: automated mass spectrometry-guided genome mining of peptidic natural products. *PLoS Comput Biol* **10** (9): e1003822.

Miethke, M., Pieroni, M., Weber, T., Brönstrup, M., Hammann, P., Halby, L., *et al.* (2021) Towards the sustainable discovery and development of new antibiotics. *Nat Rev Chem* **5** (10): 726–749.

Miller, R.D., Iinishi, A., Modaresi, S.M., Yoo, B.-K., Curtis, T.D., Lariviere, P.J., *et al.* (2022) Computational identification of a systemic antibiotic for gram-negative bacteria. *Nat Microbiol* **7** (10): 1661–1672.

Mitchell, A.M., and Silhavy, T.J. (2019) Envelope stress responses: balancing damage repair and toxicity. *Nat Rev Microbiol* **17** (7): 417–428.

Mohimani, H., Kersten, R.D., Liu, W.-T., Wang, M., Purvine, S.O., Wu, S., *et al.* (2014a) Automated genome mining of ribosomal peptide natural products. *ACS Chem Biol* **9** (7): 1545–1551.

Mohimani, H., Liu, W.-T., Kersten, R.D., Moore, B.S., Dorrestein, P.C., and Pevzner, P.A. (2014b) NRPquest: Coupling Mass Spectrometry and Genome Mining for Nonribosomal Peptide Discovery. *J Nat Prod* **77** (8): 1902–1909.

Mordstein, C., Savisaar, R., Young, R.S., Bazile, J., Talmane, L., Luft, J., *et al.* (2020) Codon Usage and Splicing Jointly Influence mRNA Localization. *Cell Syst* **10** (4): 351-362.e8.

Mori, N., Ishii, Y., Tateda, K., Kimura, S., Kouyama, Y., Inoko, H., *et al.* (2012) A peptide based on homologous sequences of the β-barrel assembly machinery component BamD potentiates antibiotic susceptibility of Pseudomonas aeruginosa. *J Antimicrob Chemother* **67** (9): 2173–2181.

Neumann, C.S., Fujimori, D.G., and Walsh, C.T. (2008) Halogenation strategies in natural product biosynthesis. *Chem Biol* **15** (2): 99–109.

Newman, D.J., and Cragg, G.M. (2016) Natural Products as Sources of New Drugs from 1981 to 2014. *J Nat Prod* **79** (3): 629–661.

Newman, D.J., and Cragg, G.M. (2020) Natural Products as Sources of New Drugs over the Nearly Four Decades from 01/1981 to 09/2019. *J Nat Prod* **83** (3): 770–803.

Nguyen, B.X., Gurusinga, F.F., Mettal, U., Schäberle, T.F., and Yokoyama, K. (2024) Radical-Mediated Nucleophilic Peptide Cross-Linking in Dynobactin Biosynthesis. *J Am Chem Soc* **146** (46): 31715–31732.

Nguyen, H., Made Kresna, I.D., Böhringer, N., Ruel, J., La Mora, E.d., Kramer, J.-C., *et al.* (2022) Characterization of a Radical SAM Oxygenase for the Ether Crosslinking in Darobactin Biosynthesis. *J Am Chem Soc* **144** (41): 18876–18886.

Nichols, D., Cahoon, N., Trakhtenberg, E.M., Pham, L., Mehta, A., Belanger, A., *et al.* (2010) Use of ichip for high-throughput in situ cultivation of "uncultivable" microbial species. *Appl Environ Microbiol* **76** (8): 2445–2450.

Nightingale, Z.D., Lancha, A.H., Handelman, S.K., Dolnikowski, G.G., Busse, S.C., Dratz, E.A., *et al.* (2000) Relative reactivity of lysine and other peptide-bound amino acids to oxidation by hypochlorite. *Free Radic Biol Med* **29** (5): 425–433.

Nikaido, H. (2003) Molecular basis of bacterial outer membrane permeability revisited. *Microbiol Mol Biol Rev* **67** (4): 593–656.

Noinaj, N., Kuszak, A.J., Gumbart, J.C., Lukacik, P., Chang, H., Easley, N.C., *et al.* (2013) Structural insight into the biogenesis of β-barrel membrane proteins. *Nature* **501** (7467): 385–390.

Okuda, S., Sherman, D.J., Silhavy, T.J., Ruiz, N., and Kahne, D. (2016) Lipopolysaccharide transport and assembly at the outer membrane: the PEZ model. *Nat Rev Microbiol* **14** (6): 337–345.

O'Neill, J. (2016) *Tackling drug-resistant infections globally: Final report and recommendations: The review on antimicrobial resistance*.

Ortega, M.A., Cogan, D.P., Mukherjee, S., Garg, N., Li, B., Thibodeaux, G.N., *et al.* (2017) Two Flavoenzymes Catalyze the Post-Translational Generation of 5-Chlorotryptophan and 2-Aminovinyl-Cysteine during NAI-107 Biosynthesis. *ACS Chem Biol* **12** (2): 548–557.

Otten, H. (1986) Domagk and the development of the sulphonamides. *J Antimicrob Chemother* **17** (6): 689–696.

Oves-Costales, D., Kadi, N., and Challis, G.L. (2009) The long-overlooked enzymology of a nonribosomal peptide synthetase-independent pathway for virulence-conferring siderophore biosynthesis. *Chem Commun (Camb)* (43): 6530–6541.

Palaniyandi, S.A., Yang, S.H., Zhang, L., and Suh, J.-W. (2013) Effects of actinobacteria on plant disease suppression and growth promotion. *Appl Microbiol Biotechnol* **97** (22): 9621–9636.

Parret, A.H., Besir, H., and Meijers, R. (2016) Critical reflections on synthetic gene design for recombinant protein expression. *Curr Opin Struct Biol* **38:** 155–162.

Payne, D.J., Miller, L.F., Findlay, D., Anderson, J., and Marks, L. (2015) Time for a change: addressing R&D and commercialization challenges for antibacterials. *Philos Trans R Soc Lond B Biol Sci* **370** (1670): 20140086.

Piccionello, A.P., Pibiri, I., Buscemi, S., and Pace, A. (ed.) (2019) *Fluorine in Life Sciences: Pharmaceuticals, Medicinal Diagnostics, and Agrochemicals: Recent development in fluorinated antibiotics:* Elsevier.

Piel, J. (2010) Biosynthesis of polyketides by trans-AT polyketide synthases. *Nat Prod Rep* **27** (7): 996–1047.

Pohanka, A., Menkis, A., Levenfors, J., and Broberg, A. (2006) Low-abundance kutznerides from Kutzneria sp. 744. *J Nat Prod* **69** (12): 1776–1781.

Power, E. (2006) Impact of antibiotic restrictions: the pharmaceutical perspective. *Clin Microbiol Infect* **12 Suppl 5:** 25–34.

Qiao, S., Luo, Q., Zhao, Y., Zhang, X.C., and Huang, Y. (2014) Structural basis for lipopolysaccharide insertion in the bacterial outer membrane. *Nature* **511** (7507): 108–111.

Ramaswamy, A.V., Sorrels, C.M., and Gerwick, W.H. (2007) Cloning and biochemical characterization of the hectochlorin biosynthetic gene cluster from the marine cyanobacterium Lyngbya majuscula. *J Nat Prod* **70** (12): 1977–1986.

Ricci, D.P., Hagan, C.L., Kahne, D., and Silhavy, T.J. (2012) Activation of the Escherichia coli β-barrel assembly machine (Bam) is required for essential components to interact properly with substrate. *Proc. Natl. Acad. Sci. U.S.A.* **109** (9): 3487–3491.

Riley, M.A., and Wertz, J.E. (2002) Bacteriocins: evolution, ecology, and application. *Annu Rev Microbiol* **56:** 117–137.

Rosano, G.L., and Ceccarelli, E.A. (2014) Recombinant protein expression in Escherichia coli: advances and challenges. *Front Microbiol* **5:** 172.

Rutledge, P.J., and Challis, G.L. (2015) Discovery of microbial natural products by activation of silent biosynthetic gene clusters. *Nat Rev Microbiol* **13** (8): 509–523.

Sanada, M., Miyano, T., Iwadare, S., Williamson, J.M., Arison, B.H., Smith, J.L., *et al.* (1986) Biosynthesis of fluorothreonine and fluoroacetic acid by the thienamycin producer, Streptomyces cattleya. *J Antibiot (Tokyo)* **39** (2): 259–265.

Scherlach, K., and Hertweck, C. (2006) Discovery of aspoquinolones A-D, prenylated quinoline-2-one alkaloids from Aspergillus nidulans, motivated by genome mining. *Org Biomol Chem* **4** (18): 3517–3520.

Scherlach, K., Schuemann, J., Dahse, H.-M., and Hertweck, C. (2010) Aspernidine A and B, prenylated isoindolinone alkaloids from the model fungus Aspergillus nidulans. *J Antibiot (Tokyo)* **63** (7): 375–377.

Schrödinger (2024) *SiteMap.* LLC, New York, NY.

Segala, F.V., Bavaro, D.F., Di Gennaro, F., Salvati, F., Marotta, C., Saracino, A., *et al.* (2021) Impact of SARS-CoV-2 Epidemic on Antimicrobial Resistance: A Literature Review. *Viruses* **13** (11).

Seidel, S.A.I., Dijkman, P.M., Lea, W.A., van den Bogaart, G., Jerabek-Willemsen, M., Lazic, A., *et al.* (2013) Microscale thermophoresis quantifies

biomolecular interactions under previously challenging conditions. *Methods* **59** (3): 301–315.

Seipke, R.F., Kaltenpoth, M., and Hutchings, M.I. (2012) Streptomyces as symbionts: an emerging and widespread theme? *FEMS Microbiol Rev* **36** (4): 862–876.

Seyedsayamdost, M.R. (2014) High-throughput platform for the discovery of elicitors of silent bacterial gene clusters. *Proc Natl Acad Sci U S A* **111** (20): 7266–7271.

Seyfert, C.E., Müller, A.V., Walsh, D.J., Birkelbach, J., Kany, A.M., Porten, C., *et al.* (2023a) New Genetically Engineered Derivatives of Antibacterial Darobactins Underpin Their Potential for Antibiotic Development. *J Med Chem* **66** (23): 16330–16341.

Seyfert, C.E., Porten, C., Yuan, B., Deckarm, S., Panter, F., Bader, C.D., *et al.* (2023b) Darobactins Exhibiting Superior Antibiotic Activity by Cryo-EM Structure Guided Biosynthetic Engineering. *Angew Chem Int Ed Engl* **62** (2): e202214094.

Sharp, P.M., and Li, W.H. (1987) The codon Adaptation Index--a measure of directional synonymous codon usage bias, and its potential applications. *Nucleic Acids Res* **15** (3): 1281–1295.

Shima, J., Hesketh, A., Okamoto, S., Kawamoto, S., and Ochi, K. (1996) Induction of actinorhodin production by rpsL (encoding ribosomal protein S12) mutations that confer streptomycin resistance in Streptomyces lividans and Streptomyces coelicolor A3(2). *J Bacteriol* **178** (24): 7276–7284.

Silhavy, T.J., Kahne, D., and Walker, S. (2010) The bacterial cell envelope. *Cold Spring Harb Perspect Biol* **2** (5): a000414.

Sinnige, T., Weingarth, M., Daniëls, M., Boelens, R., Bonvin, A.M.J.J., Houben, K., and Baldus, M. (2015) Conformational Plasticity of the POTRA 5 Domain in the Outer Membrane Protein Assembly Factor BamA. *Structure* **23** (7): 1317–1324.

Sklar, J.G., Wu, T., Kahne, D., and Silhavy, T.J. (2007) Defining the roles of the periplasmic chaperones SurA, Skp, and DegP in Escherichia coli. *Genes Dev* **21** (19): 2473–2484.

Smith, R., and Coast, J. (2013) The true cost of antimicrobial resistance. *BMJ* **346:** f1493.

Storek, K.M., Auerbach, M.R., Shi, H., Garcia, N.K., Sun, D., Nickerson, N.N., *et al.* (2018) Monoclonal antibody targeting the β-barrel assembly machine of Escherichia coli is bactericidal. *Proc. Natl. Acad. Sci. U.S.A.* **115** (14): 3692–3697.

Storek, K.M., Sun, D., and Rutherford, S.T. (2024) Inhibitors targeting BamA in gram-negative bacteria. *Biochim Biophys Acta Mol Cell Res* **1871** (1): 119609.

Strieker, M., Tanović, A., and Marahiel, M.A. (2010) Nonribosomal peptide synthetases: structures and dynamics. *Curr Opin Struct Biol* **20** (2): 234–240.

Sun, D., Storek, K.M., Tegunov, D., Yang, Y., Arthur, C.P., Johnson, M., *et al.* (2024) The discovery and structural basis of two distinct state-dependent inhibitors of BamA. *Nat Commun* **15** (1): 8718.

Tambong, J.T. (2013) Phylogeny of bacteria isolated from Rhabditis sp. (Nematoda) and identification of novel entomopathogenic Serratia marcescens strains. *Curr Microbiol* **66** (2): 138–144.

Tanaka, Y., Hosaka, T., and Ochi, K. (2010) Rare earth elements activate the secondary metabolite-biosynthetic gene clusters in Streptomyces coelicolor A3(2). *J Antibiot (Tokyo)* **63** (8): 477–481.

Tharp, J.M., Wang, Y.-S., Lee, Y.-J., Yang, Y., and Liu, W.R. (2014) Genetic incorporation of seven ortho-substituted phenylalanine derivatives. *ACS Chem Biol* **9** (4): 884–890.

Tobias, N.J., Shi, Y.-M., and Bode, H.B. (2018) Refining the Natural Product Repertoire in Entomopathogenic Bacteria. *Trends Microbiol* **26** (10): 833–840.

Tomasek, D., and Kahne, D. (2021) The assembly of β-barrel outer membrane proteins. *Curr Opin Microbiol* **60:** 16–23.

Traxler, M.F., and Kolter, R. (2015) Natural products in soil microbe interactions and evolution. *Nat Prod Rep* **32** (7): 956–970.

Trimble, M.J., Mlynárčik, P., Kolář, M., and Hancock, R.E.W. (2016) Polymyxin: Alternative Mechanisms of Action and Resistance. *Cold Spring Harb Perspect Med* **6** (10).

Typas, A., Banzhaf, M., van Berg Saparoea, B., Verheul, J., Biboy, J., Nichols, R.J., *et al.* (2010) Regulation of peptidoglycan synthesis by outer-membrane proteins. *Cell* **143** (7): 1097–1109.

U. S. Centers for Disease Control and Prevention (2024) Antimicrobail Resistance Facts: Antibiotic use in food animals. [WWW document]. URL

https://www.cdc.gov/narms/resistance/index.html#cdc_facts_stats_trends-antibiotic-use-in-food-animals.

Ullrich, K.K., Hiss, M., and Rensing, S.A. (2015) Means to optimize protein expression in transgenic plants. *Curr Opin Biotechnol* **32:** 61–67.

Vaillancourt, F.H., Yin, J., and Walsh, C.T. (2005) SyrB2 in syringomycin E biosynthesis is a nonheme FeII alpha-ketoglutarate- and O2-dependent halogenase. *Proc Natl Acad Sci U S A* **102** (29): 10111–10116.

van Heel, A.J., Jong, A. de, Montalbán-López, M., Kok, J., and Kuipers, O.P. (2013) BAGEL3: Automated identification of genes encoding bacteriocins and (non-)bactericidal posttranslationally modified peptides. *Nucleic Acids Res* **41** (Web Server issue): W448-53.

van Pée, K.H. (1996) Biosynthesis of halogenated metabolites by bacteria. *Annu Rev Microbiol* **50:** 375–399.

van Pée, K.-H., and Zehner, S. (2003) Enzymology and Molecular Genetics of Biological Halogenation. In *Natural Production of Organohalogen Compounds.* Gribble, G. (ed.). Berlin, Heidelberg: Springer Berlin Heidelberg, pp. 171–199.

Ventola, C.L. (2015) The antibiotic resistance crisis: part 1: causes and threats. *P T* **40** (4): 277–283.

Vij, R., Lin, Z., Chiang, N., Vernes, J.-M., Storek, K.M., Park, S., *et al.* (2018) A targeted boost-and-sort immunization strategy using Escherichia coli BamA identifies rare growth inhibitory antibodies. *Sci Rep* **8** (1): 7136.

Voulhoux, R., Bos, M.P., Geurtsen, J., Mols, M., and Tommassen, J. (2003) Role of a highly conserved bacterial protein in outer membrane protein assembly. *Science* **299** (5604): 262–265.

Wade, N., Wesseling, C.M.J., Innocenti, P., Slingerland, C.J., Koningstein, G.M., Luirink, J., and Martin, N.I. (2022) Synthesis and Structure-Activity Studies of β-Barrel Assembly Machine Complex Inhibitor MRL-494. *ACS Infect Dis* **8** (11): 2242–2252.

Waksman, S.A., Schatz, A., and Reynolds, D.M. (2010) Production of antibiotic substances by actinomycetes. *Ann N Y Acad Sci* **1213:** 112–124.

Wang, Y.-S., Fang, X., Wallace, A.L., Wu, B., and Liu, W.R. (2012) A rationally designed pyrrolysyl-tRNA synthetase mutant with a broad substrate spectrum. *J Am Chem Soc* **134** (6): 2950–2953.

Watts, A., Sankaranarayanan, S., Watts, A., and Raipuria, R.K. (2021) Optimizing protein expression in heterologous system: Strategies and tools. *Meta Gene* **29:** 100899.

Welch, M., Govindarajan, S., Ness, J.E., Villalobos, A., Gurney, A., Minshull, J., and Gustafsson, C. (2009) Design parameters to control synthetic gene expression in Escherichia coli. *PLoS One* **4** (9): e7002.

Welsch, M.E., Kaplan, A., Chambers, J.M., Stokes, M.E., Bos, P.H., Zask, A., *et al.* (2017) Multivalent Small-Molecule Pan-RAS Inhibitors. *Cell* **168** (5): 878-889.e29.

WHO (2021) *2020 ANTIBACTERIAL AGENTS IN CLINICAL AND PRECLINICAL DEVELOPMENT: an overview and analysis: An Overview and Analysis.* Geneva: World Health Organization.

WHO (2023) *2023 Antibacterial agents in clinical and preclinical development: An Overview and Analysis.* Geneva: World Health Organization.

WHO (2024) *WHO Bacterial Priority Pathogens List 2024: Bacterial Pathogens of Public Health Importance, to Guide Research, Development, and Strategies to Prevent and Control Antimicrobial Resistance.* Geneva: World Health Organization.

Wilson, M.C., Mori, T., Rückert, C., Uria, A.R., Helf, M.J., Takada, K., *et al.* (2014) An environmental bacterial taxon with a large and distinct metabolic repertoire. *Nature* **506** (7486): 58–62.

Wink, M. (1997) Special Nitrogen Metabolism. In *Plant Biochemistry:* Elsevier, pp. 439–486.

Winter, J.M., Moffitt, M.C., Zazopoulos, E., McAlpine, J.B., Dorrestein, P.C., and Moore, B.S. (2007) Molecular basis for chloronium-mediated meroterpene cyclization: cloning, sequencing, and heterologous expression of the napyradiomycin biosynthetic gene cluster. *Journal of Biological Chemistry* **282** (22): 16362–16368.

Wuisan, Z.G., Kresna, I.D.M., Böhringer, N., Lewis, K., and Schäberle, T.F. (2021) Optimization of heterologous Darobactin A expression and identification of the minimal biosynthetic gene cluster. *Metab Eng* **66:** 123–136.

Yang, X., Li, X., Qiu, S., Liu, C., Chen, S., Xia, H., *et al.* (2024) Global antimicrobial resistance and antibiotic use in COVID-19 patients within health facilities: A systematic review and meta-analysis of aggregated participant data. *J Infect* **89** (1): 106183.

Yeh, E., Blasiak, L.C., Koglin, A., Drennan, C.L., and Walsh, C.T. (2007) Chlorination by a long-lived intermediate in the mechanism of flavin-dependent halogenases. *Biochemistry* **46** (5): 1284–1292.

Yeh, E., Cole, L.J., Barr, E.W., Bollinger, J.M., Ballou, D.P., and Walsh, C.T. (2006) Flavin redox chemistry precedes substrate chlorination during the reaction of the flavin-dependent halogenase RebH. *Biochemistry* **45** (25): 7904–7912.

Yeh, E., Garneau, S., and Walsh, C.T. (2005) Robust in vitro activity of RebF and RebH, a two-component reductase/halogenase, generating 7-chlorotryptophan during rebeccamycin biosynthesis. *Proc Natl Acad Sci U S A* **102** (11): 3960–3965.

Young, D.D., Young, T.S., Jahnz, M., Ahmad, I., Spraggon, G., and Schultz, P.G. (2011) An evolved aminoacyl-tRNA synthetase with atypical polysubstrate specificity. *Biochemistry* **50** (11): 1894–1900.

Young, T.S., and Schultz, P.G. (2010) Beyond the canonical 20 amino acids: expanding the genetic lexicon. *J Biol Chem* **285** (15): 11039–11044.

Zehner, S., Kotzsch, A., Bister, B., Süssmuth, R.D., Méndez, C., Salas, J.A., and van Pée, K.-H. (2005) A regioselective tryptophan 5-halogenase is involved in pyrroindomycin biosynthesis in Streptomyces rugosporus LL-42D005. *Chem Biol* **12** (4): 445–452.

Zhang, Q., Mo, T., Ding, W., Han, Y., and Deng, Z. (2021) The research on post-translational modification of RiPPs Xye catalyzed by CyFE PacB. *Synth. Biol. J.*

Zhao, S., Feng, R., Gu, Y., Han, L., Cong, X., Liu, Y., *et al.* (2024) Heterologous expression facilitates the discovery and characterization of marine microbial natural products. *Engineering Microbiology* **4** (2): 100137.